Modeling the evolution of salinity in the Motril-Salobreña aquifer using a paleo-hydrogeological model

Jonas Thu Olsen

Master Thesis in Geosciences

Discipline: Environmental Geosciences

Department of Geosciences

Faculty of Mathematics and Natural Sciences

UNIVERSITETET I OSLO

September 2016

Modeling the evolution of salinity in the Motril-Salobreña aquifer using a paleo-hydrogeological model

Jonas Thu Olsen

Master Thesis in Geosciences

Discipline: Environmental Geosciences

Department of Geosciences

Faculty of Mathematics and Natural Sciences

UNIVERSITETET I OSLO

September 2016

Modeling the evolution of salinity in the Motril-Salobreña aquifer using a paleo-hydrogeological model

This thesis is published digitally through DUO – Digitale Utgivelser ved UiO

http://www.duo.uio.no

Abstract

Contamination of groundwater in costal aquifers due to salinization is a global issue, and is only anticipated to increase as the demand for freshwater in coastal zones continues to increase. The increased anthropogenic activity in coastal zones will further lead to increased seawater intrusions. To properly address the problems connected to seawater intrusions and to prevent severe deterioration of the quality of the groundwater, variable density groundwater models are a necessity. The Motril-Salobreña aquifer in the south of Spain is an ideal aquifer to study seawater intrusions and associated processes, due to its somewhat special characteristics.

One of the controlling factors over solute transport models are heterogeneities within the aquifer, as they have a major influence on the solute transport. To address this problem the use of hydrofacies was applied. The Motril-Salobreña aquifer was divided into 6 hydrofacies units based on the study of lithological columns and the sedimentological history of the aquifer. Further, the hydrofacies units were used to construct a numerical variable density groundwater model of the aquifer.

Coastal aquifers are rarely in equilibrium with current boundary conditions, resulting in a constant modification of the salinity distribution in the aquifer. The Motril-Salobreña aquifer has undergone a rapid coastline progradation over the last 500 years, with a mean coastline advance of over 3 m/year. Previous studies on the aquifer have detected the presence of connate seawater, and it has been proposed that this is a result of the rapid coastline progradation. In this study, this was explored using a paleo-hydrogeological model, simulating the transient evolution of the groundwater salinity over the last 6000 years. It was detected that conditions similar to that found in the Motril-Salobreña aquifer could result in connate seawater. Based on the results of the simulation it was constructed a map over the relative flushing times in different parts of the aquifer.

Acknowledgement

First and foremost I would like to thank my main supervisor Carlos Duque guiding me in my work throughout the year, and giving me the opportunity to work on such an interesting topic.

I also want to thank my co-supervisors Maria Luísa Calvache, Helge Hellevang and Juan Pedro Sánches-Ùbeda for their help. Special thanks should be given to Maria Luísa for letting me join their fieldwork and helping me during my stay in Spain, and to Juampe for spending a day in the field with me, helping me out with my thesis and learning me a great deal about hydrogeology. Lastly, thanks to Per Aagaard for always keep an open door and answering many of my questions.

A great thank you to my fellow students and friends at the University of Oslo for 5 great years. Without you the last years would not have been the same. Further, I would like to thank my family and friends who have supported me throughout the last year. I really look forward to being able to spend more time with you all.

Table of contents

1 Introduction

1.1 Introduction

Pollution of groundwater due to salinization processes is regarded as one of the biggest problems in coastal aquifers (Custodio and Bruggeman, 1987; Custodio, 2010; Post and Abarca, 2010) and is only anticipated to increase in the coming decades. Small amounts of seawater can deteriorate the quality of the freshwater making it useless for human purposes. Groundwater containing one percent saltwater is unfit as drinking water (WHO, 2004), and above six percent it becomes unfit for all practical purposes besides cooling and flushing (Custodio, 2005; Werner et al., 2013) making it a very vulnerable resource. Combined with the fact that around 1.2 billion people lives in close proximity to the coast (Small and Nicholls, 2003) and relaying on groundwater as their primary source for freshwater, knowledge about seawater/groundwater interactions are of paramount importance to continue having groundwater as a reliable resource for future generations.

Water is needed in all parts of today's society, from small-scale house holding to much larger amounts used for irrigation or industrial purposes. The high demand often results in bad aquifer management and excessive usage (Steyl and Dennis, 2010), leaving the aquifer vulnerable for salinization. The most widespread reason for salinization (i.e. the process of increasing salinity) of coastal aquifers is saltwater intrusions (Werner et al 2013). Saltwater intrusions can have both natural and anthropogenic origin such as sea-level rise or climate variations (e.g. Bobba, 2002) or excessive pumping (e.g. Adepelumi et al., 2009; Narayan et al., 2003). However, salinity in coastal aquifer is not only caused by present saltwater intrusions. Other causes, which all needs to be properly addressed for correct aquifer management, include: dissolution of evaporate deposits (Tellam, 1995), mixing of unflushed old marine water present within the aquifer (Khaska et al., 2013; Bath and Edmunds, 1981), displacement of saline groundwater contained in deep formations or infiltration of saline irrigation return flow.

A general applied method for solving complex problems in hydrogeology is the use of numerical models, as seen in several studies (e.g. Lemieux and Sudicky, 2010; Calvache et al., 2009; Walther et al., 2012; Hudon-Gagnon et al., 2015; Biswas and Melesse, 2016; Kolbe et al., 2016). With the increased computational capacity in combination with easy access and

intuitive graphical user interfaces in recent times, both the use and complexity of models has expanded. With this the limitations of a groundwater model often lies in the conceptualization processes and especially in describing the geological heterogeneities of the system in question. Heterogeneities can be considered at a wide range of scales, from gigascopic, defined at the scale of depositional systems or stratigraphic sequences, to microscopic, defined at the scale of individual grains and pores (Galloway and Sharp Jr, 1998a). The scale of which heterogeneities should be considered depends on the objective of the modeling, the available information regarding aquifer properties and the desired level of accuracy. After the desired resolution is determined the process of reproducing the aquifer heterogeneity can begin. There are several ways which this can be done, falling into three general categories of structure-imitating, process-imitating and descriptive (Koltermann and Gorelick, 1996). Structure-imitating processes include the use of statistical methods to determine heterogeneities within an aquifer (e.g. Scheibe and Murray, 1998; Carle et al., 1998). Process-imitating methods include inverse modeling, which aims to solve governing groundwater flow equations to connect hydraulic heads to hydraulic properties (e.g. Carrera et al., 2005). Lastly, descriptive methods which couples geological observations and geological information about the model area to construct the aquifer architecture (e.g. Anderson, 1989; Ezzy et al., 2006). For this it is generally assumed that geological facies define the spatial arrangement of hydraulic properties dominating the groundwater flow (Koltermann and Gorelick, 1996).

Eaton (2006) showed the significance of heterogeneity when conducting groundwater flow simulations, and stressed the importance of characterizing different hydrofacies within a geological unit for improved modeling results. The term hydrofacies was first introduced by Poeter and Gaylord (1990), building on the work of Anderson (1989), who defined each facies as a homogeneous, anisotropic hydrogeological unit. Since then hydrofacies has been applied in groundwater studies to solve complex problems. Klingbeil et al. (1999) related lithofacies to hydrofacies in a Quaternary gravel deposit by defining different lithological units based on outcrop analysis, and combining these with hydrogeological measurements to distinguish hydrofacies. Asprion and Aigner (1999) combined 3D seismic with outcrop mapping to produce a 3D visualization of shallow subsurface heterogeneity in a Quaternary gravel delta. Ezzy et al. (2006) combined GPR data with direct geological observations to construct a conceptual model of a coastal alluvial plain, followed by numerical modeling to explore the effect that sedimentary heterogeneity between different hydrofacies has on

groundwater flow paths and transport. Fleckenstein et al. (2006) combined the use of geostatistical simulations to define different hydrofacies with numerical modeling of groundwater flow to look at river-aquifer interactions. In this thesis, a hydrofacies will be defined as an area within an aquifer which shows similar hydraulic properties and is delineated by geological facies and grain sizes, which again is constrained by different depositional systems. Each hydrofacies unit can further include a natural range of variability in hydrogeological properties depending on the degree of internal heterogeneity within the unit.

Groundwater flow through an aquifer is to a high degree determined by the hydraulic properties of the aquifer. However, it is also controlled by spatial differences within the chemical, thermal or mechanical properties of the groundwater, that eventually will determine the energy of the water (Fetter, 2001). Water flows from areas with high energy to areas with lower energy in an attempt to balance out these differences. This can be seen in coastal aquifers where the density difference between salt- and freshwater can vary significantly within a relatively short distance. The higher amount of dissolved salts in the saltwater will increase its density compared to that in freshwater, thus increasing the energy of saltwater and leading to variable-density groundwater flow. This flow of groundwater redistributes the solute concentration and alters the density field, which again affects the groundwater movement. The two, variable-density groundwater flow and solute transport, are interconnected. Because of the density feedback of solute transport on groundwater flow, a detailed mapping of the initial salinity distribution is needed for variable-density groundwater flow modeling, described by Delsman et al. (2014) as a "vicious circle of having to know the salinity distribution to model the salinity distribution".

A commonly used approach to determine the salinity distribution and the initial salinity conditions when conducting variable-density simulations is to assume that the sea- and freshwater is in a steady-state condition. However, this assumption is often not correct, as the present conditions is still a transient moment in the evolution of the groundwater. The historical modeling of landscape and the hydrogeology of an aquifer, here referred to as paleo-hydrogeological modeling, could be used as a method to better delineate the current salinity conditions and thereby improving the initial conditions. Delsman et al. (2014) proposed that by modeling the evolution of an aquifer and starting from a point where the

salinity distribution is considered known, or is presumed to not influence the current distribution, the present conditions could be better delineated.

The amount of studies combining paleo-hydrogeological modeling with variable-density simulations is limited. Lebbe et al. (2008) modeled the historical evolution of saltwater distribution in the mouth of an estuary for the last 500 years. Delsman et al. (2014) modeled the evolution of saltwater intrusions in the Netherlands during Holocene, using variable-density simulations. Besides this the amount of studies using paleo-hydrogeological modeling combined with variable density-flow is scarce, but the importance of this type of studies is nevertheless shown by Delsman et al. (2014) who pointed out that within the 8500 years modeled period, the coastal groundwater distribution never reached equilibrium with the contemporaneous boundary conditions. Other authors have used paleo-hydrogeological modeling to address different topics then variable-density problems. Zwertvaegher et al. (2013) simulated the phreatic groundwater level in an integrated archeological and geological study over a 12000-year period to construct the old paleo-landscape in Flanders, Belgium. van Loon et al. (2009) studied fen degradation in the Netherlands over a 2000 year long period.

The Motril-Salobreña aquifer is located at the south coast of Spain, close to Sea. It is one of the best-preserved aquifers in Spain, showing little to no signs of saltwater intrusion (Calvache et al., 2009). However, Crespo et al. (2012) using a geostatistical analysis over an hydrochemical database pointed to the possibility of reminder seawater in areas located far away from the coast, without any evidence of present saltwater intrusion like salinized wells between the coastline and the detected areas. Some potential explanation of this could be old marine seawater trapped within sediments of low permeability (Duque et al., 2008): a sedimentological structure that prevents the natural flow of parts of the groundwater from the higher topographical areas of the aquifer to the sea, or; a deeper connection between sea and aquifer (Crespo et al., 2012)

The aquifer shows somewhat special characteristics due to very rapid changes in its geometry in very recent history. It has been demonstrated that over the last 500 years, the mean coastline advance of the aquifer is over 1200 meter (Jabaloy-Sánchez et al., 2014); a progradation of over 2 meters each year. As a result, the seawater interacting with the aquifer have been changing continuously and thereby modifying the natural equilibrium that is

usually reached in coastal aquifers. The rapid expansion and high sedimentation rate and the lack of equilibrium conditions between salt- and freshwater could both be possible sources for the detected saltwater within the aquifer. Also, the hypothesis of non-reaching equilibrium conditions between salt- and freshwater indicates that the assumption of using steady state to determine the initial salinity conditions when conducting variable-density groundwater flow modeling might be inadequate. Hence, the use of paleo-hydrogeological modeling could be seen as a possible solution to both detecting the source of the seawater and mapping out the current salinity conditions in the study area and thereby improving future modeling.

1.2 Objectives

The main goals for this study are:

1. Construct a sedimentological model of the Motril-Salobreña aquifer using the integrated information from lithological columns and knowledge about the sedimentological environment through literature review
2. Delineate the Motril-Salobreña aquifer into different hydrofacies based on the sedimentological model.
3. Do a sensitivity analysis over the most important hydrogeological parameters for saltwater intrusions and paleo-modeling using a generic 2D numerical model of an coastal aquifer
4. Construct a 3D-numerical model of the Motril-Salobreña aquifer integrating the proposed hydrofacies to decrease model error
5. Combine the 3D-model with paleo-hydrogeological modeling to study the transient evolution of the salinity distribution in the Motril-Salobreña aquifer and explore the possibility of connate seawater

2 Background information

2.1 Study site

2.1.1 Location and climate

The Motril-Salobreña aquifer is located in the south of Spain, at the coast of the Mediterranean Sea (Figure 2.1). Its name is derived from the two cities located on it, Motril and Salobreña, with a combined population of approximately 60000 inhabitants. During the summer months the population of these cities increases drastically because of tourism, and thus the stress over the groundwater is intensified. The aquifer has been the subject of multiple studies by the University of Granada resulting in a very complete hydrogeological dataset.

The area has a sub-tropical Mediterranean climate with little and irregular periods of rain, usually concentrated in the winter months. The average annual temperature is around 17 – 19 ^{0}C with worm summer months reaching over 25 ^{0}C and average monthly winters of over 12 ^{0}C (Jabaloy-Sánchez et al., 2014).

Figure 2.1: Motril-Saliobreña aquifer location in southern Spain, next to the Alboran Sea. The Guadalfeo River crosses the aquifer in the western part, which is fed by precipitation and snow melt in the Sierra Nevada mountain range. The terrain elevation is exaggerated by 3:1.

2.1.2 Hydrogeology and geology

The Motril-Salobreña aquifer is located over a geological unit called Alpujarrides complex, and is composed of detrital sediments of Quaternary age. It is defined as an unconfined aquifer with an area of 42 km^2 and composed of sediments deposited mainly by the Guadalfeo River, a river crossing the aquifer in the west (Figure 2.1). The thickness of the aquifer varies, ranging from 30 to 50 meter in the north to more than 250 meters in the south near the coastline (Duque et al., 2008). In the south it is in contact with the Mediterranean Sea and the unit underneath is considered as an impermeable basement. Except for a carbonate formation in the north, all surrounding formations are made of impermeable schist.

The Guadalfeo River has a very relevant role in the hydrogeological balance of the Motril-Salobreña aquifer, being one of the main sources of recharge (Duque et al., 2011). The catchment of the Guadalfeo River has elevations reaching 3479 meter in Sierra Nevada range to the north. Because of the high elevation differences the annual amount of precipitation varies greatly within the catchment, changing from 400 mm/year near the coast to over 1000 mm/year at higher elevations, with a mean value of 717.3 mm/year (Liquete et al., 2005). Discharge in the Guadalfeo River is typically characterized by seasonal variability, with two main maxima's; one in January because of winter rainfall, and one in May because of snow melt in the catchment (Lobo et al., 2006). However, in 2005 a dam was constructed to regulate the water flow in the river, which drastically changed the characteristic flow of the river now seeing a more steady flow all year.

Besides the recharge from the Guadalfeo River, the aquifer inputs are from irrigation return flow, rain and the hydraulic contact with the carbonate aquifer in the north (Duque et al., 2008). Duque et al. (2011) did a comprehensive study on recharge in the area with focus on how the different recharge sources contribute to the total recharge with stable isotopes of water. The dominating recharge input changes depending on the location on the aquifer. In the eastern part the most dominant are the irrigation return flow and rain, while in the the northwest and west sections the most important factors are the Guadalfeo River and the connection with the carbonate aquifer.

2.1.3 Historical evolution

Erosion around the Mediterranean Sea is mainly controlled by high rainfall intensity, steep land gradients, fragility of soils and human interventions such as deforestation, fires and land use changes (Poesen and Hooke, 1997). The increased progradation rate of the coastline and the increase in land area in the Motril-Salobreña aquifer can be closely linked to human interventions (García-Ruiz, 2010). The deforestation of extensive land areas used in farming, livestock farming and mining led to decreased soil stability in the Iberian Peninsula, and thereby increasing erosion and sediment discharge. This was particularly crucial between the 16th and 19th century, but human interventions have been traced back to 2000 BC (García-Ruiz, 2010).

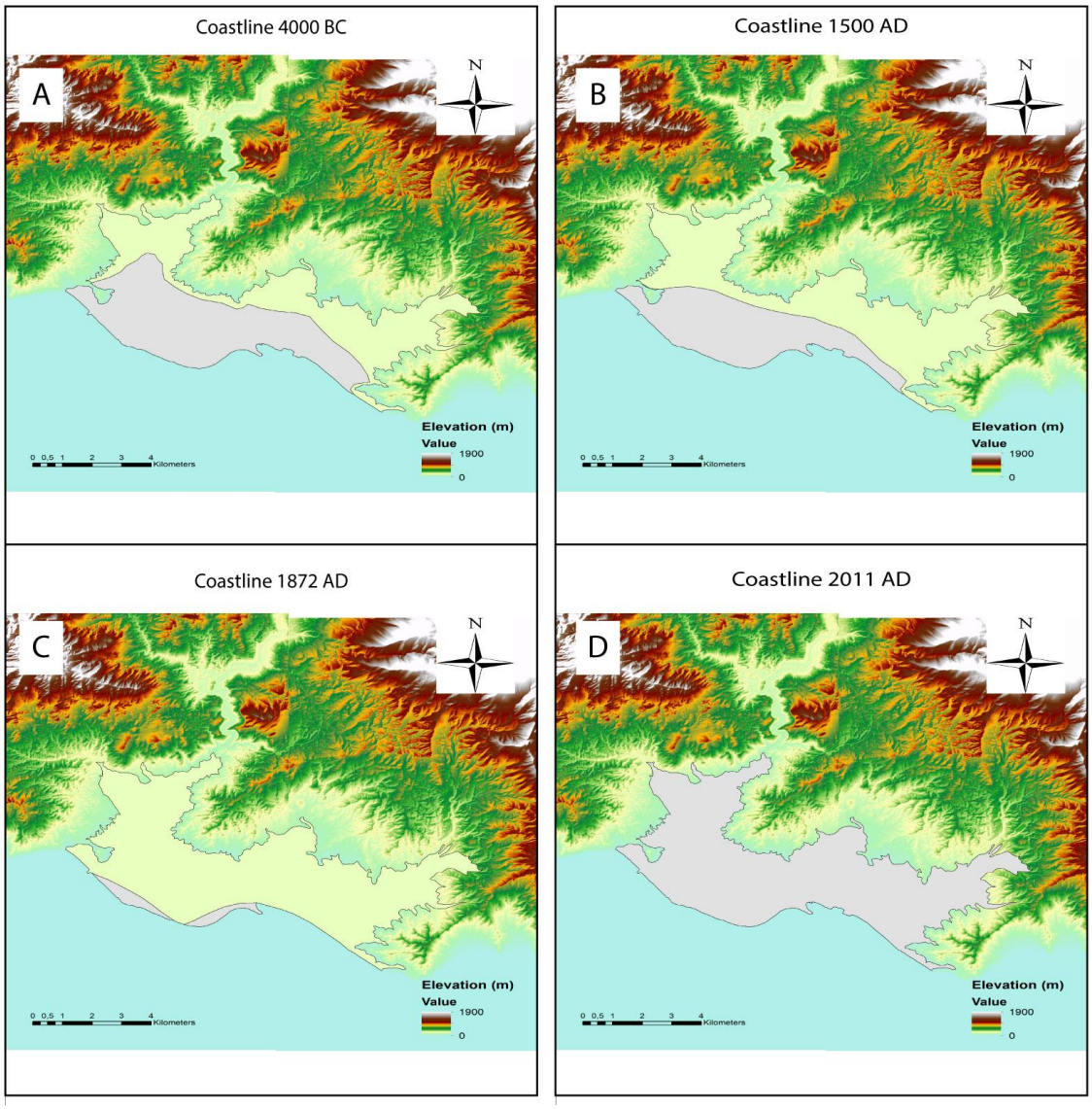

Figure 2.3: The four different stages of coastline evolution; (A) 4000-2000 BC, (B) 1500 AD, (C) 1872 AD and (D) 2011 AD (Jabaloy-Sánchez et al., 2014).

The evolution of the Motril-Salobreña aquifer coastline from 4000 BC to present time has been reconstructed by Jabaloy-Sánchez et al. (2014), based on the work of Hoffmann (1987). Using radiocarbon-dated organic matter extracted from boreholes, archaeological data and historical maps of the area they proposed three segments of coastline evolution characterized by different rates of progradation: (1) 4000-2000 BC to 1500 AD, (2) 1500 AD to 1872 AD and (3) 1872 to 2011 (Figure 2.3; Table 2.1).

According to this study, during the first period the coastline advanced at a mean rate of 0.09 – 0.15 m year^{-1}. It started out as an estuary environment before changing into narrow coastal plain at the end of the period. In the second period, from 1500 AD to 1872 AD, the delta was in a highly constructive phase with a mean coastline advance of 3.3 m year^{-1}, a considerable higher rate than earlier. At the end of this period coastline was approaching its current location (Figure 2.3, C), but continued expanding until around 1957 where it went into a more stationary condition. From then and until 2011 different parts of the coastline experienced different growth-rates, with some parts along the eastern segment even regressing (Figure 2.3, C-D). Also, in the late 1940s an anthropogenic shift of the Guadalfeo River was accomplished with the construction of walls and channeling the river for preventing flooding. This changed the river transect to its current location.

Table 2.1: Key values describing the Guadalfeo River delta evolution. Jabaloy-Sánchez et al. (2014)

Period	Mean coastline advance (m)	Yearly advance (m yr^{-1})	Delta increase (km^2)
4000-2000 BC to 1500 AD	500-510	0.09-0.15	6
1500 to 1872	1232	3.3	13.8
1872 to 2011	-	-	0.7

2.1.4 Sedimentological framework

A delta is defined as a depositional unit of sediments, fed by a terrestrial feeder system such as a river. When a river discharges into a standing body of water, the discharged material will settle and accumulate around the river mouth when sediment transport is higher than what basinal processes can redistribute. The result is a localized and often irregular progradation of the shoreline (Nemec, 1990).

The classification of deltas is not straight forward, and several approaches exist (Nemec, 1990). However, the most favored is classification of deltas depending on delta-front regime (Galloway, 1975), namely into (1) fluvial dominated, (2) wave-dominated and (3) tide-dominated. This way of classifying deltas emphasizes the basinal process, such as waves, tidal forces, wind and near-shore forces, working on the redistribution of sediments. Basinal process, or the lack of basinal processes, determines the depositional environment, and hence to a large extent the morphology of the delta and the internal facies distribution (Coleman and Wright, 1975; Dalrymple and James, 2010). For instance, in wave-dominated deltas the ratio between sediment reworking from waves and fluvial discharge is high, resulting in sediments being transport by longshore currents and redistribute along the delta front building beaches, barrier bars and spits (Boggs, 1995).

The formation of Gilbert-type deltas (Gilbert, 1885) is typically composed of coarse-grained sediments. As sediment deposition progrades basinward, the delta sediment architecture typically displays a topset, foreset and bottomset arrangement of beds (Figure 2.4). The bottomset beds are created from the lightest and most fine-grained material, reaching farthest away from the river mouth before being deposited. The foreset in turn consists of coarser and more variable sediments, deposited mainly around in the vicinity of the river mouth. This typically constitutes the river bed load. Topsets are constructed with finer sediments, and sedimentation is mainly dominated by distributary channel migration and fluvial processes such as channel and point-bar deposition and overbank flooding (Boggs, 1995).

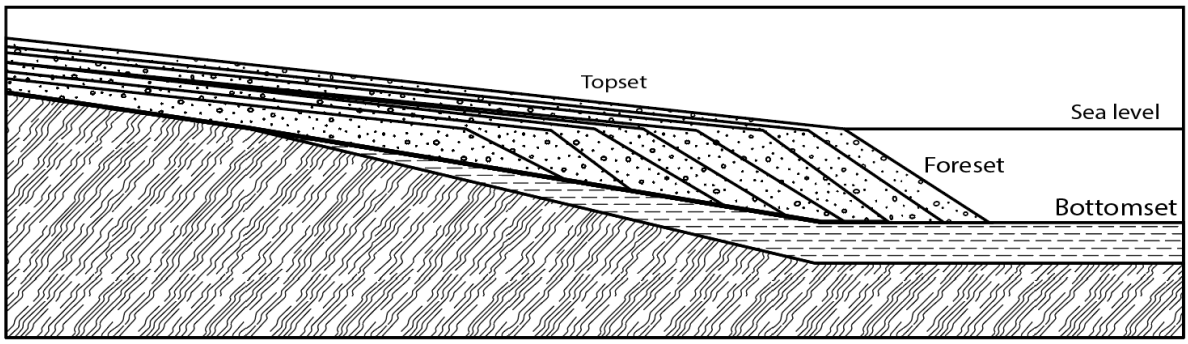

Figure 2.4: An idealized Gilbert delta with the characteristic topset, foreset and bottomset.

Coastal plains are another type of depositional environment found in marginal-marine environments. While a delta is the result of a single distributary channel, coastal plains are

derived from a number of deltas that have coalesced laterally and/or prograded at the same time (Alexander, 1989).

Depositional wise, coastal plains show a lot of similarities with deltas, and it is often hard to separate the two (Alexander, 1989). In a cross section perpendicular to the shoreline, the deposits from the two are very similar. However, if looking at a cross section parallel to the shore they become significantly different, with coastal plains showing more lateral changes in facies and permeability (Galloway and Sharp Jr, 1998b). Because of the different distributary channels they often display high heterogeneity, and from a hydreogeological viewpoint, unconfined, semiconfined and confined aquifers are found in close vertical proximity (Galloway and Sharp Jr, 1998b). If the coastal plain is narrow and connected to areas of high relief, alluvial fan and fan deltas are often common geomorphological and depositional elements connected to the coastal plain (Galloway and Sharp Jr, 1998b). A fan delta, as defined by (Boggs, 2006), is a coastal prism of sediments delivered by an alluvial fan system and deposited in the interface between the active fan and a standing body of water.

The depositional processes on an alluvial fan are commonly determined by topographic relief, sediment texture, climate and vegetation, and the three main processes are debris flows, channelized flow and sheet flow (Galloway and Hobday, 2012). Following periods of intense rainfall, ephemeral current can occur, giving rise to sheetflooding and streamflood processes. Fan deposits generally show an upward coarsening succession of sediment and grain size is reduced downfan as the gradient decreases (Galloway and Hobday, 2012).

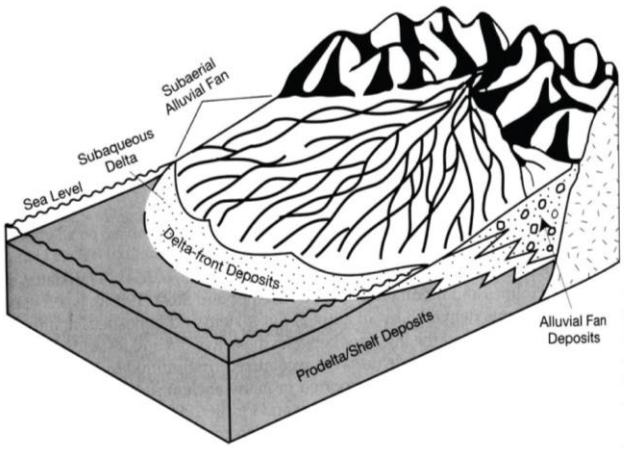

Figure 2.5: Sedimentological architecture of a fan delta. (modified from Boggs (2006)).

The forgone sedimentological information is connected to the sedimentology of the Motril-Salobreña. The aquifer can be divided into three parts, West, East and North (Figure 2.6), depending on the depositional processes that have prevailed (Jabaloy-Sánchez et al., 2014). The west sector is composed of a delta that is mainly fed with sediments deposited by the Guadalfeo River. Whereas in the East area is a coastal plain coupled to the outlet of several dry streams in the area, locally known as ramblas. The streams present high flow during periods of hours to days associated with storms and intense rainfall while most of the year they are dry. During the periods of high flow they contribute to sediment deposition in the area. The evolution of the coastal plain in the east and the delta in the west are interconnected, but they show different depositional characteristics due to the type of genetic processes that have influenced their development (Maldonado, 2009). The third area comprises alluvial sediments in the north which are mainly deposited by the Guadalfeo River.

The delta at the mouth of the Guadalfeo River has been characterized by Maldonado (2009) as a wave-dominated delta, with longshore currents transporting parts of the deposited sediments east and west. Lobo et al. (2006), studying the prodeltaic wedges of the delta, proposed that the delta constitutes an end-member of river deltas, showing many similarities with fan deltas. This includes fast sedimentation rate and limited lateral redistribution, processes favored by areas comprising high-gradient river systems, marked seasonal river discharge and significant amounts of available loose sediments. The depositional processes have resulted in a decrease in hydraulic conductivity from north to south, corresponding to an increase in the portions of silts and clays (Duque et al., 2008). Also, borehole logs from the area show an increase in silts and clays in the deeper parts of the aquifer. The occurrence of channel deposits and overbank deposits in the area greatly determines both the vertical and horizontal heterogeneity (Calvache et al., 2009). Duque et al. (2008), using TDEM soundings, interpreted the presence of high-transmissivity sediments corresponding with coarse-grained material in an old paleo-channel of the Guadalfeo River.

In the eastern section, Maldonado (2009) did a geomorphological analysis using aerial photos and detailed topographic maps. He described it as a series of depositional lobes oriented parallel to the coast. These lobes have been developed as alluvial fans that prograded seaward and led to the formation of fan deltas. Duque et al. (2008) observed that the amount of silt and clay increases in the coastal plain, and consequently argues that there is a decrease in aquifer permeability eastward. However, Calvache et al. (2009) estimated

through model calibration that some of the highest values for hydraulic conductivity were located in the eastern part.

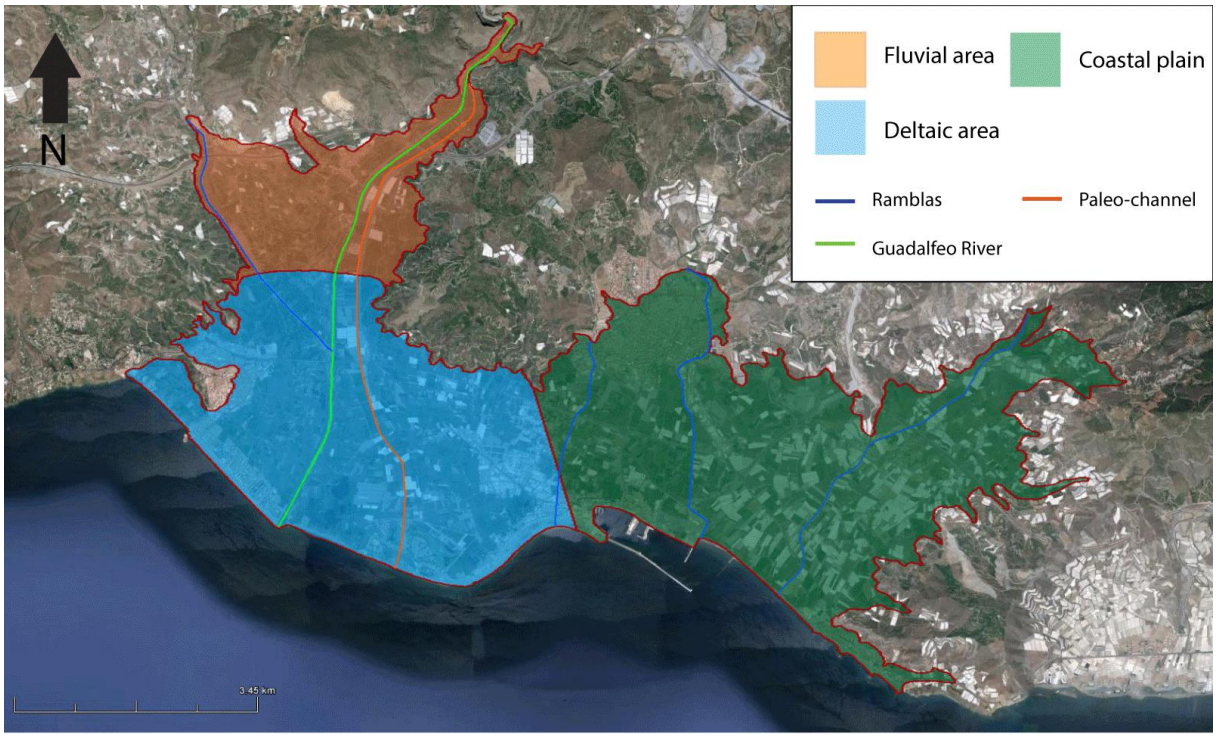

Figure 2.6: Main sedimentological areas of the Motril-Salobreña aquifer; Location of the current and paleo channel of the Guadalfeo River and the local ramblas in the east. (Jabaloy-Sánchez et al., 2014).

2.2 Salinization processes of coastal aquifers

2.2.1 Saltwater intrusion

In coastal areas and aquifers fresh groundwater from inland areas encounters the saline groundwater from the ocean. Oceanic water has higher density than fresh continental groundwater because of the amounts of dissolved salt. As a consequence, saltwater penetrates inland beneath the less dense freshwater (i.e. saltwater intrusion) and the two fluids will start to mix. However, the flow motion prevents the complete mixing of both fluids and the establishment of equilibrium in spite of their density differences, resulting in an interface called mixing zone or transition zone (Figure 2.7).

The principles of saltwater intrusions were first described by W. Badon-Ghyben in 1888, and later and independently by A. Herzberg in 1901 and is thus referred to as the Ghyben-Herzberg relationship. In the Ghyben-Herzberg relationship it is assumed that the weight of a unit column of fresh water going from the water table down to a point at the interface is

balanced by a column of saltwater going from the sea level down to the same point. This assumption holds for areas in hydrostatic condition within a homogeneous, unconfined costal aquifer, and the fluids (fresh- and saltwater) are immiscible and is expressed as:

$$H = \frac{\rho_f}{(\rho_s - \rho_f)} * h \qquad (2.1)$$

where h is the head of the water table above sea level, H is depth from the sea level (0 m.a.s.l) down to the fresh/saltwater interface and ρ_f and ρ_s is the density of fresh- and saltwater, respectively. Given the commonly used average density of 1025 kg m^{-3} for saltwater and 1000 kg m^{-3} for freshwater, equation 2.31 can be simplified to:

$$H = \frac{\rho_f}{(\rho_s - \rho_f)} * h = \alpha * h \qquad (2.2)$$

In natural circumstances the value of α is usually 40, which implies that for each meter the water table rises or sinks, the saltwater wedge will rise or sink 40 times as much for the same concentration values as above. In some cases the value of α can be changed to an empirical value based on local observations to better calculate the position of the mixing zone (Custodio and Bruggeman, 1987).

The Ghyben-Herzberg relationship shows that saltwater intrusion forms naturally to some degree in most coastal aquifers. However, anthropogenic effects can lead to enhanced saltwater intrusions by lowering the phreatic surface which leads to landward intrusion of seawater or reducing the groundwater gradients which allows saline water to displace freshwater in the aquifer (Adepelumi et al., 2009).

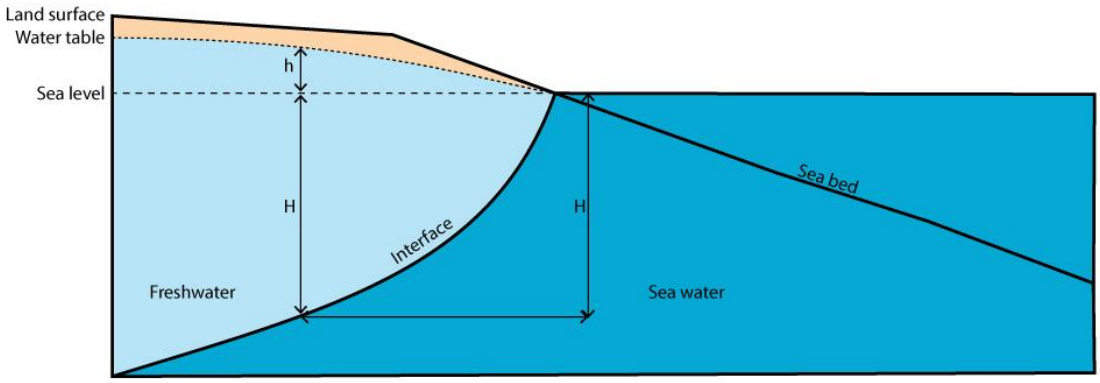

Figure 2.7: Illustration showing the basic principle of Ghyben-Herzberg relationship.

2.2.2 Other sources of salinization

Despite saltwater intrusions being the most common reason for salinization in coastal aquifer (Custodio and Bruggeman, 1987), other sources of salt must also be taken into consideration.

The mixing of freshwater with unflushed old marine water is observed in several aquifers. Old marine water found in aquifers is usually connected to low permeability formations (silt and clay lenses), confined aquifers and at the bottom of aquifers containing a very flat surface (Custodio and Bruggeman, 1987). It is typically two sources of marine water within aquifers (Custodio and Bruggeman, 1987): (1) connate marine water and (2) old seawater. Connate water is water trapped inside the sediments at the time of deposition, usually found in lagoons and advancing coasts. Old seawater is defined as all marine water in an aquifer that is currently not in direct contact with the present oceanic water. This can be a result of a change in the hydrodynamic system, which changes the location of the saltwater intrusion. Reasons for this can be sea level changes, tectonic activity that lift/sink the aquifer or other processes that produced changes in hydraulic head and in the groundwater flow patterns (Edmunds and Milne, 2001).

2.3 MODFLOW-SEAWAT

MODFLOW (McDonald and Harbaugh, 1988) is a three-dimensional finite-difference groundwater model developed by USGS used for simulating groundwater flow and groundwater/surface-water interactions, and is a commonly used program by hydrogeologists for simulating groundwater processes. It uses the following partial differential equation to solve groundwater flow:

$$\frac{\partial}{\partial x}\left(K_{xx}\frac{\partial h}{\partial x}\right)+\frac{\partial}{\partial y}\left(K_{yy}\frac{\partial h}{\partial y}\right)+\frac{\partial}{\partial z}\left(K_{yy}\frac{\partial h}{\partial z}\right)+W=S_y\frac{\partial h}{\partial t} \qquad 3.3$$

where K_{ii} are values for hydraulic conductivity along the x, y and z axis [L T^{-1}], h is the piezometric head [L], W is the water going into or out from the system [L^3 T^{-1}], S_s is the specific storage [L^{-1}]and t is time [T].

MT3DMS (Zheng and Wang, 1999) is used for simulating solute transport equations. It is based upon the three types of solute transport; advection, dispersion/diffusion and chemical reactions under normal hydrogeological conditions. It is used for simulating the three-dimensional transport of contaminants within a transient groundwater system applying the following equation:

$$\frac{\partial(\theta C^k)}{\partial t}=\frac{\partial}{\partial x_i}\left(\theta D_{ij}\frac{\partial C^k}{\partial x_j}\right)-\frac{\partial}{\partial x_i}(\theta v_i C^k)+q_s C_s^k+\sum R_n \qquad (3.4)$$

where C^k is the dissolved concentration of species k [M L^{-3}], θ is the porosity [dimensionless], t is time [T], x_i is the distance along coordinate axis I [L], D_{ij} is the hydrodynamic dispersion coefficient tensor [L^2T^{-1}], v_i is the linear pore water velocity [L T^{-1}], q_s is the volumetric flow rate per unit volume of aquifer [M^3 T^{-1}], C_s^k is the concentration of source of sink flux of species k [M L^{-3}] and $\sum R_n$ is the chemical reaction term [M L^{-3} T^{-1}].

The coupling of MODFLOW and MT3DMS into a single program and including variable density flow resulted into SEAWAT (Guo and Langevin, 2002). It is used to solve the coupled groundwater flow and solute-transport equations, to simulate three-dimensional, variable-density groundwater flow and multi-species transport. SEAWAT is based upon the concept of equivalent freshwater head in a saline groundwater environment:

$$h_f=\frac{P_N}{\rho_f g}+Z_N \qquad (3.5)$$

where h_f is the equivalent freshwater head [L], P_N is the pressure at point N [M L^{-1} T^{-2}], ρ_f is the density of freshwater [M L^{-3}], g is acceleration due to gravity [L T^{-2}], Z_N is the elevation of point N over datum [L].

Then the following variation of the variable-density groundwater flow equation:

$$\nabla\left[\rho\frac{\mu_0}{\mu}K_0\left(\nabla h_0+\frac{\rho-\rho_0}{\rho 0}\right)\right]=\rho S_{s,0}\frac{\partial h_0}{\partial t}+\theta\frac{\partial\rho}{\partial C}\frac{\partial C}{\partial t}-\rho_s q'_s \quad 3.6$$

where ρ_0 is the fluid density [M L^{-3}], μ is the dynamic viscosity [M L^{-1} T^{-1}], K_0 is the hydraulic conductivity tensor of the material saturated with reference fluid [L T^{-1}], h_0 is the hydraulic head of the refrence fluid [L], $S_{s,0}$ is the specific storage [L^{-1}], t is time [T], θ is porosity [dimensionless], C is salt concentration [M L^{-3}] and q'_s is the source or sink of fluid with density ρ_s [T^{-1}].

3 Methods

3.1 Grain size distribution

3.1.1 Theory

Hydraulic conductivity, K, is directly related to particle size and inversely related to particle size standard deviation (Fetter, 2001). As a result hydraulic conductivity will generally be higher for well-sorted (low standard deviation) sediments with coarse grain size, compared to little sorted sediments with fine grain size.

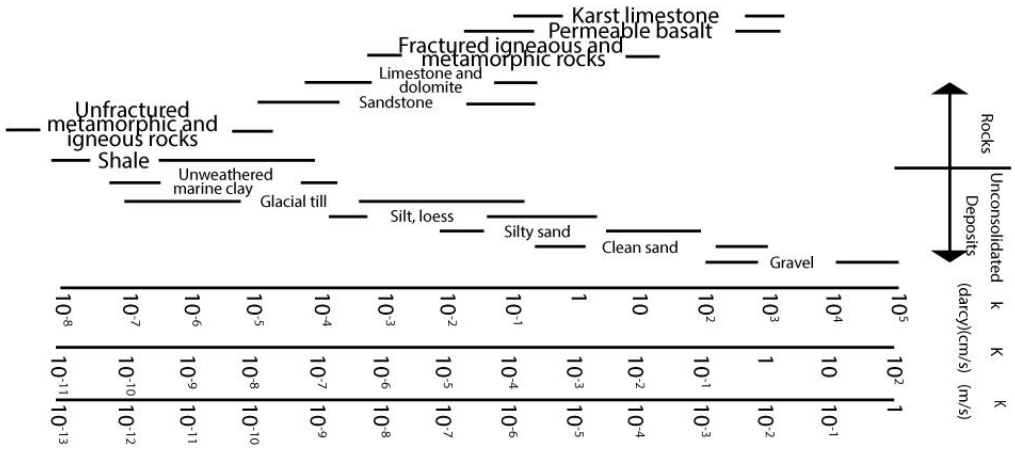

Figure 3.1: Range of values of hydraulic conductivity for different sediment sizes typically found in nature. (Freeze and Cherry, 1979)

Hydraulic conductivity can be estimated from grain size distribution of sediment samples from the field. The grain size mean value of a sample is usually connected to hydraulic conductivity by an empirical formula. One of the most applied methods for this is the Hazen method (Hazen, 1892). It consists in using the effective grain size diameter obtained from the cumulative grain size curve to obtain an estimate for hydraulic conductivity:

$$K = C(d_{10})^2 \qquad (3.1)$$

where K is hydraulic conductivity (cm/s), d_{10} is the effective grain size (cm) and C is an empirical coefficient based on the degree of sorting.

In order to make the cumulative grain size distribution curve, the sediment sample is sorted into different fractions based on particle grain size. This is usually done by sieving the sediments through a number of sieves, each with different grid size. The portion of the

sample that is coarser will be retained in the sieve, whereas the portion with finer grain size proceeds to the next sieve and the processes continues. When this is done for the entire sample, and the sample is divided into fractions depending on the grain size, each weight fraction are plotted in a semilogarithmic plot with grain size on one axis and the cumulative portion retained on the other. Then d_{10} can be read of the plot, which corresponds to the intercept line at 10% (Figure 3.2).

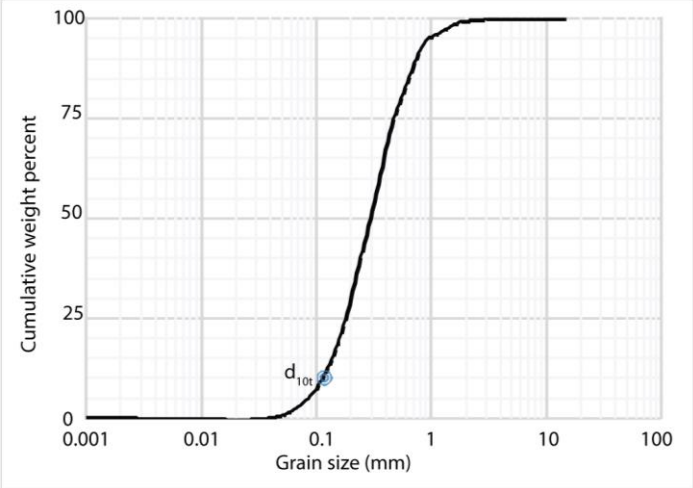

Figure 3.2: Example of the cumulative grain size distribution. d_{10} marks the point for the effective grain size.

3.1.2 Sediment sampling

It was selected 8 samples from sediment cores of 8 boreholes from the Motril-Salobreña aquifer (Figure 3.3). The cores are are stored from previous drilling in the area at the University of Granada. Since the objective of the experiment was to distinguish different hydrofacies, each sample was taken within a range of depth can be assigned to the same unit (Table 3.1).

Table 3.1: Depth at which sediments were collected for grain size analysis.

	Location							
	REC	*INT*	*DEC*	*UP*	*MIDDLE*	*DOWN*	*PALEO*	*EAST*
Depth (m)	10-50		155-245	12	30	10-40	20-50	10-40

Figure 3.3: The Motril-Salobreña aquifer with the location to where the 8 samples used in grain size distribution was taken.

3.1.3 Procedure

Each sample was dried for 18 hours at 105 ^{0}C to make sure they were completely dry before being sorted. After that the grain size distribution of each sample was determined using 10 different sieves with varying hole spacing (Table 3.2; Figure 3.4). To separate the material all of the sieves were shaken manually until the material was separated completely, afterwards the sediment retained in each sieve was measured using a precision weight.

HydrogeoSieveXl (Devlin, 2015), an Excel-based spreadsheet program, was then used to estimate a range of hydraulic conductivity value for each of the samples. It uses different methods to determine hydraulic conductivity based on the grain size distribution, and gives a range of possible values that might apply for each sample. It also estimates value for porosity applying the following equation:

$$n = 0.255 * (1 + 0.83^{U}) \quad (3.2)$$

Where n (dimensionless) is porosity and U is uniformity coefficient (dimensionless).

Table 3.2: Sieve sizes used in the grain size sorting

Sieve	Size (mm)
1	16
2	8
3	4
4	2
5	1
6	0.5
7	0.250
8	0.125
9	0.063
10	<0.063

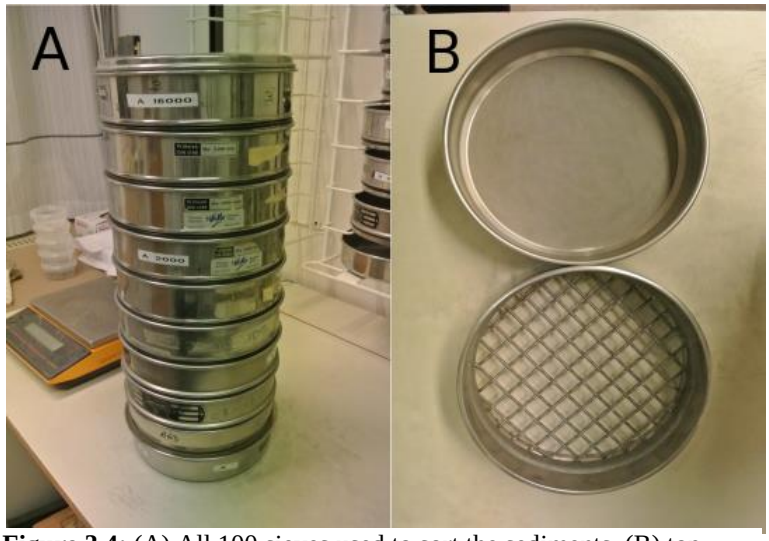

Figure 3.4: (A) All 100 sieves used to sort the sediments, (B) top sieve is the smallest one, javing 0.063 mm grid spacing, bottom sieve is the coarsest, having a grid space of 16 mm

However, only some of the methods were used here since not all of them were appropriate for the objectives of this study. The Zamarin (Zamarin, 1928) and the Slichter (Slichter, 1905) methods were chosen as they provided the highest and lowest values for hydraulic conductivity in all of the samples. The Beyer (Beyer, 1964) method was chosen as it gives an intermediate value for all the samples, and it applicable for all the effective grain sizes. The Hazen method, despite being applicable for effective grain size between approximately 0.1 and 3 mm, was also chosen as it is the most commonly applied method in grain size analysis; hence its value could be interesting for comparison.

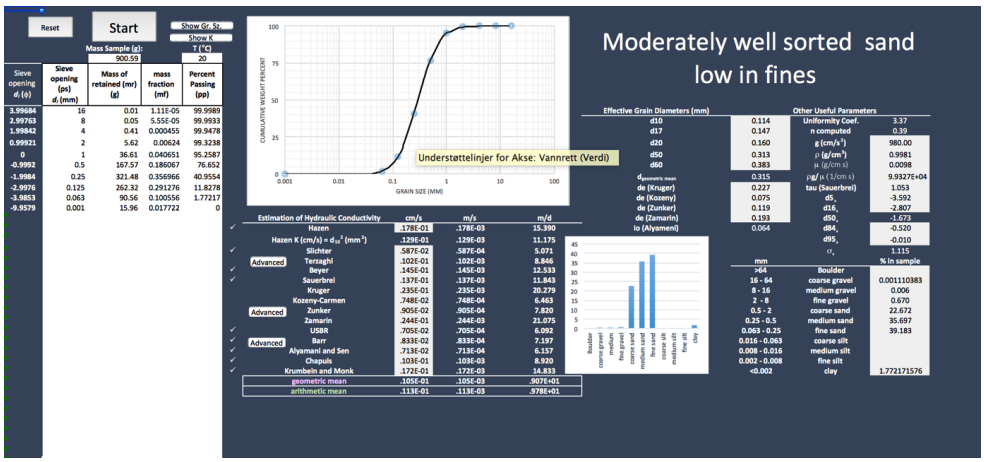

Figure 3.5: Example of the HydrogeoXL interface. Estimations of K are calculated automatically once the grain size distribution is tabled (Devlin, 2015).

3.2 Sedimentological model and hydrofacies

3.2.1 Sedimentological models of the study area

A sedimentological model of the aquifer was constructed to divide the aquifer into hydrofacies units. It was made by interpreting the lithological columns from boreholes and considering the sedimentological framework presented in section 2.1.4 and the history of the evolution of the aquifer summarized in section 2.1.3.

The aquifer was divided into three sections depending on the prevailing deposition systems: eastern, western and northern area (Figure 3.6). Thereafter the lithological columns and the knowledge about the depositional environment were used to define the major lithofacies that constitute the aquifer, whereupon the lithofacies were applied to construct the sedimentological model of the aquifer.

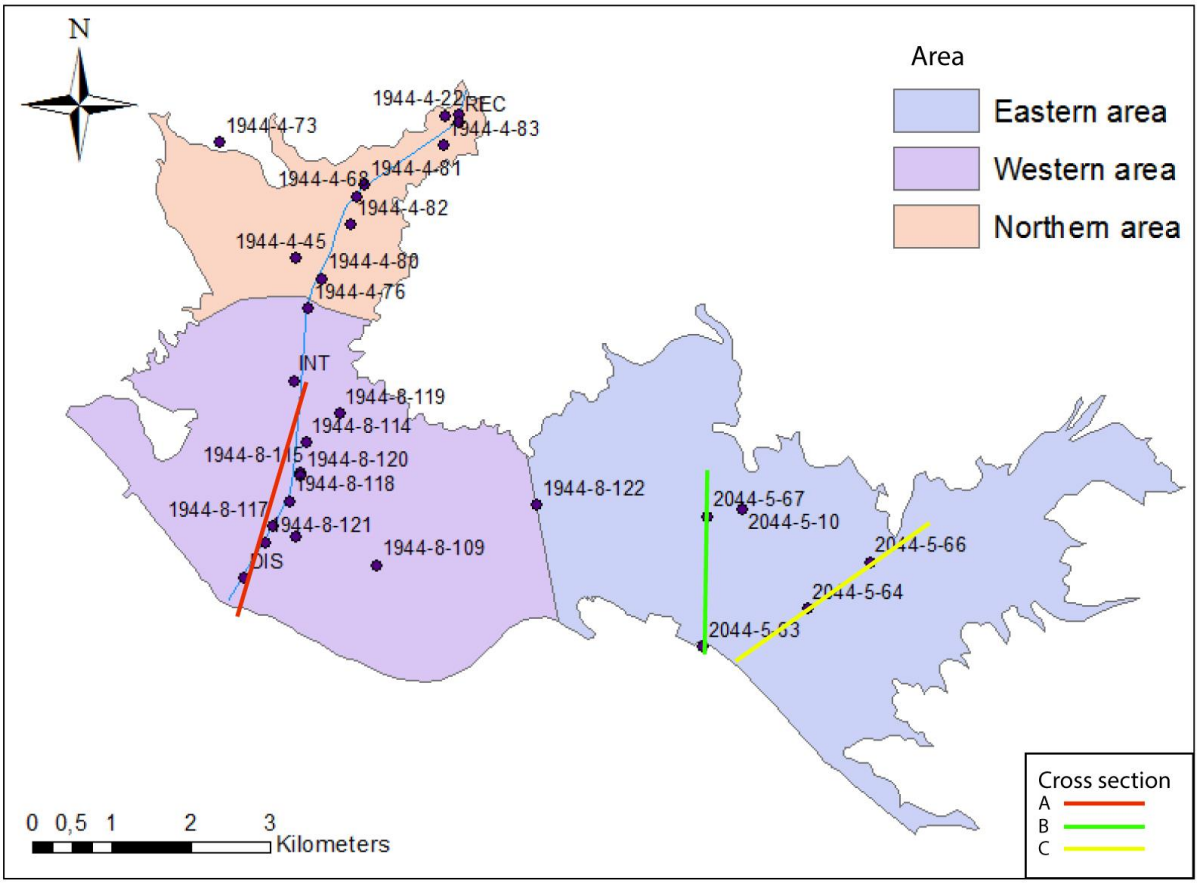

Figure 3.6: Distribution of the lithological columns in the Motril-Salobreña aquifer and the location of the cross sections used for the sedimentological models (see section 4.2.1 for description of the cross sections). The subareas within the aquifer are determined from the dominating depositional processes.

3.2.2 Hydrofacies

The information provided by the sedimentological model was used to divide the aquifer into different hydrofacies units. These units were characterized based on an initial assumption that grain sizes would determine the hydraulic conductivity, and that the dominating depositional environment was a controlling factor in the spatial distribution of grain sizes within the aquifer. In this way, grain size was considered as a major indicator of the hydraulic properties for each unit; and in fact, hydraulic conductivity is often the most dominant hydraulic property (Carrera et al., 2005).

The range of values for hydraulic conductivity assigned to each unit was determined based on the field estimates as well as previous studies in the area, including values estimated through numerical modeling. This gives a range of possible values for hydraulic conductivity for each unit that could all be feasible.

3.3 2D-Model

A synthetic 2D numerical model was constructed for testing how to implement the changes in the coastline movement (section 2.1.3), to conduct a sensitivity analysis on the most important parameters for saltwater intrusion modeling and to study the effect of the heterogeneities resulting from the sedimentological construction of the aquifer (section 4.2). Werner et al. (2013) notes that the variability of possible geological structures in a aquifer presents a significant barrier to the generalization of heterogeneity effects on seawater intrusion modeling, and that the application of simplified heterogeneous configurations are necessary to get enhanced understanding.

A sensitivity analysis measures how sensitive the model is to changes in a specific model parameter. In this particular case the salinity distribution was analyzed to know how it responds to changes in the model parameters. If a parameter has high sensitivity, a small change in its value will result in a significant change in the simulation results. On the contrary, changes to a parameter with low sensitivity will result in a significantly smaller change.

3.3.1 2D-conceptual model

For the 2D modeling a cross section of a generic unconfined coastal aquifer was considered (Figure 3.7). Freshwater infiltrates from the right vertical boundary and parts of the upper

horizontal boundary before being transported through the aquifer and discharging into the sea. The total thickness of the aquifer is B with a horizontal length L, divided into two sections L_s and L_L representing the sea and land parts of the aquifer, respectively.

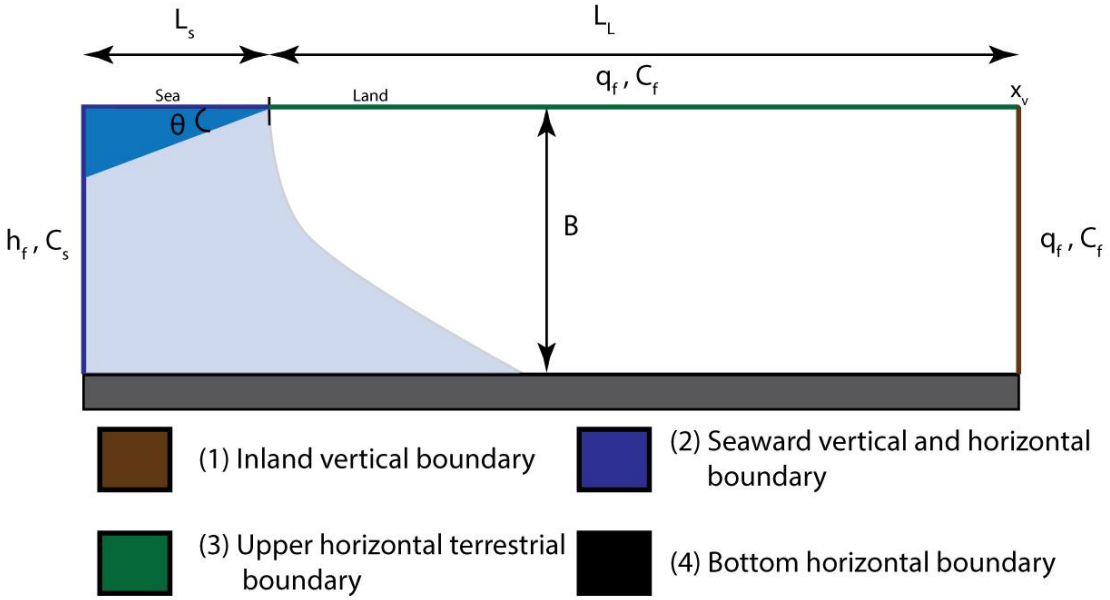

Figure 3.7: Conceptual model of a 2D cross section. θ is the slope of the seabed. B is the total thickness of the aquifer, q_f is the specific discharge, h_f is hydraulic head, C_s and C_f is the salt concentration of salt- and fresh water, respectively and L_s and L_L is the sea and land parts of the aquifer, respectively

3.3.2 Boundary conditions

The boundary conditions for the model include: (1) inland vertical boundary, (2) seaward vertical and horizontal boundary, (3) upper horizontal terrestrial boundary and (4) bottom horizontal boundary.

Table 3.3: Type and description of the boundary conditions used in the 2D-model.

Boundary Description	Boundary type	Description
Inland vertical boundary	Specific flow	Constant flux from groundwater flow. Constant concentration (0.35 kg/m^3)
Seawater	Specific head (constant head)	Constant head (0m) and constant concentration (35 kg m^{-3})
Top boundary (terrestrial)	Specific flow	Constant input from natural recharge
Bottom boundary (Basement)	Specific flow (no flow)	Impermeable basement

1. The inland vertical boundary simulates the general flow of groundwater towards the sea originated from inland recharge beyond the model domain.

$$C(x_v, z) = C_f, \qquad -B \leq z \leq 0 \quad (3.7)$$

$$Q_V(x_v, z) = q_f B, \qquad -B \leq z \leq 0 \quad (3.8)$$

where C_f is the salt concentration of terrestrial groundwater at any depth Z, at the distance X_v from the coastline, Q_V is the volumetric Darcy's flux [L^3 T^{-1} L^{-2}] and q_f is the uniform, specific discharge per unit length of boundary [L T^{-1}]. For this boundary, C_f represents the salt concentration often found in fresh water and is 0.35 g/L. The value of q_f is however problem dependent, and was calculated using field data and Darcy's equation:

$$q_f = \frac{Q}{A} = -K\frac{\Delta h}{l} \quad (3.9)$$

where Q is Darcy's flow, K is hydraulic conductivity, A is the area perpendicular to the flow direction and Δh is the difference in head between two observation and l is the distance between them.

2. The seabed boundary condition is defined along the left-most vertical column and parts of the upper horizontal boundary.

$$C(x, z) = C_s, \qquad -B \leq z \leq 0, -L_s \leq x \leq 0 \quad (3.10)$$

$$h_f(x, z) = 0, \qquad -B \leq z \leq 0, -L_s \leq x \leq 0 \quad (3.11)$$

were C_s is the salt concentration of saltwater defined as 35 g/L and h_f is the hydraulic head value, and L_s is the sea portion of the upper horizontal boundary. It represents the sea part where the groundwater discharges.

3. Upper horizontal terrestrial boundary defines the subaerial portion of the aquifer with constant recharge, simulating the recharge from precipitation, irrigation and the Guadalfeo River that recharges the aquifer. This was calculated using available information from previous numerical studies in the Motril-Salobreña aquifer.

$$Q_H(x, 0) = q_L L_L, \qquad 0 \leq x \leq L_L \quad (3.12)$$

$$C(x, 0) = C_f, \qquad 0 \leq x \leq L_L \quad (3.13)$$

where Q_H is the volumetric Darcy's flux [L^3 T^{-1} L^{-2}] and q_L is the uniform, specific discharge per unit length of border [L T^{-1}].

4. The bottom horizontal boundary symbolizes an impermeable aquifer basement.

$$Q(x, -B) = 0, \quad -L_s \leq x \leq L_L \qquad (3.14)$$

$$C(x, -B) = 0, \quad -L_s \leq x \leq L_L \qquad (3.15)$$

3.3.3 Base model

To have a reference point to compare the effect of the model parameters it was made a reference model. It is based on the conceptual model (Figure 3.10) and considered homogeneous with respect to hydrogeological parameters. To make it similar to reality parameters values used in the model are based on field data from the Motril-Salobreña aquifer and earlier studies in the area (Table 3.4).

Table 3.4: Initial aquifer and flow parameters used in the 2D model. (*)(Calvache et al., 2009), (**) (Duque et al., 2010)

Flow model parameters					
K_x (m/d)	K_y (m/d)	K_z (m/d)	S_y	S_s (m^{-1})	Θ
10*	10*	10*	0.20*	0.0018*	0.2**
Transport model parameters					
α_L (m)	α_{TH} (m)	α_{TV} (m)	D_m (m^2/d)	K_d (m^3/kg)	
30*	3*	3*	0.3*	$1*10^{-7}$*	

The slope of the seabed was defined with the average slope of the Motril-Salobreña prodelta with an average slope of 1.3^0 (Jabaloy-Sánchez et al., 2014).

The model has a total length of 2700 m in the x-direction, divided into L_S and L_L (Figure 3.10). The length of these sections was initially determined using a modified aspect ratio of L_L/B and L_S/B, as defined by Smith (2004), which states that the aspect ratio needs to be chosen high enough so that the position of the vertical model boundaries does not significantly influence the shape and location of the saltwater/freshwater interface. Since one of the objectives was to implement a dynamic coastline (see section 3.3.2.5) the length of L_L was increased to a ratio of 15. To compensate for the increased run time due to increased length of L_L, the length of L_S was decreased after trial simulations showed that an aspect ratio of 3 was adequate.

The finite-difference grid used in the models has one row, 270 columns and 30 layers, with cell dimensions 10x10x5 m in the x-, y- and z-plane, respectively. X-origin is at -500 m, so that the coastline is located at the 0 m and X_v is at 2200 meter.

3.3.4 Model parameters and sensitivity runs

Hydraulic conductivity and anisotropy

Hydraulic conductivity (K) is a measure of how easily a fluid can flow through the effective pores in a medium. For unconsolidated sediments hydraulic conductivity increases with grain size, and decrease with increased standard deviation of particle size (Fetter, 2001). This parameter is often very variable even inside the same geological unit because of variability in grain size material. The determination of the hydraulic conductivity from field methods depends on the method applied (e.g. slug test, pumping tests, laboratory analysis of sediment samples or geophysics logging), and different methods can give different results (Butler Jr, 2005). A detailed mapping of hydraulic conductivity in complex sedimentary deposits is difficult (Rehfeldt et al., 1992; Sudicky, 1986), and even a high number of field measurements can result in great uncertainty in the value applied for the groundwater flow simulation.

In the Motril-Salobreña aquifer hydraulic conductivity has been estimated through pumping tests to range between 35-210 m/d (Castillo, 1975), and further numerical studies have estimated horizontal hydraulic conductivity values ranging from 12 – 300 m/d (Calvache et al., 2009).

When hydraulic conductivity is different along the x,- y,- and z-axis in an aquifer, the aquifer is anisotropic. This is often a direct consequence of the natural deposition of sediments and the associated geological processes. In sedimentary aquifers this is especially related to multiple sedimentary structures that can generate a significant difference in the flow circulation. For example, bedding planes due to sediment deposition resulting in flow channels parallel to the bedding plane, thus generating higher hydraulic conductivity in the horizontal direction compared to the vertical (Bear and Cheng, 2010).

In the Motril-Salobreña aquifer there is no previous field studies about anisotropy. However, because of the different sedimentological environments it is natural to assume that different

areas exhibit different values of anisotropy. This has also been estimated in previous numerical models, where a horizontal and vertical anisotropy ratio (K_h/K_v) between 1 - 120 were applied (Calvache et al., 2009).

A sensitivity analysis of the effect of hydraulic conductivity and anisotropy was tested in two phases with the numerical model. First anisotropy was kept constant while a range of values for hydraulic conductivity was tested. Thereupon hydraulic conductivity was kept constant while different values of anisotropy were applied in the simulations.

Dispersion

Water flowing through a sand layer is forced to move around particles, resulting in a spreading of the concentration front in a process called dispersion (Appelo and Postma, 2005). For practical purposes, dispersion is considered as the sum of the two processes mechanical dispersion and diffusion (the migration of fluids particles from zones with high concentration to zones with lower concentration (Fetter, 2001)) (3.16).

$$D_x = \alpha_x v_x + D_e \qquad (3.16)$$

Where D_x is hydrodynamic dispersion in x-direction [L^2 T^{-1}], α_x is the longitudinal dispersivity [L], v_x is the linear groundwater velocity in x-direction [L T^1] and D_e is the coefficient of effective diffusion [L^2 T^{-1}]. However, diffusion does not play a significant role in the transport of solutes when groundwater velocities are high, and only becomes important when velocities are very low (Kresic, 2006).

When groundwater velocities are high (>50 m/yr), dispersion becomes a characteristic property of the porous medium denoted by the dispersivity (Appelo and Postma, 2005):

$$\alpha_x = \frac{D_x}{v} \qquad (3.17)$$

Dispersivity can be subdivided into longitudinal dispersivity (α_L), transversal dispersivity (α_T) and vertical dispersivity (α_v) (Kresic, 2006).

The general practice in modelling studies is to use horizontal transverse dispersivity one magnitude lower than longitudinal dispersivity, and vertical horizontal dispersivity 1 or 2 magnitudes lower than longitudinal dispersivity (Kresic, 2006).

Both field studies and numerical modelling studies have previously proven that dispersivity is important for the characteristics of the mixing zone of a saltwater intrusion. Shoemaker (2004) demonstrated through numerical modelling that increased dispersivity leads to more mixing between seawater and freshwater. As a consequence, the saltwater becomes less dense and flows toward the sea resulting in a broader vertical mixing zone and a less defined salt wedge toe. On the contrary, decreased dispersivity results in less seawater/freshwater mixing, a sharper defined salt water toe and allows the saltwater intrusion to reach further inland. Shoemaker (2004) stated that simulated salinities are more sensitive to transverse dispersivity (both horizontal and vertical) than to longitudinal dispersivities because groundwater flows mostly parallel to lines of equal solute concentration in the transition zone. Because dispersivity plays such an important role on the characteristics of the mixing zone, a thorough understanding of how the model reacts to different values is necessary.

There is no measured data available about the dispersion in the study area. However, Calvache et al. (2009) estimated through numerical modelling that values for longitudinal dispersivity ranges between 30 – 65 m and transversal and vertical dispersivity between 3 – 6.5 m. However, similar studies from other alluvial aquifers show dispersivity values as small as 1 m (Gelhar et al., 1992).

The effect of dispersivity on the groundwater system was tested in the same way as hydraulic conductivity and anisotropy. Different values of dispersivity were applied to the base model to see how it affected the geometry and location of the saltwater intrusion.

Recharge

Recharge is previously found to be the most important factor for determining the extent of the saltwater intrusion in coastal aquifers (Shoemaker, 2004; Hill, 1998). The primary source of recharge is from infiltration of surface water derived from precipitation. However, recharge can also be induced by anthropogenic effects, such as return from irrigation (Schmidt and Sherman, 1987) or artificial recharge (Bouwer, 2002). Factors influencing aquifer recharge are, amongst other: climate, land cover and land use, porosity and permeability of soil cover and geological and geomorphological characteristics (Kresic, 2006).

In the Motril-Salobreña aquifer the main contributors to recharge are irrigation return flow (especially during the summer months), the Guadalfeo River and the carbonate aquifer (Duque et al., 2011). To determine the recharge for the 2D-numerical model, it was delineated two recharge boundaries considering the previous sources of recharge (Figure 3.10). The horizontal terrestrial boundary represents the irrigation return flow, Guadalfeo River and recharge from precipitation over the model domain, while the vertical represents the general flow of groundwater towards the sea originated from inland recharge beyond the model domain (referred to as horizontal and vertical recharge boundary from now). Both have their origin in the surficial recharge, however they are different in respect to how the water infiltrates into the model domain (i.e. one infiltrates from the top and the other through a vertical section at the border) as well as their overall quantitative input.

In order to specify which type of infiltration (i.e. horizontal or vertical recharge) had more impact over the simulation, several tests using different ratio between the two was conducted, calculated as

$$Q^* = \frac{Q_V}{Q_H} \qquad (3.18)$$

where Q^* is the ratio between the vertical and horizontal inflow [dimensionless], Q_V is the total inflow from the vertical boundary (m^3/d) and Q_H is the total inflow from the horizontal boundary (m^3/d).

Also, the influence of the total inflow was tested to see how this influences the seawater intrusion.

$$Q_T = Q_H + Q_V \qquad (3.19)$$

where Q_T is the total inflow to the model (m^3/d).

Dynamic coastline

A coastline is the border between land and ocean and the region where interaction between land and sea processes occur. It is commonly the base level to which sediment is being transported too, and when they accumulate it leads to the progression of the coasline. The implications over hydrogeological studies is a boundary condition that defines where groundwater exits the system and where interaction between the dense saltwater and less

dense freshwater occur. As a consequence, changes to the coastline position could significantly influence the hydrogeological regime in an aquifer.

The rapid coastline progradation that the Motril-Salobreña aquifer has experienced could influence the present day hydrodynamic conditions in the area. The groundwater system could still be affected by the past hydrogeological conditions meaning that the present location of the saltwater wedge is not in equilibrium, or that some areas within the aquifer contains paleo water or connate water still undergoing a flushing process.

For the previous sensitivity analysis of model parameters it was assumed a static environment with a stationary coastline, which is often a valid assumption. However, to study the changes in the coastline over Motril-Salobreña aquifer, a dynamic coastline was implemented to study its impact on the saltwater-freshwater interface. Barring Delsman et al. (2014) who studied the salinity distribution in the Netherlands, not many studies of this type exists. The information regarding the general practice of how it should be accomplished and how it affects the modeling result are very scarce. It was therefore necessary to consider how to include a moving boundary condition and which parameters are important for the salinity distribution in this type of studies. Also, since this was a transient study, it was important to determine which parameters are most influential for the time it takes the groundwater system to achieve equilibrium with the new coastline position.

To implement a dynamic coastline the base model (Figure 3.7) was extended to include a prograding coast (Figure 3.8). This was done by dividing the simulation into one or more "time slices" (Delsman et al., 2014), where each time slice represents a shift in the aquifer geometry that modifies the model boundaries. For the prograding coast the aquifer geometry is changed between time slices by activating previous inactive cells and changing the location of cells containing the boundaries (Figure 3.9). That is, the model domain was extended with a distance by activing cells such as the extent corresponds to the advance of the coastline. By dividing the model into time slices, it was possible to change the aquifer geometry between each simulation and thereby modelling the historical evolution of an area.

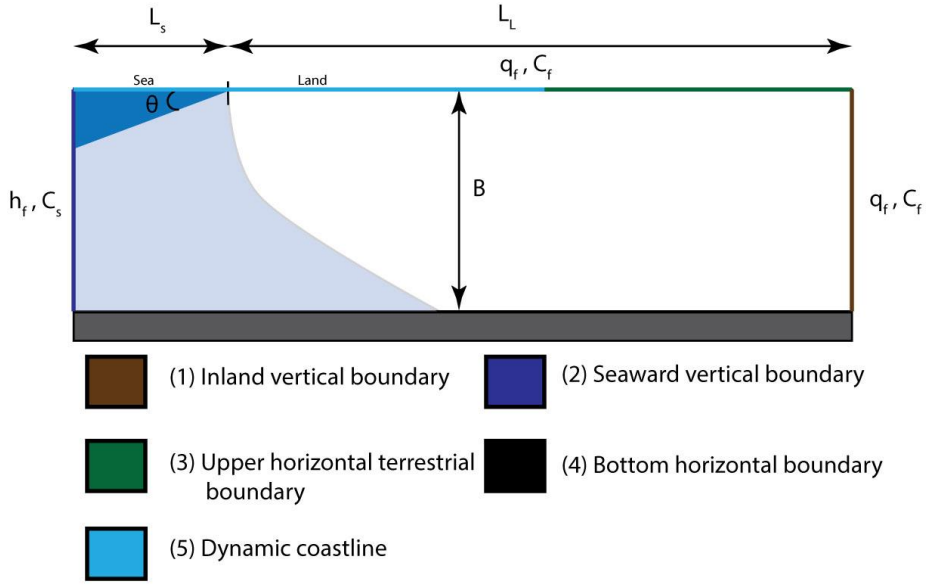

Figure 3.8: Expanded conceptual model of the reference model to include a dynamic coastline. The boundary conditions used along the (5) dynamic coastline boundary is different from one time slice to another.

The initial salt concentration and hydraulic head for the first time slice was determined by running the simulation until a steady state condition was achieved. Afterwards, the grey cells were activated and the boundaries were moved to the location of the new boundaries, marking a new time slice and thus simulating a prograding coast.

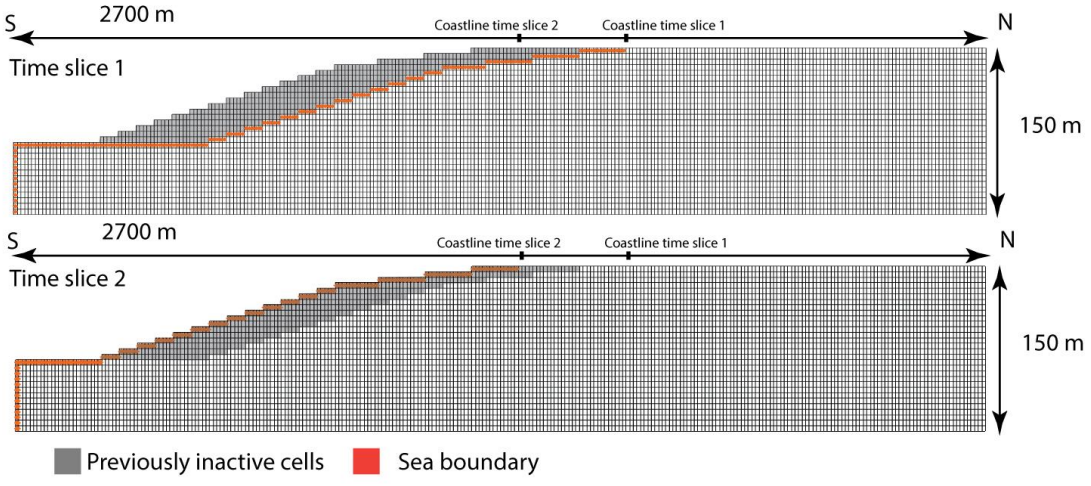

Figure 3.9: An example of the numerical grid used for two "time slices". The model domain is extended between the two time slices by activating previous inactive cells simulating a prograding coast.

The initial conditions for hydraulic head and salt concentration of each time slice (except for the first one) were determined by the results of the preceding time slice. As a consequence,

previously inactive cells had no initial value (since these were inactive in the previous time slice), and hence had to be determined in another way.

There are three different ways the salt concentration of the previously inactive cells can be determined: (1) salt water, (2) freshwater or (3) brackish water. Different geological scenarios could generate different salt concentration for the cells. For example, if the sedimentation rate is high so that clean ocean water is trapped inside sediments, the initial concentration in the cells would be added as saltwater. If this water is partially flushed or chemically altered, the result could be brackish or even clean freshwater, and hence the initial values would respectively be added as such. To see if there was a notable difference in the modeling results between the three scenarios, each case was tested in combination with a dynamic coastline.

A sensitivity analysis on the model parameters and their influence on this type of modeling were also accomplished. Since the assumption behind the motivation for this type of modelling is that the present salinity condition measured in an aquifer is only a transient moment in the evolution, and therefore not in equilibrium with current boundary conditions, it is especially important to determine which parameters have a major influence on the time that it takes for the hydrodynamic system to be in equilibrium with the new boundary conditions. If a simulation reaches equilibrium with the new boundary conditions within a time slice, all the previous time slices becomes irrelevant for future modeling, and the simulation could successfully have been started at that time.

The two parameters that were analyzed were total inflow and hydraulic conductivity as they highly influence the velocity of the water and the hydraulic gradient of the groundwater system. When analyzing the influence of the parameters it is important to consider the length and the amount of time steps used in the simulation (Reilly and Harbaugh, 2004). The amount of time steps needs to be high enough so that the development of the groundwater system can be explored in detail, and that any changes are captured. Therefore, it was used time steps small enough so that the simulations could be explored at the scale of tens of days. However, when the saltwater intrusion approached equilibrium changes in its location from one time step to another became increasingly smaller, so it was impossible to determine the exact time when the simulation reached equilibrium. Therefore it was determined to use ranges of one thousand days. Despite the relatively coarse resolution on the time frame, the

general trend of each parameter and its effect was considered to be captured satisfactory for the objectives of this test.

Sedimentological units

The sedimentological interpretation of the Motril-Salobreña (section 4.2.1) indicates that there are 3 sedimentological characteristics in the aquifer that can have an important effect over the groundwater system: (1) occurrence of sedimentological layers and thereby vertical changes in hydraulic conductivity resulting from a progressive delta, (2) changes inside the same geological unit due to presence of areas with different (hydro)geological properties, or (3) lateral changes in hydraulic conductivity because of changes in depositional environment.

The first sedimentological characteristic that was tested was vertical changes in hydraulic conductivity due to layers within the aquifer (Figure 3.10). Several simulations were conducted with different values of hydraulic conductivity in the different layers to evaluate the effect. For most of the simulations hydraulic conductivity was assumed to decrease with depth after what was interpreted from the Motril-Salobreña aquifer. Each scenario was quantitatively evaluated based on the distance the saltwater toe would penetrate inland.

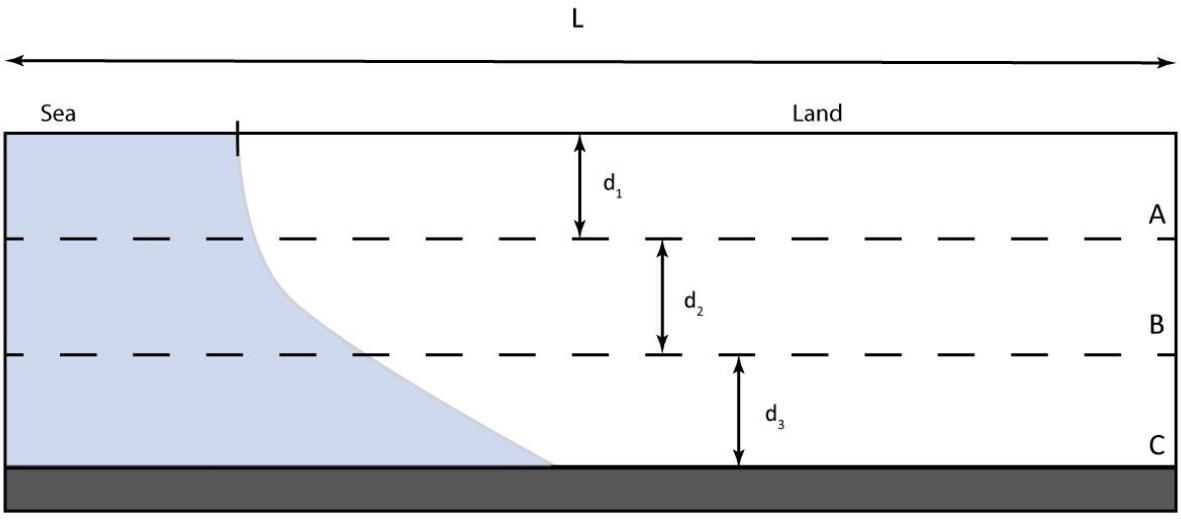

Figure 3.10: Conceptual model of the layered aquifer used to represent the vertical changes in hydraulic conductivity interpreted to be in the Motril-Salobreña aquifer.

The second sedimentological characteristic that was tested was the changes of hydraulic conductivity within a geological unit, or more specific a low permeable zone within a high permeable formation (Figure 3.11).

The presence of a low permeable formations within a geological unit has been detected in the Motril-Salobreña aquifer, and the possibility of connate saltwater within these units has been proposed. The assumption is that saltwater will be contained in the low permeable formation if the contrast between K_1 and K_2 is high enough. This was tested running several simulations with different values of K_1 and K_2, and calculating the residual concentration in the cells comprising K_2 after some time, in combination with a dynamic coastline. When the coastline was moved from A to B (Figure 3.11) the hydrodynamic system in the aquifer changed and thereby the saltwater-freshwater interface moved. The low permeable formation which initially was situated inside the saltwater would now be located within the freshwater region of the aquifer, and any saltwater trapped within the formation would experience freshwater flushing.

Another working hypothesis is what will happen when the low permeable areas are disconnected from the surrounding aquifer. In this care, diffusion becomes the dominant factor for flushing the salt from the formation. According to Kresic (2006), the effect of diffusion on the transport of solutes only becomes significant when the groundwater velocity is very low, and in this case the exchange of solute will happen mainly due to diffusion. The effective diffusion coefficient depends on the solute in question, but for major ions like Cl^- and Na^+ typical values found in nature varies between $1*10^{-9}$ and $2*10^{-9}$ m^2/d (Kresic, 2006). To test this, different simulations using variable values for diffusion were conducted and the residual concentration was calculated. If the cells are partially or fully disconnected from the surrounding aquifer, the residual concentration should increase with lower values of diffusion and hence decrease with higher values.

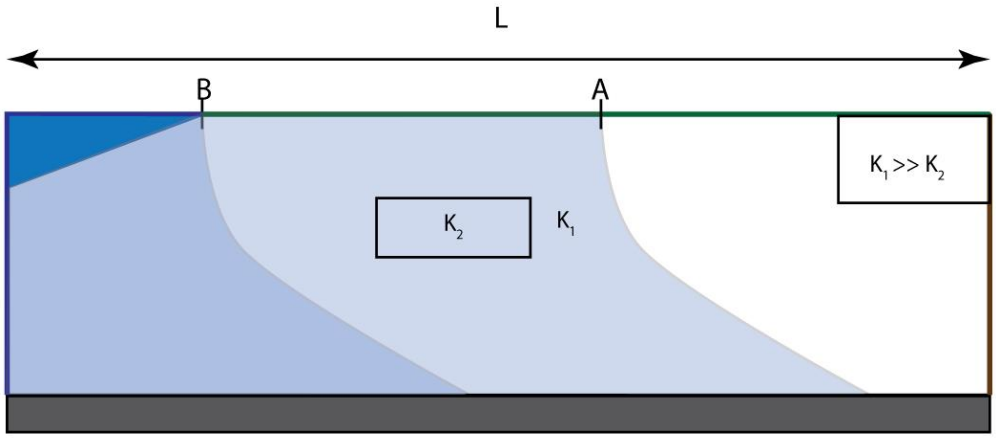

Figure 3.11: Conceptual model used to simulate the presence of low permeable layers within the aquifer. K_1 and K_2 denotes the hydraulic conductivity of the aquifer the low permeable formation respectively. Point A and B show the location of the coastline for time slice 1 and 2, respectively.

The last sedimentological characteristic that was tested is to the effect of the lateral changes in hydraulic conductivity found throughout the aquifer. Lateral changes within a unit can lead to heterogeneities that can influence the flow pattern within the aquifer and generate preferential flow paths. This can result in limited flow in certain areas of the aquifer and enhanced flow in other regions, and consequently affect the required time for the groundwater system to reach equilibrium or disconnect some areas from the surrounding aquifer.

The main type of lateral change that can be expected in the Motril-Salobreña aquifer is presented in a cross section of the aquifer in figure 3.12. The cross section is divided into 4 units with different hydraulic conductivity interpreted from the sedimentological model of the area. To implement the dynamic coastline two time slices were included. In time slice 1 the coastline was located at point A before being changed to point B for time slice 2.

In this simulation there are two objects of interest. The first is to evaluate how lateral changes in the aquifer influences the necessary time to reach equilibrium with the new boundary conditions when a dynamic coastline is included to the simulation. For this the procedure of adding a coastline presented in section 3.3.2.5 was applied. The second object to be explored was how heterogeneities affect the discharge of water through the aquifer, and if it could lead to preferential flow paths.

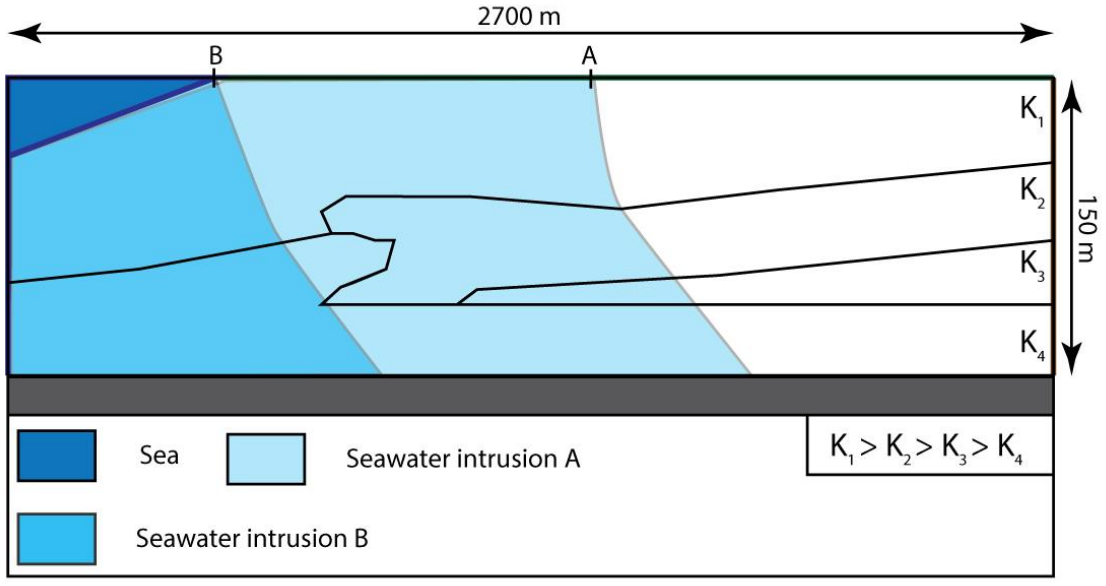

Figure 3.12: Conceptual model of the major lateral changes present in the Motril-Salobreña aquifer.

3.4 3D-model

3.4.1 Conceptual model of the Motril-Salobreña aquifer

The numerical 3D-model of the Motril-Salobreña aquifer is based one single unconfined aquifer composed of detrital sediments (Figure 3.13).

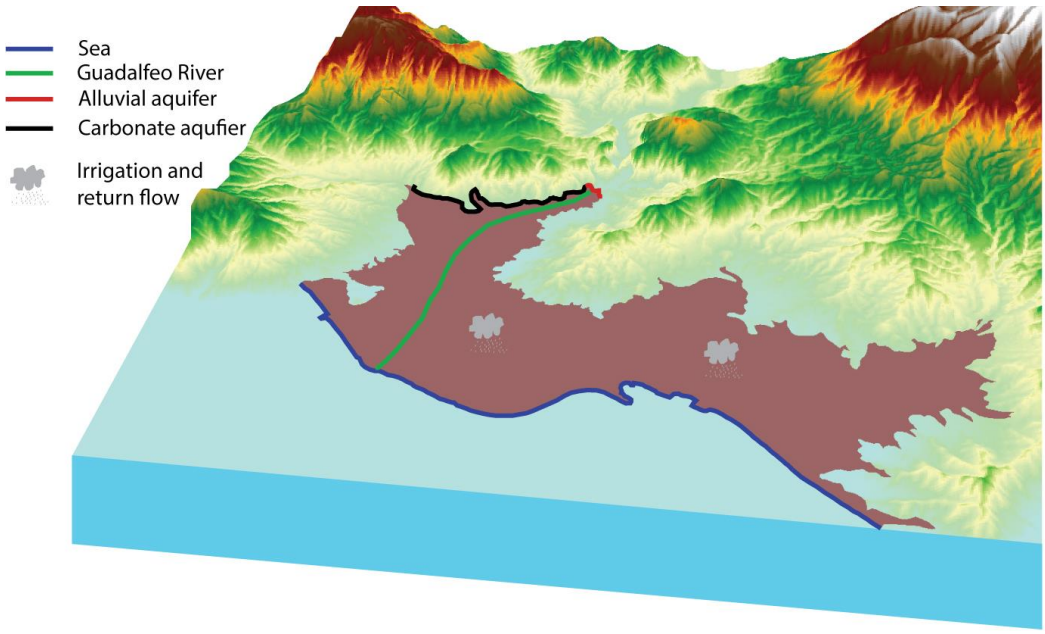

Figure 3.13: Conceptual model over the Motril-Salobreña aquifer.

The general flow pattern in the aquifer is towards the sea; which acts as the primary source of discharge from the aquifer besides well extraction and discharge to the Guadalfeo River (the latter only to a small degree). The recharge to the aquifer is derived from 4 primary sources: (1) the carbonate aquifer in the north-western parts, (2) the alluvial aquifer where the Guadalfeo River enters the aquifer, (3) the Guadalfeo River and (4) recharge from rain and irrigation return flow.

Earlier studies have estimated the aquifer's flow budget and listed the contribution of the different sources (Table 3.4).

Table 3.4: Estimated flow budget over the Motril-Salobreña aquifer estimated in previous studies. Modified from (Duque et al., 2011).

	Water budget for the Motril-Salobreña aquifer					
	(Heredia et al., 2003)		(Calvache et al., 2009)		(Duque, 2009)	
	Mm^3/year	%	Mm^3/year	%	Mm^3/year	%
Inputs						
Alluvial aquifer	3.5	9.8	4.7	13.8	5.9	25.3
Carbonate aquifer	4	11.1	4.2	12.3		
Guadalfeo River	11.6	32.3	11.6	24	4.8	20.6
Irrigation return flow and rain	16.8	46.8	13.6	39.9	12.6	54.1
Total	35.9	100	34.1	100	23.3	100
Outputs						
Sea	16.8	51.5	26.2	77.0	18.9	73.8
Pumping	15.4	47.3	7.5	22.1	6.6	25.8
Guadalfeo River	0.4	1.2	0.3	0.9	0.1	0.4
Total	32.6	100	34.0	100	25.6	100

3.4.2 Boundary conditions and initial values

It was defined a total of 7 boundary conditions in the model based on physical characteristics in the study area (Table 3.5).

1. The ocean boundary was defined as a constant head boundary with constant concentration along the border between the aquifer and the ocean.
2. The schist surrounding most of the aquifer was considered impermeable and thereby simulated with a no-flow boundary.
3. The carbonate aquifer to the north was defined as a Cauchy boundary with the groundwater flux dependent on the head gradient and the conductance between the two formations, calculated as:

$$C = \frac{kA}{L} \quad (3.20)$$

where C is conductance (m^2/d/m), k is the hydraulic conductivity (m/d), A is the gross cross-sectional area (m) and L is the flow length (m). From this the flow into the aquifer is calculated as

$$Q = C\Delta H \quad (3.21)$$

where Q is the flow into the aquifer (L^3/T) and ΔH is the head difference between the two aquifers. Head in the Motril-Salobreña aquifer is simulated from the model while head stage in the carbonate aquifer varies accordingly to the head stage measured in a well located within the aquifer.

4. In the north where the Guadalfeo River enters the aquifer is in contact with an alluvial aquifer. This contact was defined as a Dirichlet boundary with varying head. The head values were taken from a well in the alluvial aquifer just at the border between the two aquifers.
5. The Guadalfeo River was defined as a Cauchy boundary. It was simulated with the SFR2-packaged (Niswonger and Prudic, 2005), which allows for no flow in the river and thereby preventing the possibility of unlimited amount of recharge. The flow between the river and the aquifer is the product of the head gradient between the two and the riverbed conductance, calculated with equation (3.20). The flow in the river changes accordingly to monthly field data, and the river geometry was assumed to be constant along the river transect, being 20 meter wide and exhibiting a constant river bed thickness of 1 meter.
6. Groundwater extraction from wells in the study area was simulated with the well-package using field data from the area. There are 18 registered wells located at the aquifer, with pumping rates ranging between 0 and 8000 m^3/month.
7. Recharge to the aquifer from precipitation and irrigation return flow was combined and simulated with a specific flow boundary. The amount of water used for irrigation depends on the crop types in the area, which has been mapped by the University of Granada. The amount of precipitation was derived from surrounding meteorological stations in the vicinity of the aquifer. The volume of water reaching the aquifer was calculated based on irrigation supply, irrigation system in use and the percentage of estimated irrigation return (Calvache et al., 2009).

Initial conditions represent the starting boundaries (heads and concentration) at the beggining of the simulation, and can therefore be regarded as a boundary condition in time for the transient response of the groundwater model solution (Reilly and Harbaugh, 2004). Contrary to steady state simulations, the initial conditions in transient simulations influences the final solution.

Initial head values for the simulation were acquired from field measurements and interpolated to the remaining model domain. The initial head values correspond to the observed wells from the first stress period (November 2001). For the initial concentration values it was assumed that the system was in a steady state condition, hence the initial salt concentration were determined thereafter.

Table 3.5: Boundary conditions used in the numerical model of the Motril-Salobreñä aquifer.

Name	Boundary type	Description	Characteristic
(1) Sea	Dirichlet boundary	Ocean/aquifer boundary	Constant head and concentration (0 m 35 g/L)
(2) Impermeable schist	Neumann boundary	Surrounding impermeable schist	Constant flow (no flow)
(3) Carbonate aquifer	Cauchy boundary	Carbonate aquifer	Head dependent, constant concentration (35 g/L)
(4) Alluvial aquifer	Dirichlet boundary	Alluvial aquifer where Guadalfeo River enters	Constant head (varying between stress periods), constant concentration (35 g/L)
(5) Guadalfeo River	Cauchy boundary	Discharge from the Guadalfeo River	River stage varies accordingly to measured field data
(6) Wells	Neumann boundary	Extraction through pumping	Monthly withdrawal from wells according to field data
(7) Recharge	Neumann boundary	Irrigation and precipitation	Excess rainfall and irrigation return flow

3.4.3 Model geometry

The numerical grid used in the model consists of 16921 cells with 100x100 m dimensions in the horizontal plain, distributed over 10 layers (Figure 3.14). A high number of layers were chosen as variable-density groundwater models require a finer vertical resolution than constant density groundwater models to accurately calculate flow velocities (Langevin, 2003). The thickness of each cell is 20 meters, except for the cells in the top layer and the cells in contact with the basement.

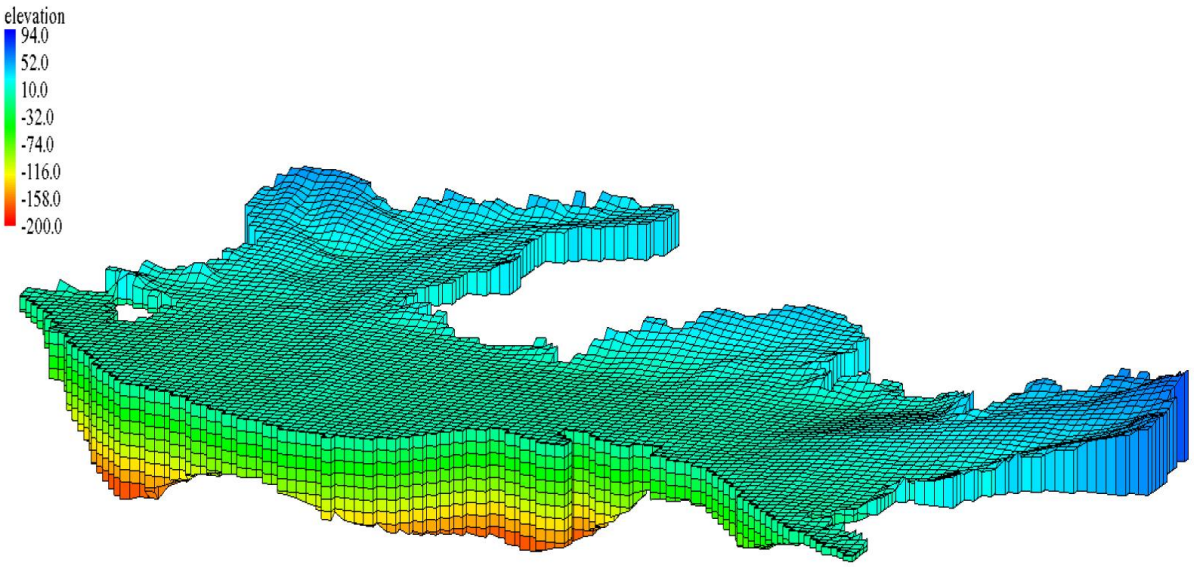

Figure 3.14: The numerical grid used in the 3D-numerical simulation of the Motril-Salobreña aquifer.

The top elevation of layer 1 corresponds to the topography in the area, and is thus spatial dependent. It was determined by a digital terrain map with a 5x5 m resolution. The basement of the aquifer was interpolated from geophysical points around the aquifer obtained through geophysical methods (Duque et al., 2008), together with pseudo points placed around the aquifer border to prevent interpolation artifacts in areas far away from information points. Kriging was chosen as the desired interpolation method as it's often an appropriate interpolation method for geological topics (Davis and Sampson, 1986), however it also yielded the most realistic basement geometry after comparing with the results from inverse distance weighting, natural neighbor and linear interpolation.

The pseudo points where placed around the borders of the aquifer to help acquire the desired basement geometry, which corresponds to: (1) reflects what looks like a realistic basement geometry (i.e. did not include any improbable geological features) and (2) a basement that is deep enough so that the aquifer thickness becomes appropriate for the numerical model. The second point proved to be especially challenging in the study area as the semi-arid climate and the small thickness of the aquifer at certain places would result in dry cells, and consequently preventing the model from converging. This was circumvented by making the basement of the aquifer to be one meter below sea level along the contact between the schist and the aquifer and thereby assuring for groundwater flow in the cells. Also, some areas in the northern parts of the aquifer where the topography was especially steep were removed from the model domain. The removed areas were small compared to the total size of the

model domain as well as constituting no important hydrogeological features. It was therefore considered to have no significant impact on the modeling result, or at least to not be very relevant for the coastal areas where this research has major focus.

3.4.4 Parameterization, model calibration and validation

The hydrogeological properties of the aquifer were determined by a first initial determination based on the hydrofacies and then inverse modeling for tuning the details about the properties in each of them. Inverse modeling is the process of gathering information (i.e. hydrogeological properties) about the model from the measurements that is being modeled (i.e. groundwater flow) (Carrera et al., 2005). For this the aquifer was divided into 6 zones after the defined hydrofacies units (Figure 3.15, see section 4.2.2 for explanation about the division). Thereafter, a possible range of hydraulic conductivity was assigned to each unit based on available field data and previous studies.

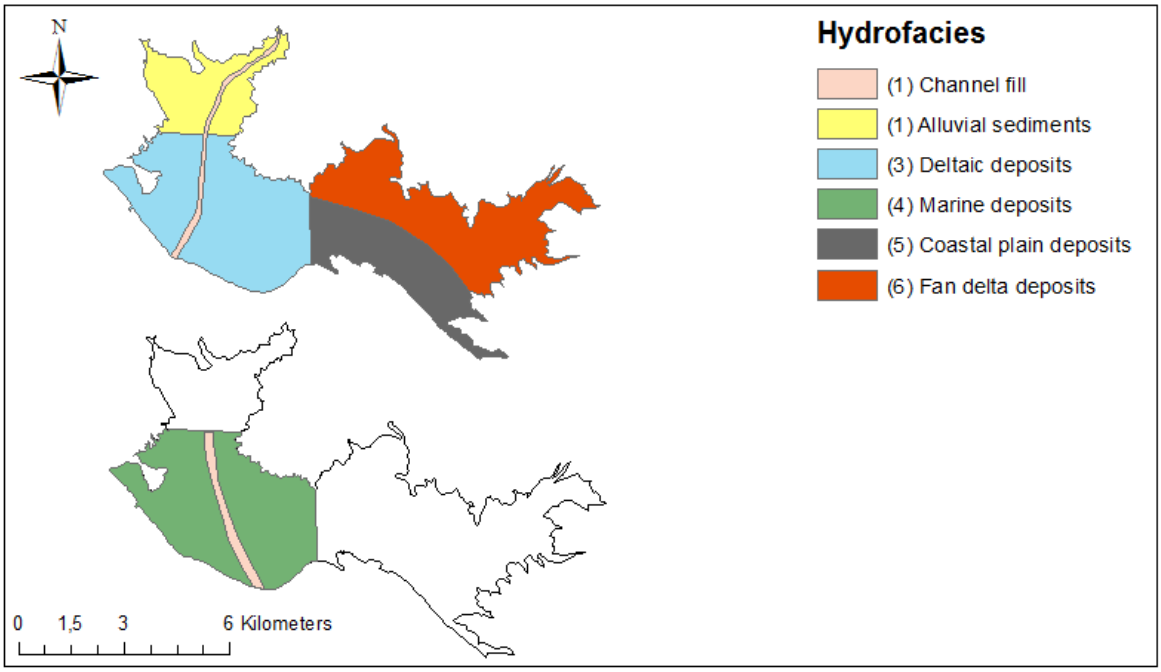

Figure 3.15: Delineation of hydrofacies. UP: distribution of the hydrofacies at the top of the aquifer; down: hydrofacies at 100 m depth.

Model calibration was carried out using a trial and error technique by matching measured groundwater head observations from the study area with the estimated values from the model, as well as comparing the computed flow budget of the aquifer with that from previous studies (Table 3.4). To quantify the model calibration is was used the mean error (ME), mean

absolute error (MAE) and root mean squared error (RMSE) to achieve the best possible result between observed and measured head values (Anderson et al., 2015).

$$ME = \frac{1}{n}\sum_{i=1}^{n}(h_m - h_s)_i \qquad (3.22)$$

$$MAE = \frac{1}{n}\sum_{i=1}^{n}|(h_m - h_s)|_i \qquad (3.23)$$

$$RMSE = \left[\frac{1}{n}\sum_{i=1}^{n}(h_m - h_s)_i^n\right]^{0.5} \qquad (3.24)$$

where n is the number of targets, h_m is measured head (m) and h_s is simulated head (m).

The hydraulic conductivity of the riverbed material and the conductance of the carbonate aquifer boundary were estimated using automated parameter estimation (PEST). PEST uses an inverse modeling process to minimize the difference between field observations and model simulation by using an algorithm to determine the optimal set of parameter values (Poeter and hill, 1997) However, the range of possible values for both were constrained such that their contribution to the total recharge of the aquifer would be in the same order of magnitude as that of earlier research.

The hydraulic conductivity distribution for each hydrofacies was estimated using PEST with pilot points. Pilot points estimates the hydraulic conductivity at discrete locations throughout the model domain by spatial interpolation (Anderson et al., 2015). In the calibration process each hydrofacies was given a unique set of pilot points to determine the hydraulic conductivity distribution within, and each set of pilot points were constrained to only affect the distribution within that unit. That is, the pilot points within hydrofacies 2 (alluvial sediments) would only influence the hydraulic conductivity in that unit, and would not influence the distribution within unit 3 (deltaic deposits). In this way, prior estimates of hydraulic conductivity could be used to constrain the possible values for estimated hydraulic conductivity within each unit. When determining where to place the pilot points it was followed the guidelines by Doherty and Hunt (2010) for irregular pilot point distribution. It was used a total of 44 pilot points divided over the aquifer, with the highest density of pilot points found in unit 3 where the majority of the lithological columns are situated (Figure 3.16).

Values for specific storage, specific yield and the ratio of horizontal and vertical hydraulic conductivity anisotropy were determined for each hydrofacies unit as a constant value. There are no prior information about horizontal and vertical anisotropy in the aquifer, while specific yield and specific storage has previously only been estimated through model calibration. In GMS horizontal anisotropy is calculated as the ratio of the flow along the Y-axis to the X-axis in GMS. For zone 5 and 6, where the main direction of the flow is along both axis depending location, horizontal anisotropy was assumed to be 1.

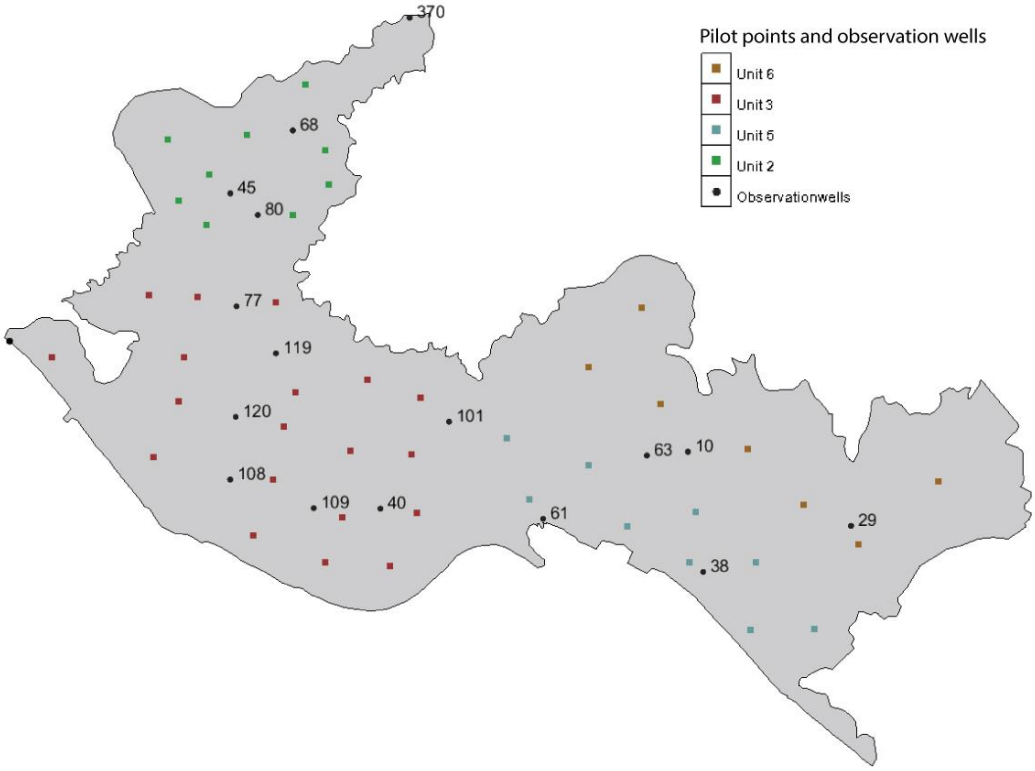

Figure 3.16: Pilot points and observation wells

The model was calibrated for the time period 01.11.2001 – 01.11.2004. The calibrated model was validated using the data from the period 01.11.2004 – 01.11.2007.

3.5 Paleo-hydrogeological model of the Motril-Salobreña aquifer

The effect of the changes in the location of the coastline was tested with the constructed model of the Motril-Salobreña aquifer. For this the model domain and the boundary

conditions were modified corresponding to the changes in coastline position at different time periods. This method is a simplification of reality since the coastline is not changing its location in one single motion, but rather in a more gradual process. However, this is the first time that this type of model has been implemented in Motril-Salobreña aquifer and it represents a new perspective that can be explored with more details in future studies.

For the paleo-hydrogeological model of the Motril-Salobreña aquifer it was used 2 successive time slices. Each time slice corresponds to changes in the location of the coastline motivated by the historical reconstruction of the coastline (Jabaloy-Sánchez et al., 2014) (Figure 2.3). The start of the simulation corresponds to the location at 4000 BC, marking the first known reference point of the coastline. The first time slice corresponds to the change in coastline position from 4000 BC to 1500 AD and time slice 2 corresponds to the change from 1500 AD to 2007 AD.

Table 3.6: Description of the time slices used in the paleo-hydrogeological model.

Time slice	Description
4000 BC – 1500 AD	Mean coastline advance 0.09 – 0.15 m/year. Constant values of recharge.
1500 AD – 2007 AD	Mean coastline advande 3.3 m/year. Constant recharge for 1500 AD – 2001 AD, varieng values from 2001 – 2007.

The model was constructed according to the model described in section (3.3.3), except for the location of the coastline which was dynamic. Hydraulic properties was determined after the best set of parameter values obtained in calibration process (see section 4.2.3). For the period 4000 BC – 2001 AD, it was used the average values from 2001-2007 for river flow, recharge from precipitation and the head values used for the alluvial and the carbonate aquifer. For the last 7 years of time slice two (2001-2007) it was used the complete dataset obtained from field measurements.

Transport parameters were initially assigned based on the values applied by Calvache et al. (2009), which calibrated the parameters by matching the saline wedge with that from 7 observations points in the aquifer. For the diffusion coefficient it was used a value of $1*10^{-9}$ m^2/s which corresponds to the diffusion coefficient of Cl^- and Na^+, the dominating ions in seawater.

Table 3.16: Transport parameters used in the paleo-hydrogeological model.

Transport model parameters					
Unit	α_L (m)	α_{TH} (m)	α_{TV} (m)	D_m (m^2/d)	K_d (m^3/kg)
1,2,3,4	30*	3*	3*	$1*10^{-4}$	$1*10^{-7}$*
5-6	65*	6.5*	6.5*	$1*10^{-4}$	$1*10^{-7}$*

* Values from (Calvache et al., 2009)

To evaluate the effect of the paleo-hydrogeological model the simulation was compared to the steady state salinity distribution obtained in the 3D numerical model of the Motril-Salobreña aquifer. This allows for a detailed comparison of the salinity evolution, and to examine the effect of the geological environment in the aquifer over the salinity distribution. To carry out this analysis it is needed to consider the time that it takes for the aquifer to reach equilibrium (if it is reached). This will allow for a study of the impact of the changes in the coastline position over the current salinity distribution, or provide some insight about the recovery capacity of the aquifer for flushing future saltwater intrusion events.

4 Results

4.1 Grain size distribution

The grain size distribution has been used to provide estimates for hydraulic conductivity in the different hydrogeological units (Table 4.1).

Table 4.1: K values from grain size distribution. Locations with a bracket containing a number indicate the depth at which the sample is taken.

Location	d_{10}	Hydraulic conductivity (m/d)				Porosity	$C_u(d_{60}/d_{10})$
		Hazen	Slichter	Beyer	Zamarin		
UP	0.089	-	-	7.4	-	0.38	3.83
MIDDLE	0.071	-	-	5.3	-	0.42	2.27
DOWN	0.086	-	-	7.3	-	0.40	3.01
PALEO	0.172	30.2	8.7	26.6	48	0.36	4.88
EAST	0.114	15.4	5.0	12.5	-	0.39	3.37
DIS(39)*	0.095	-	0.75	3.5	-	0.26	67.4
DIS(72)*	1.03	-	233.46	918.58	-	0.343	5.7
DIS(87)*	1.03	-	1.01	5.84	-	0.255	41.36
DIS(102)*	0.11	-	0.94	5.18	-	0.255	46.23
DIS(132)*	2.6	6987	2308	6557	-	0.392	3.35
DIS(153)*		-	-	0.00151	-		
DIS(167)*		-	-	0.00167	-		
DIS(207)*		-	-	0.00039	-		
DIS(237)*		-	-	0.00117	-		
INT(22)*	1.1	-	262	1044	-	0.341	5.82
INT(45)*	0.6	-	60.8	291	-	0.316	7.67
INT(62)*	0.095	-	0.86	5.93	-	0.266	16.84
INT(76)	0.095	-	0.89	5.56	-	0.260	20.84
REC(19)*	0.61	-	54	288	-	0.302	9.03
REC(30)*	1.83	3287	1035	3161	764	0.38	3.83
REC(44)*	0.4	-	28.4	131	-	0.321	7.25
REC(58)*	1.1	-	2.93	18.4	-	0.281	12.25

* Samples are provided by the University of Granda

The samples of UP, MIDDLE, DOWN, PALEO and EAST differs from the other three sample locations as they provide a range of depth at which they are taken, contrary to the other samples where hydraulic conductivity is estimated at specific depths. For these 5 samples hydraulic conductivity values are in the same order of magnitude. The lowest values are found along a line of UP, MIDDLE and DOWN, with values ranging from 5.3 – 7.4 m/d. The highest values are found at PALEO with 26.6 m/d, and EAST have a value between the two, with 12.5 m/d (estimated with the Byer method).

INT, REC and DIS provides a more detailed value of hydraulic conductivity, and consequently values change between 3 orders of magnitude within the same borehole. The highest value is found at DIS(132) where a value of 6557 m/d is estimated, corresponding to gravel or clean sand. The lowest value estimated, 3.6 m/d, corresponds to clean or silty sand (Freeze and Cherry, 1979).

4.2 Sedimentological model and hydrofacies

4.2.1 Sedimentological model

The Motril-Salobreña aquifer was interpreted to constitute of 7 major lithofacies (Table 4.2), with the majority of the lithological columns located along the Guadalfeo River.

Table 4.2: Lithofacies interpreted to constitute the Motril-Salobreña aquifer.

Facies	Sediment composition	Depositional environment
1	Gravel/sand with some silt	Deltaic
2	Silt, sand and gravel	Estuary
3	Clay/silt with some gravel/sand	Marine
4	Gravel with some sand	Channel fill
5	Gravel/sand	Fan delta
6	Silt/sand with some gravel	Coastal plain
7	Gravel/sand with occurrence of silt	Alluvial

In the deltaic area, the deepest parts of the aquifer are dominated by clay and silt with some gravel (lithofacies 3, marine; Figure 4.1). The high portion of fine grained material indicates a low energy depositional environment, and hereby the sediments are considered as a product of marine deposits or sediments deposited at a distance from the feeder system (the

Guadalfeo River). The gravel present in this facies is considered to result from periods of higher sediment transport or debris flows connected to the occurrence of alluvial fans. Above the bottom marine deposits the sedimentological structure becomes more complicated, with increased lateral changes in sediment composition. Lithofacies 2 (estuary) consists of finer grained sediments, mainly silt and sand, but the occurrence of gravel is not uncommon. This lithofacies can possibly be connected to the early stages of an estuary environment described by Jabaloy-Sánchez et al. (2014) which were the dominant depositional system around 4000 – 2000 BC. Then, going basinward the material becomes coarser (lithofacies 4, channel fill). This lithofacies contains very coarse grained material, mainly gravel with some sand. It is not perfectly clear what the source for the gravel in this lithofacies is, as it contradicts with what would be expect (upward coarsening due to prograding delta). A possible explanation is that it is connected to increased sediment yield in the catchment and the alluvial fans. Another explanation, and maybe more likely, is that it could be channel fill of an old paleo channel of the Guadalfeo River. Then, constituting the upper part of the western area is lithofacies 1 (deltaic). The section of the boreholes located in this lithofacies all show an upward coarsening sequence, going from mostly gravel and silt to gravel and sand. This indicates a Gilbert-delta with bottomsets, foresets and topsets that have progressed basinward.

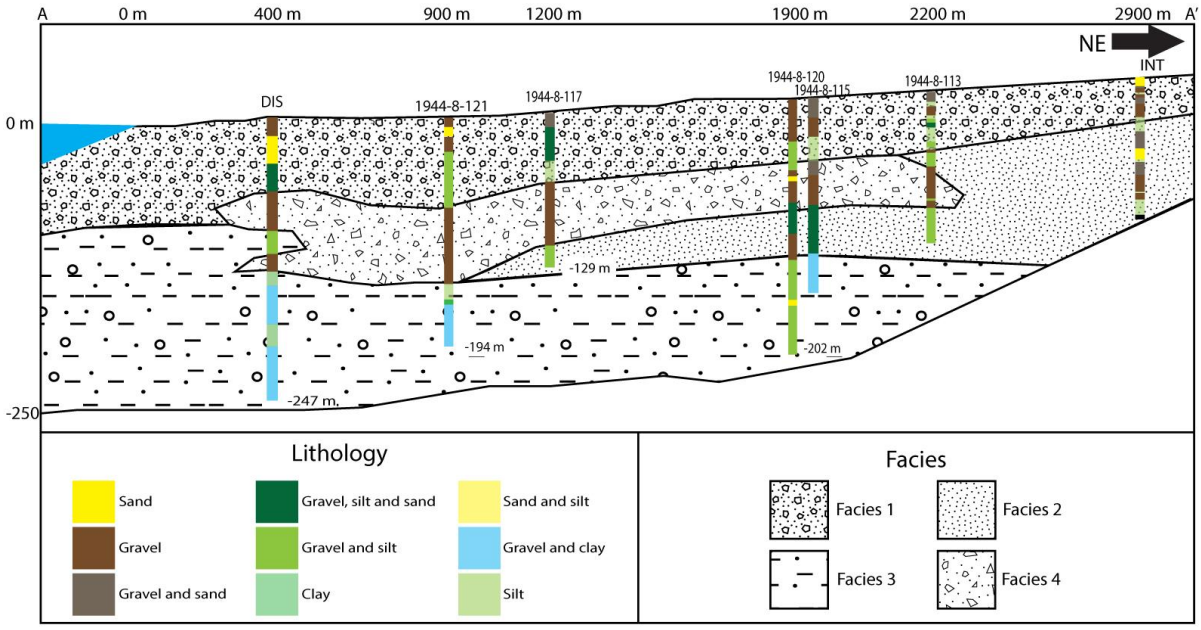

Figure 4.1: The interpretation of the sedimentological model of the western delta area along cross section A.

The eastern area is represented in two cross sections, with lithological columns that indicate that the area consist of two lithofacies (Figure 4.2). Close to the mountain the dominant

sediment types are sand and gravel, resulting from the sediment deposition from alluvial fans (lithofacies 5, fan delta). Then, as the aquifer progressed basinward and the river gradient decreased the depositional environment changed and became more influenced by marine and low energy depositional processes marking lithofacies 6 (coastal plain). Consequently, sediments are finer grained with higher amounts of silts compared to lithofacies 5 which is mostly dominated by sand and gravel. As a consequence the area is divided into two geological formations depending on lithology.

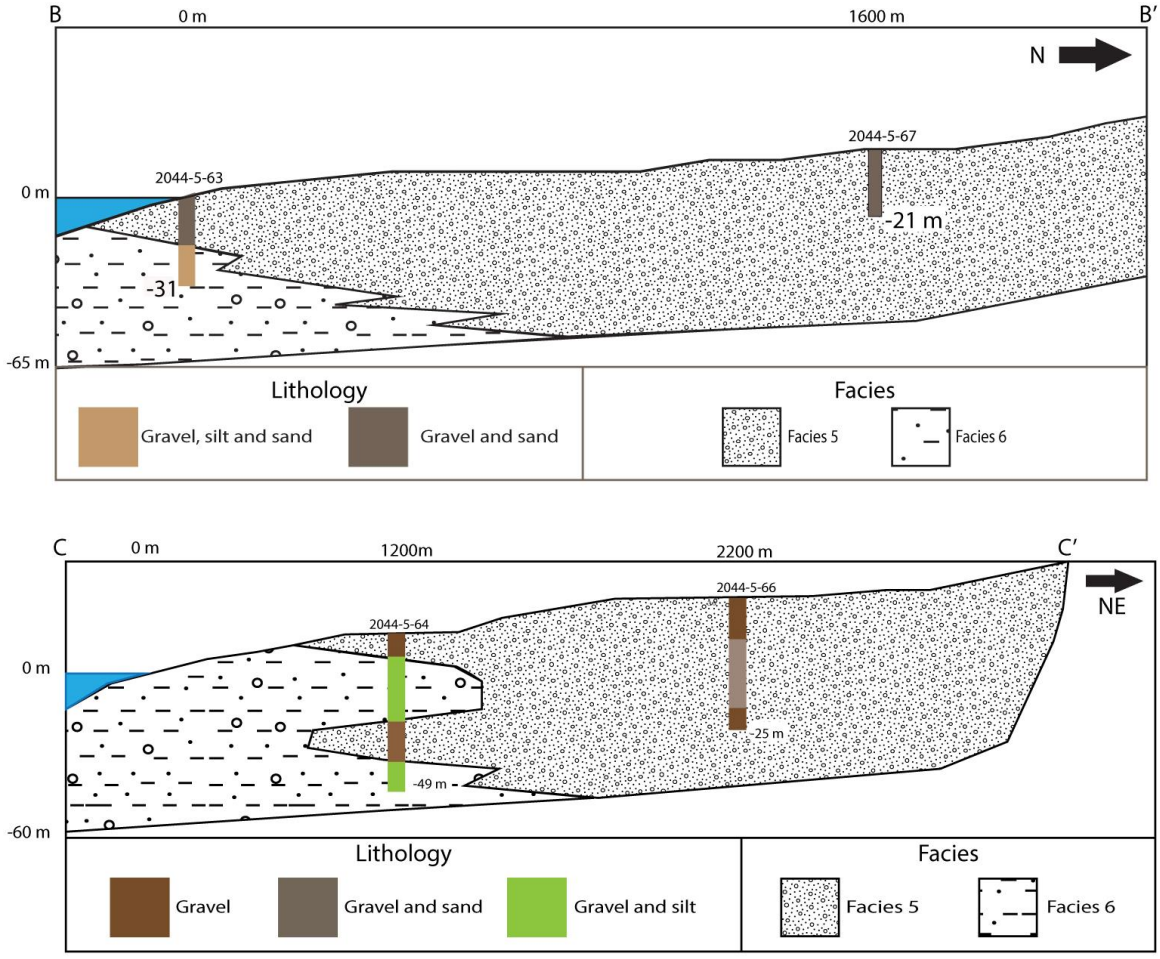

Figure 4.2: Interpreted sedimentological model of the eastern area of the Motril-Salobreña aquiferbased on the boreholes information.

The area north of the delta is interpreted to be an alluvial depositional system (lithofacies 7, alluvial). Sedimentation is derived from fluvial depositional processes, and hereby sediment facies consists of a combination of channel fill, point bars and floodplain deposits. This can be detected in the lithological columns, where layers of silt, gravel and sand are intermixing. However, noted by Galloway and Hobday (2012), outcrop analysis or closely spaced well or core data is necessary for a detailed mapping of fluvial facies. Hence, a detailed model of this facies was not possible. However, the boreholes indicate that the amount of coarse grained

material is higher compared to the other two areas of the aquifer, and that the silts found in the area are mainly connected to the occurrence of silt lenses.

4.2.2 Hydrofacies

The following 6 hydrofacies units were interpreted to constitute the Motril-Salobreña aquifer.

Table 4.3: Description of the different hydrofacies in the Motril-Salobreña aquifer and hydraulic conducitivity properties based on field data /table 4.1) and values obtained by Calvache et al. (2009).

Unit	Description	K (m/d)
1	Channel fill	200 – 900
2	Alluvial sediments	45 - 300
3	Deltaic deposits	3 – 27
4	Marine deposits	0.0001 – 12
5	Coastal plain deposits	5 – 50
6	Fan delta deposits	20 – 50

- Unit 1 consists of fluvial sediments with high permeability deposited within the current- and paleo channel of the Guadalfeo River. This unit shows the highest hydraulic conductivity of all the units. Estimation from numerical modeling indicates a value of 300 m/d (Calvache et al., 2009), while the grain size distribution indicates values of over 900 m/d.
- Unit 2 represents the alluvial deposition in the northern parts of the aquifer. The main sediment types are gravel with silt and sand, and because of the fluvial domain in this part this unit is considered to have internal heterogeneities resulting from the deposition of floodplains, channel fill and point bars. This hydrofacies unit is assumed to contain the second highest hydraulic conductivity out of all the units with values ranging between 45– 300 m/d.
- Unit 3 comprises the shallow sediments in the western deltaic area described in the forgone section, namely lithofacies 1, 2 and 4. It is assumed to reach 140 meters below sea level. Because of the diverse depositional processes and hereby a complex sedimentary structure, this unit has high internal heterogeneity in the form of intermixing layers and zones of silt, clay and gravel. However, the complex sedimentary structure makes a more detailed delineation of the unit difficult, despite

the relatively detailed interpretation of the unit in the sedimentological model. Further delineation of hydraulic properties is considered to be best done through stochastic simulations. Hydraulic conductivity for the unit ranges from 3 – 27 m/d.

- Unit 4 represents the marine sediments deposited in the deepest parts of the western delta area. It lies underneath unit 3 and goes all the way down to the basement, so the thickness of the unit depends on the total depth of the aquifer. It consists of mainly finer grained sediments with a high portion of clay, and thereby it is assumed to contain the lowest hydraulic conductivity of all the units, ranging between 0.0001 – 12 m/d. Based on the relatively uniform lithology observed in the lithological columns the internal heterogeneity in this unit is considered limited compared to that found in unit 3, despite the occurrence of sand and gravel lenses.
- Unit 5 represents the coastal plain sediments deposited in the most seaward parts of the eastern area (Figure 4.3). The depositional processes that have dominated in this area are mainly transport of finer sediments by longshore current from the Guadalfeo River and deposition of coarser grained sediments by the local Ramblas. As a consequence, this unit contains a wide mix of sediments sizes and thereby a relative low hydraulic conductivity compared to the other units, with values ranging between 5 – 50 m/d.
- Unit 6 is composed by alluvial sediments deposited within the fan delta in the eastern area, between unit 5 and the aquifer border (Figure 4.3). Sediments are deposited mainly by alluvial fans, and are thereby relatively coarse grained ranging mainly from sand to gravel with corresponding high values of hydraulic conductivity, with values between 20 – 50 m/d.

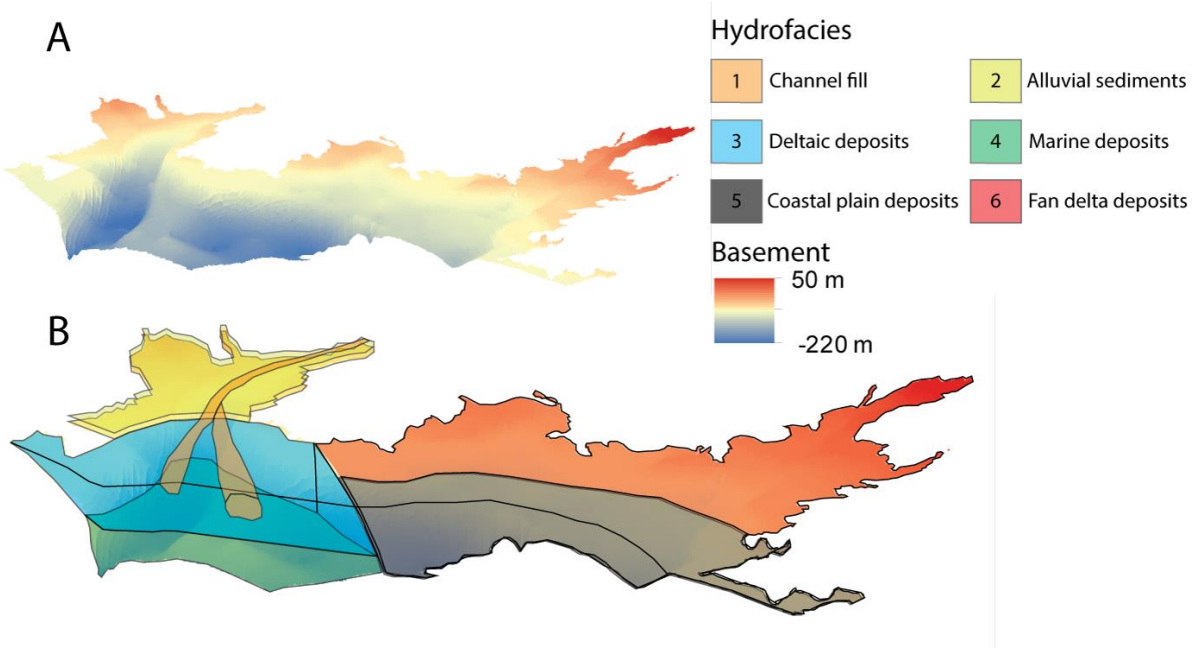

Figure 4.3: (A) Basement of the aquifer interpolated with kriging and (B) delineation of hydrofacies within the Motril-Salobreña aquifer based on the sedimentological models. Vertical exaggeration 5:1.

4.3 2D-model

4.3.1 Effect of hydraulic conductivity

Hydraulic conductivity values of 5, 10, 20 and 40 m/d were tested to evaluate the effect that hydraulic conductivity has on saltwater intrusions. These values were chosen as it is a mean value of what could be expected in the study area; despite the occurrence of some areas exhibiting higher or lower values.

Table 4.4: The values of hydraulic conductivity tested and the distance the saltwater toe penetrated inland.

K (m/d)	5	10	20	40	50
Distance (m)	200	440	800	1350	1580

The general trend in the simulations was that when hydraulic conductivity was increased the saltwater toe would penetrate further inland (Figure 4.4, Table 4.4), which was true for all values of hydraulic conductivity that was tested. Changing hydraulic conductivity from 5 to 50 m/d, which were the lowest and highest values applied, resulted in a difference in penetration distance of the seawater intrusion of 1380 m. The increase in penetration distance was not changing linearly between different values of hydraulic conductivity. In the conducted simulations, the increase in penetration distance was gradually decreasing for higher values of hydraulic conductivity (Figure 4.4, right). That is, when hydraulic

conductivity was increased from 10 to 20 the toe would penetrate 360 m further inland compared to 230 m when hydraulic conductivity was changed from 40 to 50 m/d.

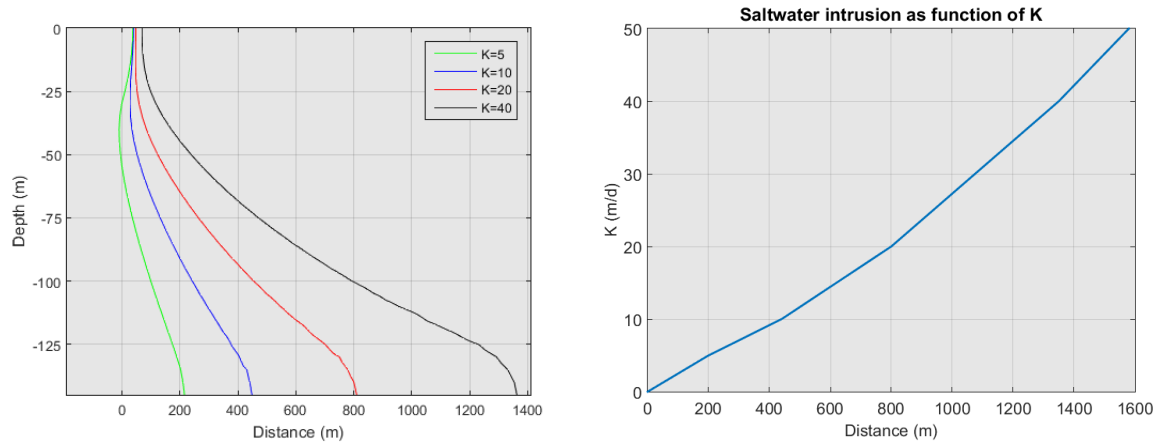

Figure 4.4: (Left) Location and shape of the interface with different values of hydraulic conductivity, the distance for the penetration depth is measured at the 15 g/L isoline. (Right) distance of saltwater wedge toe measured at the 15 g/L isoline for increasing values of K.

The ratios for vertical anisotropy that were tested range between 1 and 120 after the values estimated by Calvache et al. (2009) (Table 4.5). All ratios were tested with two constant values of hydraulic conductivity.

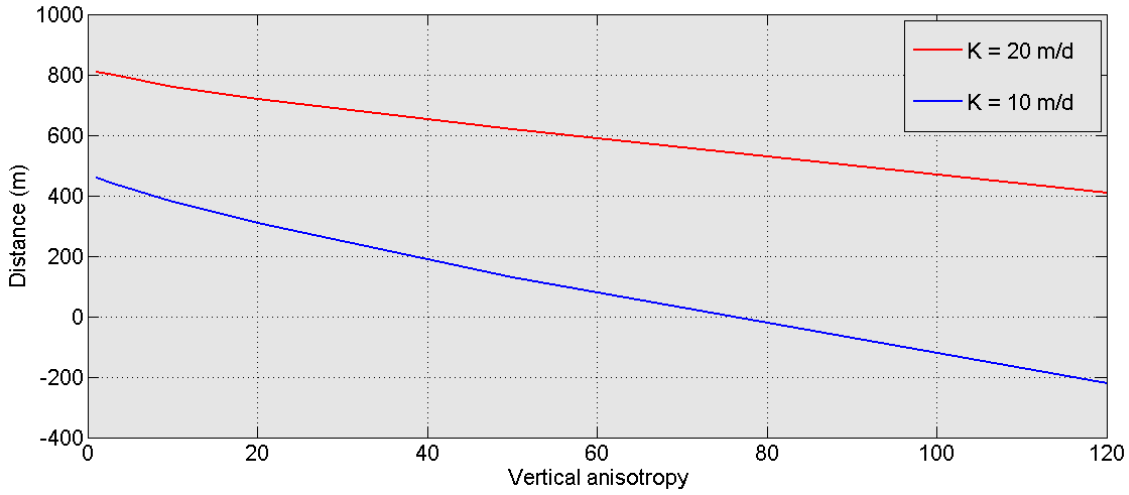

Figure 4.5: The distance the saltwater toe penetrated inland using different values of vertical hydraulic anisotropy. The distance for the penetration depth is measured at the 15 g/L isoline.

In all of the simulations the saltwater toe penetrated less inland when the anisotropy was increased (Figure 4.5). For example, between case 2 and 6 when hydraulic conductivity was 10 m/d and anisotropy was increased from 1 to 120, the location of the saltwater toe changed from 460 m inland to 220 outside the coast, a difference of 680 m. For case 8 and 12 where hydraulic conductivity was 20 m/d, the penetration distance changed less with a similar increase in anisotropy, resulting in a decreased penetration distance of 390 m (Figure 4.5).

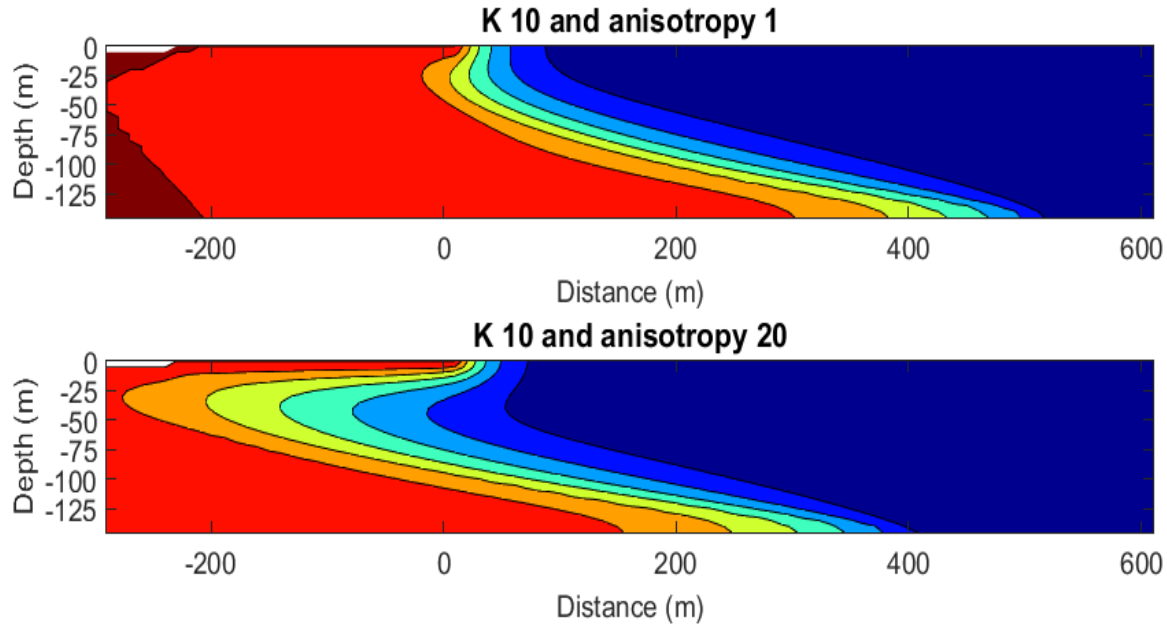

Figure 4.6: Shape of the mixing zone using two different values of vertical anisotropy.

Table 4.5: Cases of different ratios for anisotropy tested with the numerical model. Distance is the distance from the coast to the saltwater wedge toe. The distance for the penetration depth is measured at the 15 g/L isoline.

Case	K (m/d)	Anisotropy	Distance (m)
1	10	3	440
2	10	1	460
3	10	10	380
4	10	20	310
5	10	50	130
6	10	120	-220
7	20	3	800
8	20	1	810
9	20	10	760
10	20	20	720
11	20	50	620
12	20	120	410

Besides the change in location of the toe, the shape and geometry of the saltwater wedge would also change drastically, becoming more stretched in the horizontal direction when anisotropy was increased (Figure 4.6). This was especially observed in the shallower parts (at

around 30-40 m depth), where the thickness of the mixing zone was increased to over 200 m compared to around 80 m when anisotropy was changed from 1 to 10.

4.3.2 Effect of dispersion

The values for longitudinal dispersivity that were tested range between 5 - 65 m, as well as ratios of vertical transverse dispersivity to longitudinal dispersivity between 0.01 and 0.1 (Table 4.6).

Dispersion had a greater effect in the deeper parts of the aquifer where the saltwater toe would penetrate further inland when longitudinal dispersivity was reduced (Figure 4.7). When longitudinal dispersion was 65 m the saltwater toe penetrated 330 m inland, compared to 620 m when longitudinal dispersion was reduced to 5 m. For both α_V/α_L of 0.1 and 0.01 the increased penetration distance of the saltwater toe was changing nolinearly as higher values of longitudinal dispersion was applied. That is, the increased penetration between longitudinal dispersivity of 10 and 20 (case 3 and 4) m was 80 m, compared to 40 meters when longitudinal dispersivity was changed from 30 to 40 m (case 1 and 5).

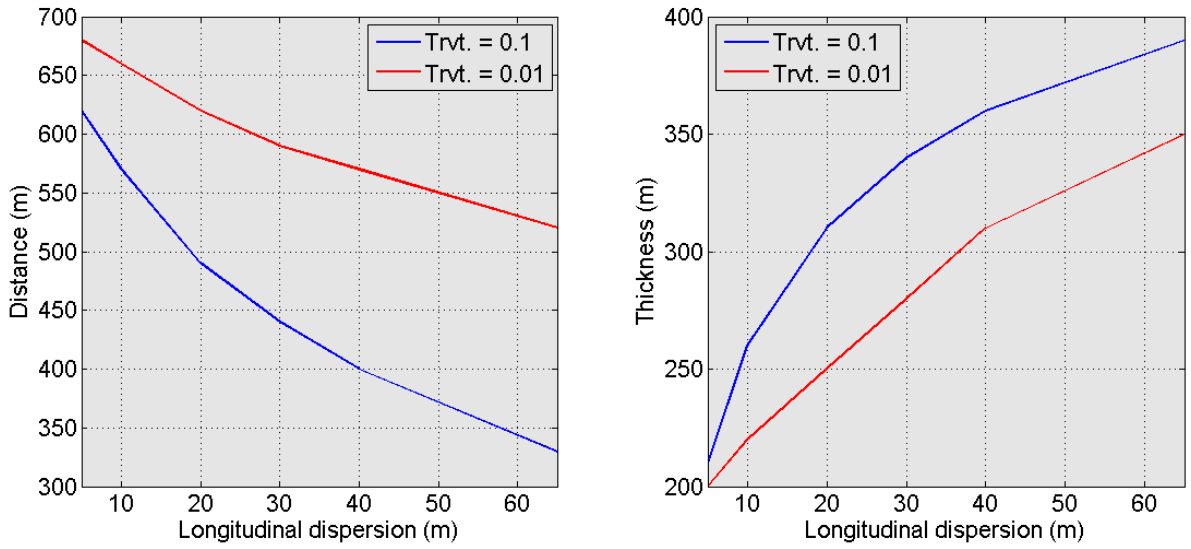

Figure 4.7: Location (Left) and thickness (Right) of the interface with different values of longitudinal dispersivity. The distance for the penetration depth is measured at the 15 g/L isoline. Trvt. is the ratio of vertical transversal dispersivity to longitudinal dispersivity.

Besides changing the location of the salt wedge toe, dispersivity also influenced the geometry of the mixing zone. When dispersivity was increased from 5 to 65, the width of the mixing zone would increase from 210 m to 390 m.

Table 4.6: Cases tested with different dispersivities. Distance is the distance between the coastline and the saltwater wedge toe and thickness is the thickness of the mixing zone measured at the thickest point measured in the horizontal direction.

Case	K(m/d)	α_L(m)	α_v (m)	Distance(m)	Thickness (m)
1	10	30	3	440	340
2	10	5	0.5	620	210
3	10	10	1	570	260
4	10	20	2	490	310
5	10	40	4	400	360
6	10	65	6.5	330	390
7	10	30	0.3	590	270
8	10	5	0.05	680	200
9	10	10	0.1	660	220
10	10	20	0.2	620	240
11	10	40	0.4	570	310
12	10	65	0.65	520	350

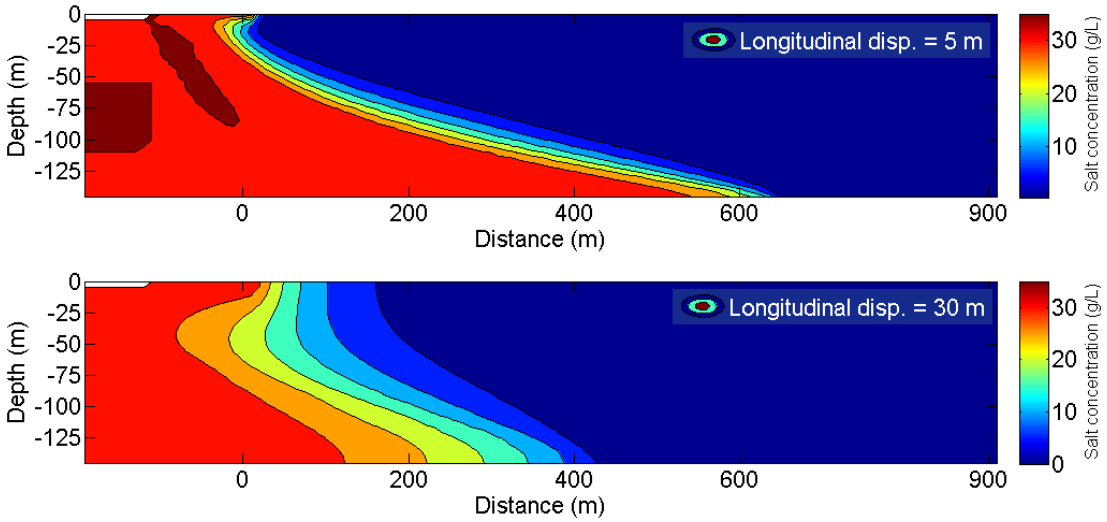

Figure 4.8: Changes in the geometry of the mixing zone with different values of longitudinal dispersivity. Hydraulic conductivity is 10 in both simulations.

When α_V/α_L was reduced by one order of magnitude (from 0.1 to 0.01) the saltwater toe would on average penetrate further inland (Figure 4.7, left). The maximum difference was observed when longitudinal dispersivity was 65 m, with a total distance of 190 m compared to 60 m difference when longitudinal dispersivity was 5 m. The mixing zone became sharper with reduced thickness for all values of longitudinal dispersivity (Figure 4.7, right).

4.3.3 Effect of recharge

Different values of total recharge as well as the ratio between horizontal and vertical inflow were tested. The total inflow estimated through Darcy's equation from field data was 30.19 m^3/d (section 3.3.2). It was tested values of Q_T between 6.2 and 45.2 m^3/d and Q^* between 0.001 and 1000.

The thickness and the distance the saltwater intrusion penetrated inland were measured for different values of total recharge (Table 4.7). When Q_T was reduced the saltwater intrusion would penetrate further inland compared to higher values (Figure 4.9). For example, between Q_T of 6.2 and 45.2 m^3/d, where the distance the saltwater toe penetrated inland changed from 1130 m to 230 m. For the simulated results the distance the saltwater wedge toe penetrated decreased nonlinearly with increasing total inflow (Figure 4.9).

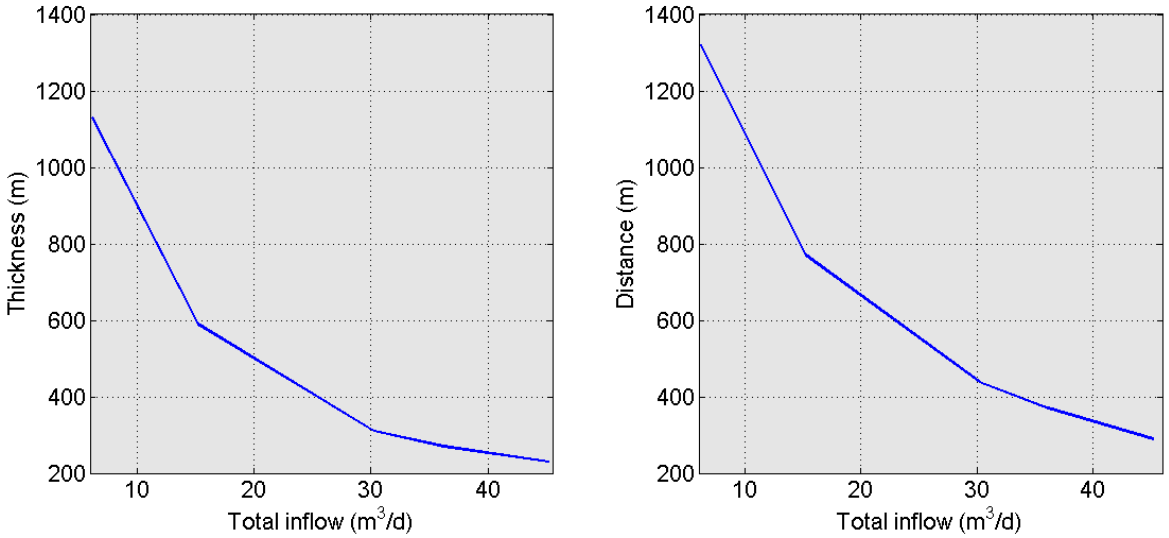

Figure 4.9: The thickness (left) and the distance (right) the interface penetrates inland for different values of Q^T, measured at the 15 g/L isoline.

The thickness of the saltwater mixing zone would increase with decreasing total inflow (Figure 4.9, left). The thickness of the mixing zone was decreasing nonlinearly with increased total inflow.

The different values of Q^* tested ranged between 0.001 and 1000 (Table 4.7). The ratios are so high that they in practice can be considered as only vertical inflow or only horizontal inflow.

Table 4.7: Values of total inflow (Q_T) and the ratio between horizontal and vertical inflow (Q*). The distance for the penetration depth is measured at the 15 g/L isoline.

Case	Q_T (m^3/d)	Q^*(dimensionless)	Distance(m)	Thickness(m)
1	30.2	150	440	310
2	15.2	75	770	590
3	6.2	30	1320	1130
4	36.2	180	370	270
5	45.2	225	290	230
6	30.2	14	440	310
7	30.2	0.6	470	340
8	30.2	0.001	500	380
9	30.2	1000	440	310

The simulations show some variations between different ratios. For example, a difference between *Q** of 0.001 and 1000 was 60 m. Higher ratios increased the distance the saltwater toe penetrated up to a ratio of 10. After this the horizontal inflow was so small compared to the vertical that it had no influence on the saltwater wedge and hereby could be neglected.

The thickness of the saltwater wedge was also found to decrease with higher ratios of *Q**. When *Q** was changed from 0.001 to 1000 the thickness of the mixing zone decreased from 310 to 380 m (Figure 4.10).

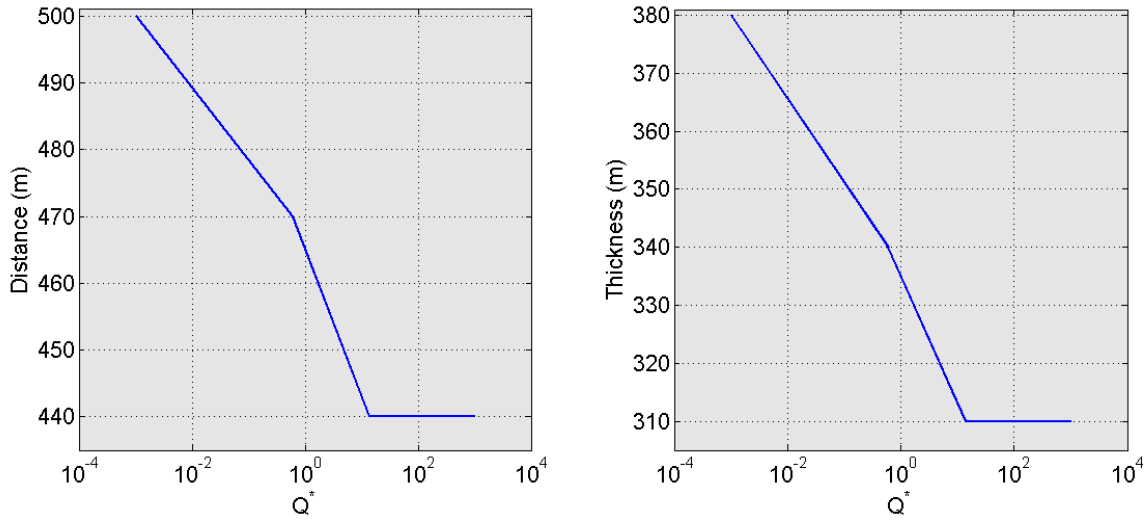

Figure 4.10: Distance (left) and thickness (right) of the saltwater wedge with different ratios of *Q**. The distance for the penetration depth is measured at the 15 g/L isoline.

4.3.4 Dynamic coastline

The effect of the coastline movement was tested with 3 simulations using one stress period of 100 years to simulate the progradation of the Motril-Salobreña aquifer, and a coastline progradation of 300 m after Jabaloy-Sánchez et al. (2014).

In the first scenario the new activated cells were filled with freshwater. After 300 days the freshwater had been flushed out and the cells had acquired the same salt concentration as the surrounding cells (35g/L). Also, the shape and location of the saltwater wedge was identical with the saltwater wedge in scenario two where the cells were filled with full saltwater. This shows that how the initial conditions are determined is only important if the study is to be explored on an extremely small time scale (less than 1 year). However, from a practical viewpoint, the time it took to set up the simulation and initiate the cells with the new values was considerable different between the three cases, with the seawater option requiring less time than the other two. Therefore, it was decided to use this option for the rest of the simulations.

The recharge to the aquifer affected the time for the simulation to reach equilibrium, and it was tested for values ranging between 18 and 45 m^3/d (Table 4.8). In all the simulations lower values of recharge were found to increase the required time to reach equilibrium (Figure 4.11, right). When recharge was 18 m^3/d equilibrium was reached after 85000 days compared to 26000 days when total inflow was 45 m^3/d. Also, time to equilibrium decreased nonlinearly for the simulated cases, with the strongest decrease observed between case 46 and 50.

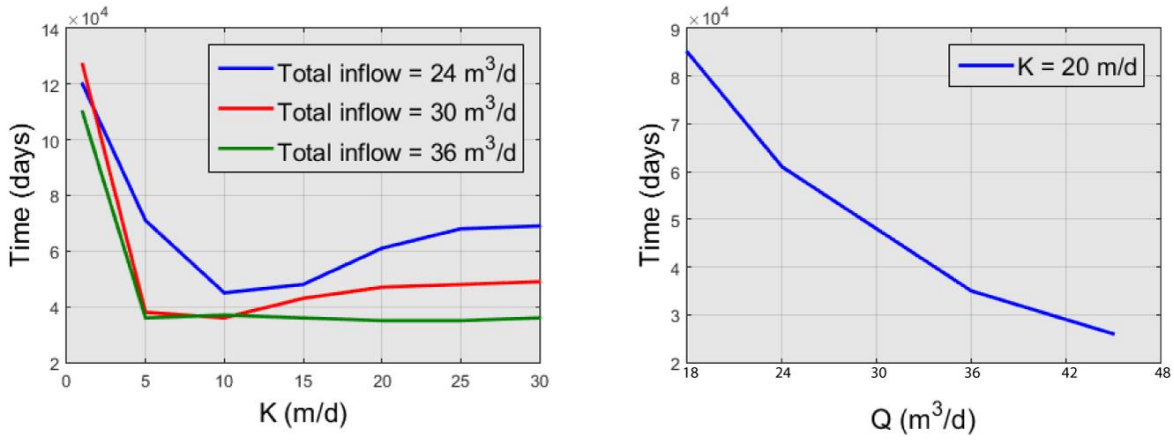

Figure 4.11: The time required for the simulations to achieve equilibrium with different values of hydraulic conductivity (left) and different values of total inflow (right).

Hydraulic conductivity values between 1 and 30 m/d were tested to see how they influenced the time it took to reach equilibrium with the new boundary conditions (Table 4.8). These values were chosen as they represent an average value of the hydraulic conductivity values measured in the Motril-Salobreña aquifer. It was also applied three values of total inflow (24, 30 and 36 m^3/d) to evaluate if the effect of hydraulic conductivity would change for different magnitudes of inflow.

Table 4.8: Cases tested to explore the effect of hydraulic conductivity and total freshwater inflow to the system and their implications on the time required reaching equilibrium with the coastal progradation boundary.

Case	K	Porosity	Time (days)	Q (m^3/d)
28	30	0.2	49000	30
29	10	0.2	36000	30
30	1	0.2	127000	30
31	25	0.2	45000	30
32	20	0.2	48000	30
33	5	0.2	38000	30
34	15	0.2	43000	30
35	30	0.2	69000	30
36	25	0.2	68000	30
37	20	0.2	61000	24
38	15	0.2	48000	24
39	10	0.2	45000	24
40	5	0.2	71000	24
41	1	0.2	120000	24
42	1	0.2	110000	36
43	5	0.2	36000	36
44	10	0.2	37000	36
45	15	0.2	36000	36
46	20	0.2	35000	36
47	25	0.2	35000	36
48	30	0.2	36000	36
49	20	0.2	85000	18
50	20	0.2	26000	45

The time required to reach equilibrium showed a rather complex relationship with hydraulic conductivity, with some ranges of hydraulic conductivity resulting in a decrease of time while other ranges leading to an increase in time (Figure 4.11, left). For all three cases the longest time to reach equilibrium was with the lowest values of hydraulic conductivity (1 m/d). After this the required time would sharply decrease to an intermediate value of hydraulic conductivity (5-10 m/d) for recharge of 24 and 30 m^3/d, after gradually increasing again up to 30 m/d. For recharge of 36 m^3/d the required time was almost constant for values higher than 5 m/d.

4.3.5 Sedimentological formations

For the layered aquifer it was tested a total of 11 cases with different hydraulic conductivity between the three layers (Table 4.9).

The distance the saltwater intrusion would penetrate inland ranged from 300 to 810 m, depending on the value of hydraulic conductivity (Figure 4.12). The hydraulic conductivity of the upper layer influenced distance that the intrusion penetrated inland the most. For example, between case 8 and 9 the only difference in hydraulic conductivity was in the top layer where they had 5 m/d and 20 m/d, respectively. Despite this, the saltwater intrusion in case 8 penetrated 330 m longer compared to case 9. Also, between case 3 and 10 which had the exact same values of hydraulic conductivity, but inverse layering (20/10/1 and 1/10/20 m/d), the saltwater intrusion penetrated 420 m longer inland when the highest values were found in the upper layers of the aquifer.

Table 4.9: The parameters used in the layered model (A/B/C) and the results from the simulations. Distance is the distance between the coastline and the seawater intrusion toe measured at the 15 g/L isoline.

Case	K(A/B/C) (m/d)	Distance (m)
1	10/5/1	300
2	20/5/1	480
3	20/10/1	500
4	20/10/5	620
5	30/10/5	810
6	10/10/10	440
7	20/1/5	540
8	20/1/1	430
9	5/1/1	100
10	1/10/20	80
11	5/10/20	310

The presence of low permeable sediments surrounded by high permeable sediments was tested as a potential explanation for the presence of salinity differences in the Motril-Salobreña aquifer. The hydraulic conductivity used in the low permeable formation ranged from 0.1 – 0.0001 m/d, which corresponds to that often found in silty sediments in the nature (Freeze and Cherry, 1979), while the surrounding aquifer had hydraulic conductivity values between 10 and 20 m/d.

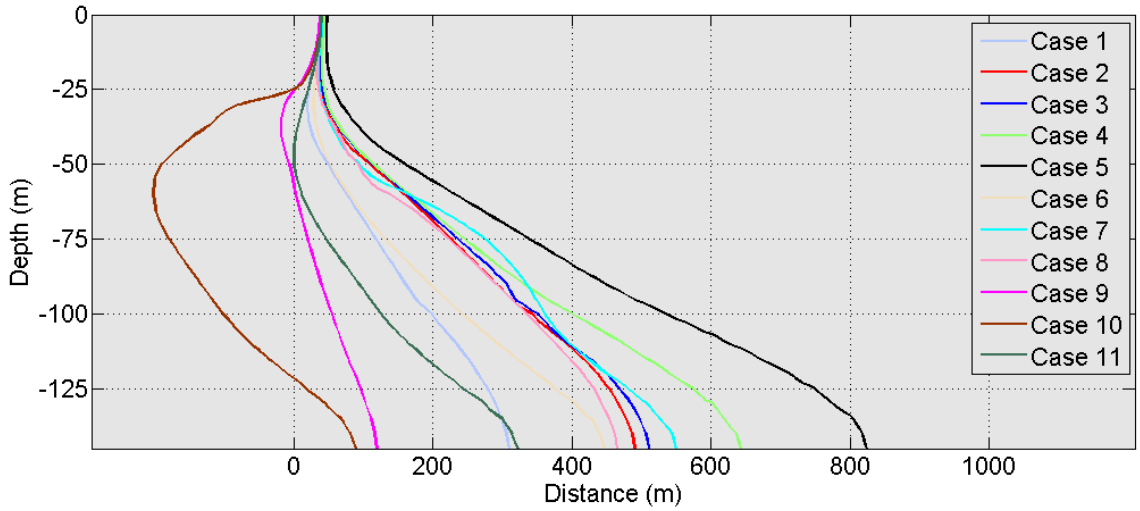

Figure 4.12: Saltwater-freshwater interface (15 g/L isoline) for different scenarios of hydraulic conductivity in the 3 layers.

The average salt concentration contained in the low permeable formation after 38 years was calculated. This specific time was chosen because in most of the simulations the high conductivity cells were flushed while the low permeable cells still contained seawater (Figure 4.13). In this way, the effect of the low permeable layer and the presence of connate saltwater could be explored.

Table 4.10: Salinity in low permeable formations for different cases. Conc. is the residual concentration in the low permeable cells after 14 000 days.

Case	K_1 (m/d)	K_2 (m/d)	α_L	Diffusion	Conc. (g/L)	Flushing (years)
1	10	0.1	30	0.01	3.7	85
2	10	0.001	30	0.01	4.8	98
3	10	0.0001	30	0.01	5.9	101
4	20	0.0001	30	0.01	6.1	101
5	10	0.1	30	-	5.5	162
6	10	0.001	30	-	18.3	-
7	10	0.0001	30	0.001	15.5	635
8	10	0.01	30	-	12.9	1180
9	10	0.01	30	0.001	12.0	411
10	10	0.1	30	0.001	3.7	85
11	10	0.01	30	0.0001	12.8	992
12	10	0.01	30	0.00001	12.9	1159
13	10	0.01	30	0.01	4.7	99
14	10	0.01	30	0.000001	12.9	1178
15	10	1	30	0.01	2.7	69
16	10	10	30	0.01	2.3	65

The residual concentration in the cells was significantly affected by the value of K_2. When K_2 was decreased, the residual concentration in the cells would increase (Figure 4.14). This was

especially noticeably between case 10 and 9 when K_2 was changed from 0.1 to 0.01 m/d, increasing the residual concentration by 8.3 g/L. Further reduction would reduce it to a smaller degree, down to 15.5 g/L in case 7 when K_2 was 0.0001 m/d. The increased contrast in hydraulic conductivity between the two formations resulted in less water going through the low permeable formation and thereby reducing the flushing process.

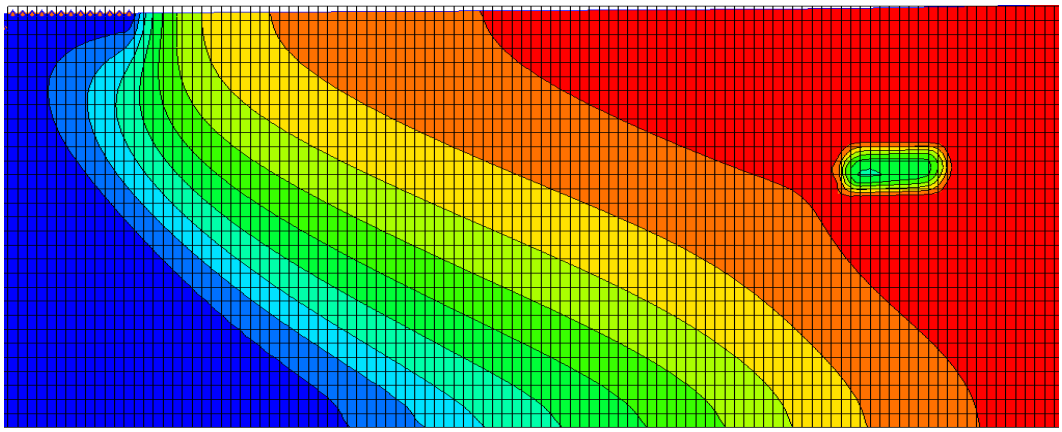

Figure 4.13: A section of the simulated salt distribution after 14 000 days in case 8. The low permeable formation is disconnected from the saltwater intrusion, yet still contains higher salt concentrations than the surrounding cells. Blue color is 35 g /L and red is 0.35 g /L.

Since less water would enter the low permeable formations, diffusion would become an increasingly important factor in the flushing process. This is evident from case 6 where diffusion was removed from the simulation and consequently preventing the cells from being flushed during the 2740 year long simulation. Further, if diffusion was decreased, the residual concentration would increase (Figure 4.14). For example, when diffusion was decreased from 0.01 in the case 13 to 0.001 in case 9, concentration increased from 4.7 to 12.0 g/L. Moreover, further reduction of diffusion only increased the residual concentration by a small amount. From here a reduction of 3 magnitudes in diffusion only resulted in 0.6 g/L higher concentration.

The time needed to flush the low permeable formation ranged from 65 years to over 2740 years (Table 4.10), with both diffusion and the contrast in hydraulic conductivity influencing the flushing time. When diffusion was decreased, the flushing time would increase. In case 14 when diffusion was decreased to $1*10^{-6}$ compared to 0.001 in case 9, the flushing time increased by 767 years. An increased contrast in hydraulic conductivity between the two layers would also result in increased flushing time. For example between case 9 and 10, when K_2 was changed from 0.1 to 0.01, the flushing time increased from 85 years to 411 years.

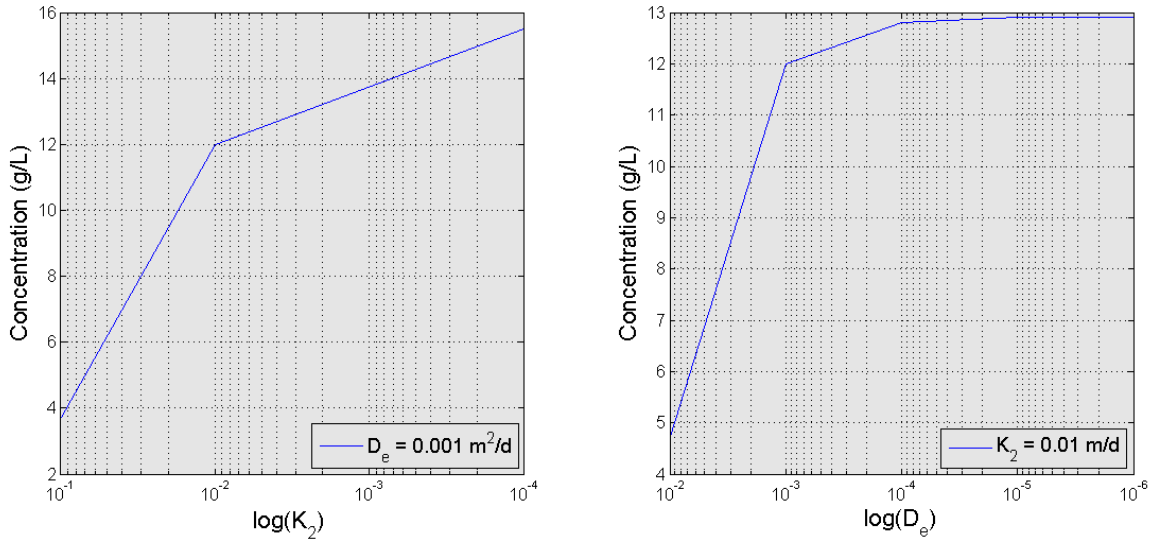

Figure 4.14: The average concentration of the cells composing the low permeable formation with (A) different values of K_2 and (B) different values of D_e.

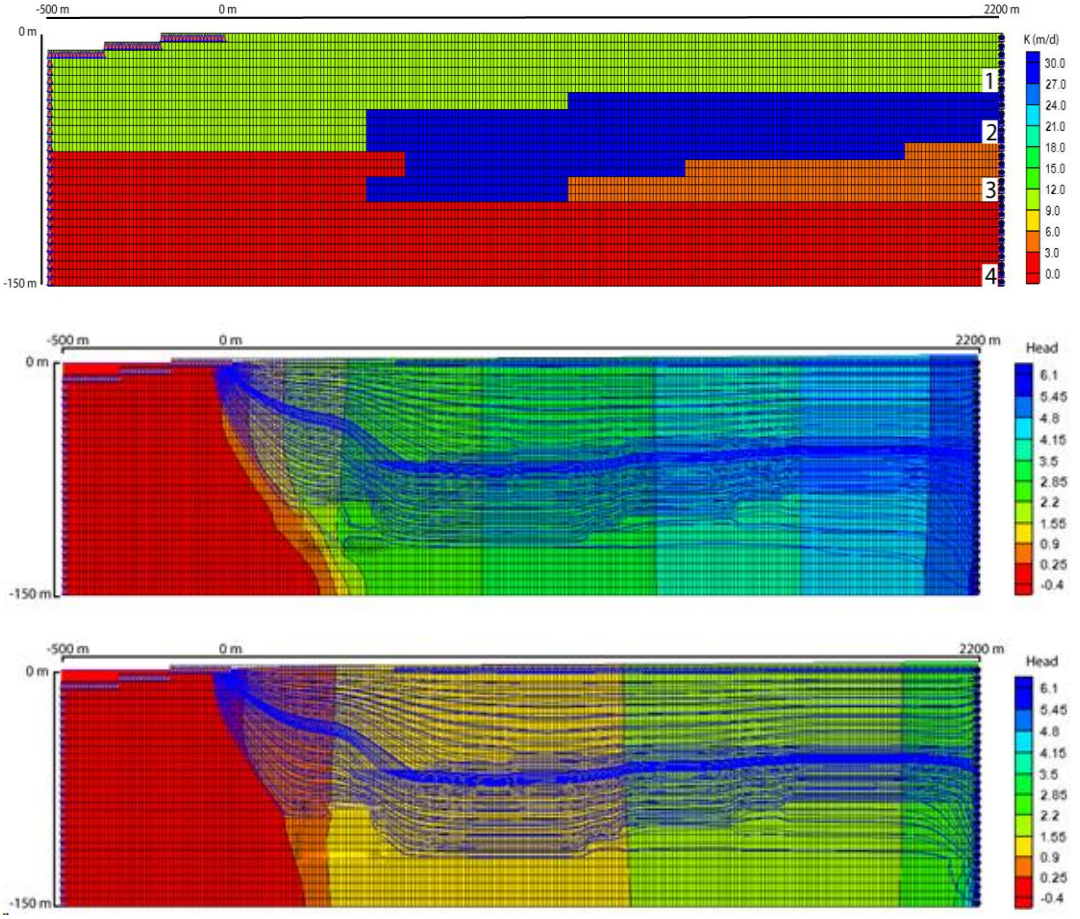

Figure 4.15: Effects of lateral changes in hydraulic conductivity. Blue lines shows the flowpaths of particles injected at the right vertical border and their flow path through the aquifer. Top: hydraulic conductivity distribution; middle: result from case1; down: result from case 2. The highlighted area (C) shows a special area of interest.

The lateral changes of hydraulic conductivity were tested based on the sedimentological interpretation of the aquifer (see section 4.2).

The analysis of the effect of lateral changes in hydraulic conductivity was accomplished with the analysis of the flow paths (Figure 4.15). Each line represents the path for a single particle injected at the right vertical boundary through the aquifer. Consequently can the density of the lines be used to describe which parts of the aquifer experiencing the highest discharge, with areas of high density having higher discharge of water compared to areas with low density.

Table 4.11: Hydraulic conductivity values tested for lateral changes in the Motril-Salobreña aquifer.

Case	K (1/2/3/4) (m/d)
Case 2	10/30/5/1
Case 3	10/3/5/0.1

The highest densities in the flowpaths are located along the coarse gravel lens in the middle of the aquifer where the hydraulic conductivity is highest. The gravel formation acts as a channel for the groundwater and leads to a preferential flow path within the aquifer. This would consequently lead to some areas experiencing less circulation of water and flushing, which increased the time needed to remove the saltwater and thereby increased the time that the simulation needed to reach equilibrium with the new coastline position.

4.4 3D-model

4.4.1 Calibration process

During the calibration process values for specific yield, specific storage and the conductance of the carbonate aquifer was adjusted manually, and as a result 7 sets (referred to as model 1-7 from here) of model parameters had to be calibrated before arriving at satisfactory model (Table 4.12). There are currently no uniform calibration standard used by the modeling community (Anderson 2015), and deciding if a model is “good enough” is therefore subjectively and depends on the modeling objectives. The objective of this calibration process was to see if the numerical model could be improved by implementing hydrofacies, so the models were evaluated using the AE, MAE and RMSE and comparing this with previous studies. Also, a evaluation of how realistic the hydrogeological parameters were

given the lithology in area was considered. Based on these criteria's, model 7 was chosen as the best model, having the third lowest error and the most realistic parameter values. Model 1 and 2 were discarded despite having lower errors than model 7, as the specific yield used in unit 2 were considered to low compared to the lithology (sand to gravel) in the unit. Furthermore, model 3, 4, 5 and 6 all showed realistic parameter values, but were discarded for having higher model errors than model 7.

Table 4.12: The different sets of model parameters estimated with associated model error.

	Parameters					
Model	C.Cond (m^2/d/m)	K_R (m/d)	HK anisotropy*	VK anisotropy *	S_y **	S_S* (10^{-3})
1	0.1	0.14	1/0.5/0.1/1/1.3/10	3/10/10/3/3/3	0.3/0.01/0.3/0.3/0.07	4/0.1/2/0.2/4/4
2	0.34	0.1	1/3/3/1/3/3	3/10/10/3/3/3	0.3/0.01/0.3/0.18/0.3	3/1/5/0.3/7/7
3	0.1	0.11	1/1/1/1/1/1	10/10/10/10/10/10	0.3/0.15/0.2/0.02/0.02	4/0.1/2/0.2/4/4
4	0.13	0.2	1/1.2/0.5/1/1.4/10	1/10/10/1/3/3	0.3/0.15/0.2/0.02/0.002	2/0.1/2/0.2/4/4
5	0.1	0.11	1/1/1/1/1/1	1/10/10/10/10/10	0.3/0.15/0.2/0.02/0.002	2/0.1/2/0.2/4/4
6	0.1	0.14	1/0.5/9.1/1/1.3/10	3/10/30/3/3/3	0.3/0.15/0.3/0.2/0.2	4/0.1/2/0.2/4/4
7	**0.12**	**0.27**	**1/0.5/0.1/1/1/1**	**3/10/6.5/3/10/3**	**0.3/0.15/0.3/0.2/0.2**	**4/1/2/0.2/4/4**

	Statistical summary					
	Calibration			Validation		
Model	ME (m)	MAE (m)	RMSE (m)	ME (m)	MAE (m)	RMSE (m)
1	0.03	0.50	0.69	-0.02	0.48	0.64
2	0.01	0.54	0.74	-0.17	0.57	0.72
3	-0.06	0.80	1.09	-0.76	1.08	1.45
4	0.47	0.87	1.30	0.41	0.76	1.01
5	-0.05	0.70	0.95	-0.63	0.88	1.19
6	0.09	0.55	0.83	-0.30	0.58	0.84
7	**-0.03**	**0.54**	**0.77**	**0.05**	**0.63**	**0.83**

* Results are listed for hydrofacies unit 1/2/3/4/5/6

** Results are listed for hydrofacies unit 1/2/3/5/6

The conductance of the carbonate aquifer was the most important parameter for the water table in the north eastern area. Low values of conductance would lead to a lower simulated water table and thereby increasing the model error, and contrary higher values would result in too much recharge. In order to avoid unrealistic values, the conductance was adjusted based on the water budget. Previous studies has estimated that the carbonate aquifer would provide between 11.1 – 12.3 % of the total recharge (Table 3.4), so a final value of 0.12 m^2/day/m was chosen, resulting in the carbonate aquifer contributing with 13.9 % of the total recharge (Table 4.13).

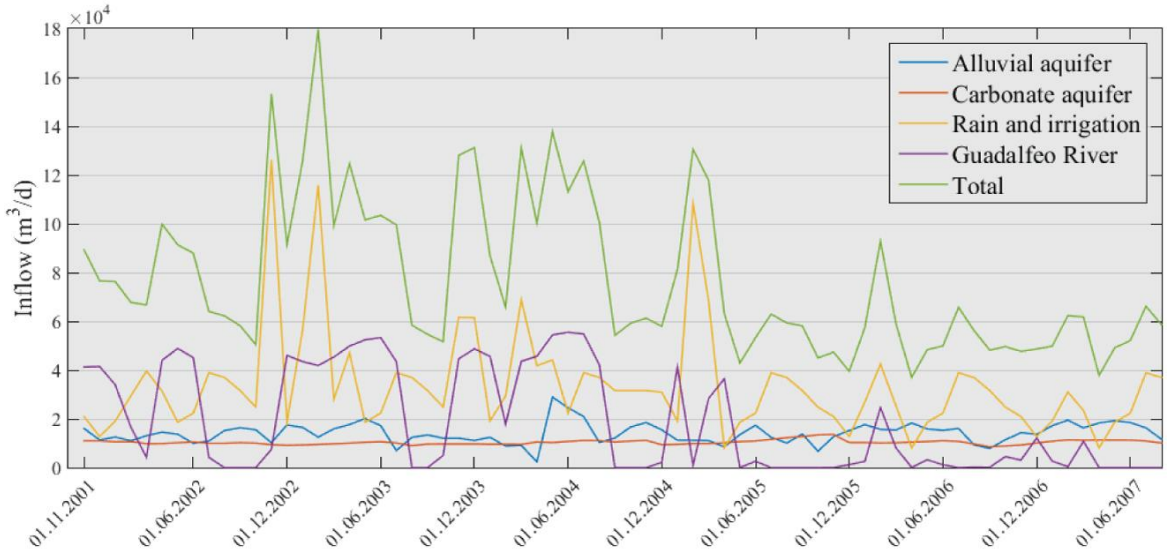

Figure 4.16: Recharge from the different sources for both calibration and validation period in model 7.

Initially, values for specific yield and specific storage were assigned to each facies based on the values estimated by (Calvache et al., 2009). However, especially in the eastern area, this resulted in a groundwater table that was too sensitive to changes in recharge compared to the observed values (Figure 4.17). It was therefore assigned new values based on the lithology in the area, with specific yield ranging between 0.15 and 0.3, corresponding with fine to medium sand and medium sand to medium gravel (Kresic, 2006).

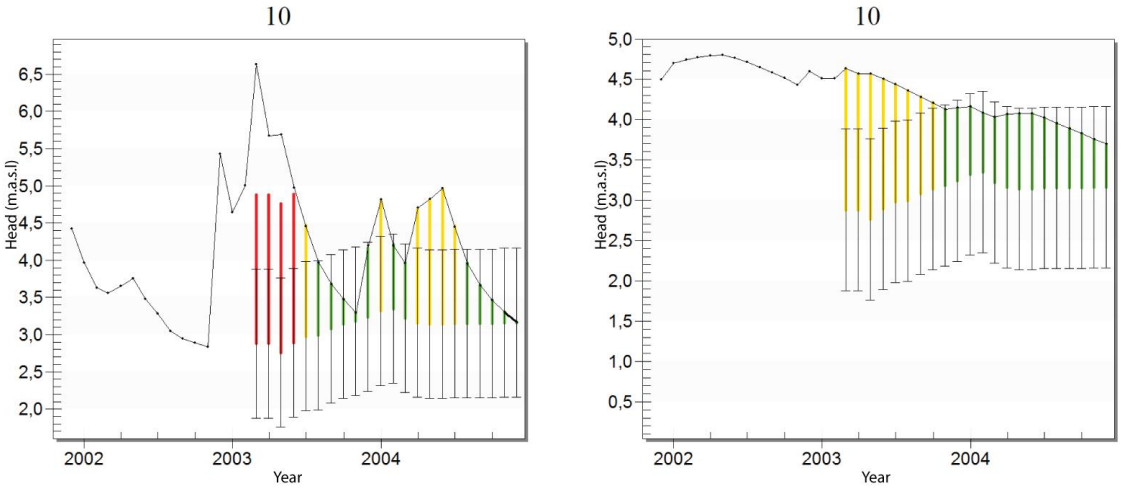

Figure 4.17: Simulated head (black line) from observations for specific yield of 0.01 (left) and 0.2 (right). Green color indicates error < 1 m, yellow 1 m ≤ error < 2 m and red error ≥ 2 m.

The recharge from the Guadalfeo River influenced the simulated head in the wells along the river transect, and the water table along the river responded fast to changes in the river flow.

The calibrated values for river bed hydraulic conductivity all ranged around 0.1 m/d in all model scenarios (Table 4.12), with model 7 having a value of 0.27 m/d. This resulted in a total recharge from the Guadalfeo River of 24.7 % (Table 4.13), which is an intermediate value compared to those obtained in previous studies (Table 3.4).

Table 4.13: Average annual recharge to the Motril-Salobreña aquifer estimated with model 7 for the calibration period.

Average annual inflow in the Motril-Salobreña aquifer		
	Mm/year	Percentage
Alluvial aquifer	5.0	18.8
Carbonate aquifer	3.7	13.9
Rain and irrigation	11.4	42.6
Guadalfeo River	6.6	24.7
Total	26.7	100

Vertical and horizontal anisotropy varied between the models, with the former having values ranging between 3 and 10, and the latter between 0.1 and 10. For model 7 the horizontal anisotropy was between 5 and 10 times higher along the Y-direction in unit 2 and 3 where the Guadalfeo River is located.

Table 4.14: Range of estimated hydraulic conductivity in the 6 hydrofacies units and the allowed possible range for hydraulic conductivity in each unit.

Unit	Estimated K (m/d)	Possible range of K (m/d)
1	245	150 – 900
2	45 – 150	45 – 200
3	3 – 27	3 – 27
4	0.1	0.0001 – 12
5	5 - 50	5 – 50
6	20 - 60	20 – 60

The distribution of hydraulic conductivity within the aquifer was calibrated to range between 0.1 m/d to 245 m/d (Figure 4.19, Table 4.14). Between the 6 hydrofacies, unit 2, 3, 5 and 6 had values corresponding to either the highest or lowest values allowed by regulation (e.g. in unit 2 the lowest value estimated was 45 m/d which was the lowest allowed by regulation). Between the units calibrated with pilot points (unit 2-6), only unit 4 had homogeneous hydraulic conductivity with a value of 0.1 m/d. The other units showed a trend of being divided in two, exhibiting one area with high and one area with low hydraulic conductivity (Figure 4.19). This resulted in the top layer being divided in 3 zones (Figure 4.19) of hydraulic conductivity; with zone A and C at the borders of the aquifer having relatively high

hydraulic conductivity compared to zone B in the middle. It should be noted that each zone contains a range of hydraulic conductivity and the delineation of each zone is based on the trend observed in the spatial distribution of hydraulic conductivity resulting from the calibration process.

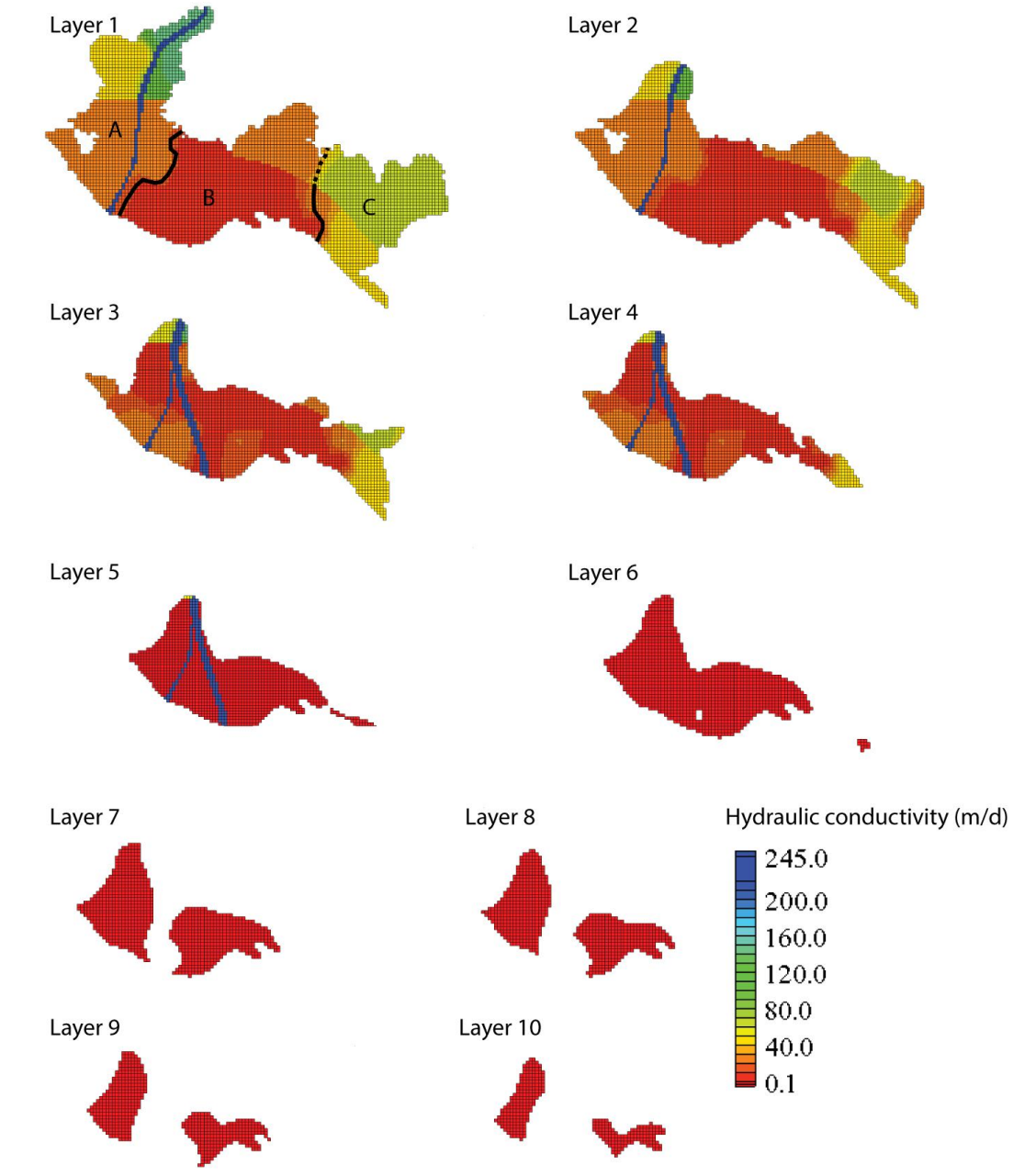

Figure 4.18: Hydraulic conductivity distribution estimated in model 7. In layer one 3 zones (A, B and C) has been delineated based on hydraulic conductivity.

4.4.2 Statistical Summary

The calibration period of model 8 has a MAE of 0.54 m, ME of -0.03 m and RMSE of 0.77 and the validation period has MAE of 0.63, ME of 0.05 and RMSE of 0.83 (Table 4.12). The low ME for both periods indicate that the model fit is not biased, with the positive and negative residuals cancelling each other out. Further, the difference in RMSE and MAE indicate that the model has some large residuals affecting the model which the MAE fails to capture. Observed heads ranges from 35.71 to 0.49 m for the calibration period, and from 29.28 to 0.48 m for the validation period. This means that the RMSE relative to the observed head is 2.2 % for the calibration period and 2.9 % for the validation period. Comparing the model error with that from previous studies in the aquifer, the model shows a rather good fit. Calvache et al. (2009) calculated an MAE relative to observed head of 1.8 % for a transient model of 1 year. Ayres (2015) calculated an MAE of 0.85, which, given that here data had the same range of observations as in this study, equals an MAE relative to observed heads of 2.5 %. For comparison model 7 had an MAE relative to observed heads of 1.5 and 1.9 % for the calibration and validation period, respectively.

4.5 Paleo-hydrogeological modeling

The paleo-hydrogeological model of the Motril-Salobreña was used to study the transient evolution of the salinity distribution in the aquifer over the last 6000 years using a simplified configuration (Figure 4.20). During the period 4000 BC – 1500 AD the coastline had a mean progradation rate of 0.09 – 0.15 m/year, and the salinity distribution reached equilibrium with the new coastline position after only 150 years. The second period (1500 – 2007) had a considerable faster coastline progradation of 3.3 m/year. Despite this, the salinity distribution did reach equilibrium with the new coastline position during the 507 year long simulation period, needing between 20 – 400 years. It was observed that the salt concentration in the aquifer would fall rapidly at the start of the simulation, needing considerable less time to go from 35 g/L to around 6 g/L than from 6 g/L to 0.35 g/L in all parts of the aquifer (Figure 4.19).

Different parts of the aquifer experienced variable rates of flushing due to the differences in recharge and hydraulic conductivity. For the period 1500 AD – 2007 AD, the fastest flushing was observed in zone C (Figure 4.18) in the east end of the aquifer where hydraulic conductivity was around 50 m/d. Here flushing of the saline water took around 20 years in

the top layers and 30 years in the deepest parts (Figure 4.20). In the western area around the Guadalfeo River (zone A) it took around 50 years in the top layers. This area also has one of the highest amounts of discharge to the sea because of the Guadalfeo River. In zone B the flushing time was 100 years in the top layers and around 300 years at depths of 100 meters.

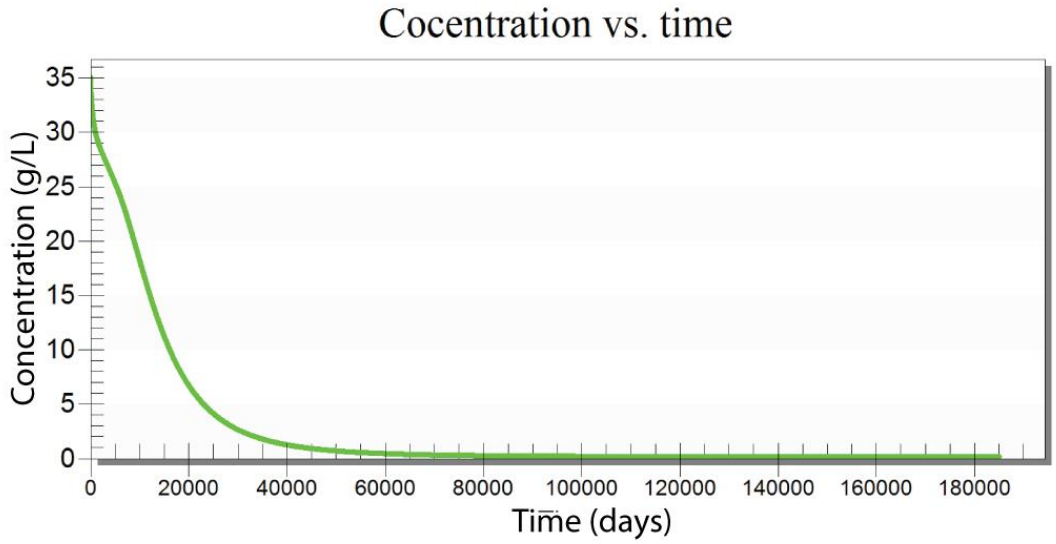

Figure 4.19: Typical flushing time observed in the cells. The concentration would fall rapidly to ~6 g/L before decreasing more gradually.

In the deepest parts of the aquifer where hydraulic conductivity was 0.1 m/d, the flushing time was considerable longer and a clear distinction in flushing time was observed between the high permeable sediments in the top and the low permeable in the bottom (Figure 4.21). At 1520 AD the top layers (layer 1-5) were almost completely flushed, while the bottom layers still had a salt concentration of 35 g/L. 60 years later, in 1580 AD, a clear reduction in salt concentration was observed in the bottom layers, whereas the top layers were now completely flushed. From there, the concentration in the bottom layers was steadily reduced until 1910 AD when they were completely flushed, and the saltwater wedge was in the same location as that of 2007 AD.

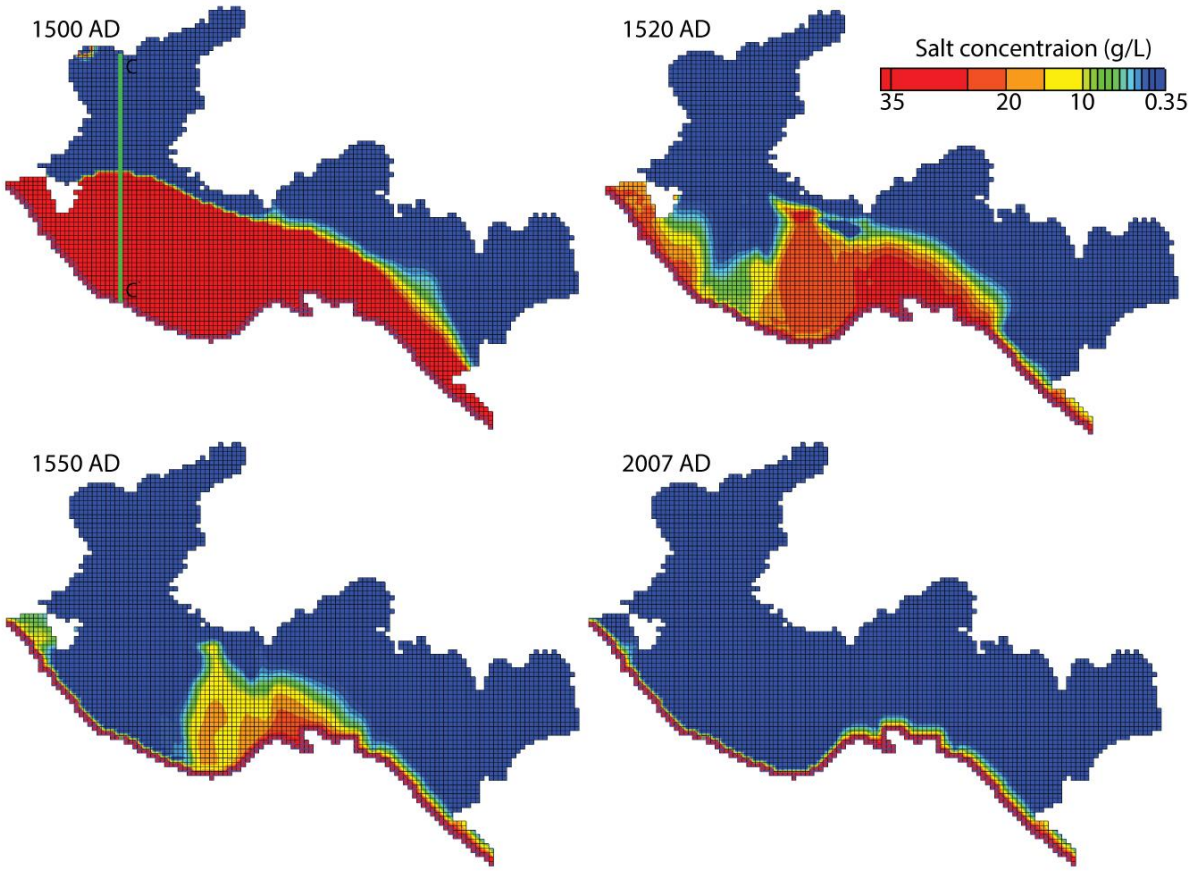

Figure 4.20: Transient evolution of the salinity distribution in the Motril-Salobreña aquifer during time slice 2 in layer 1. C-C` marks the line for figure 4.21.

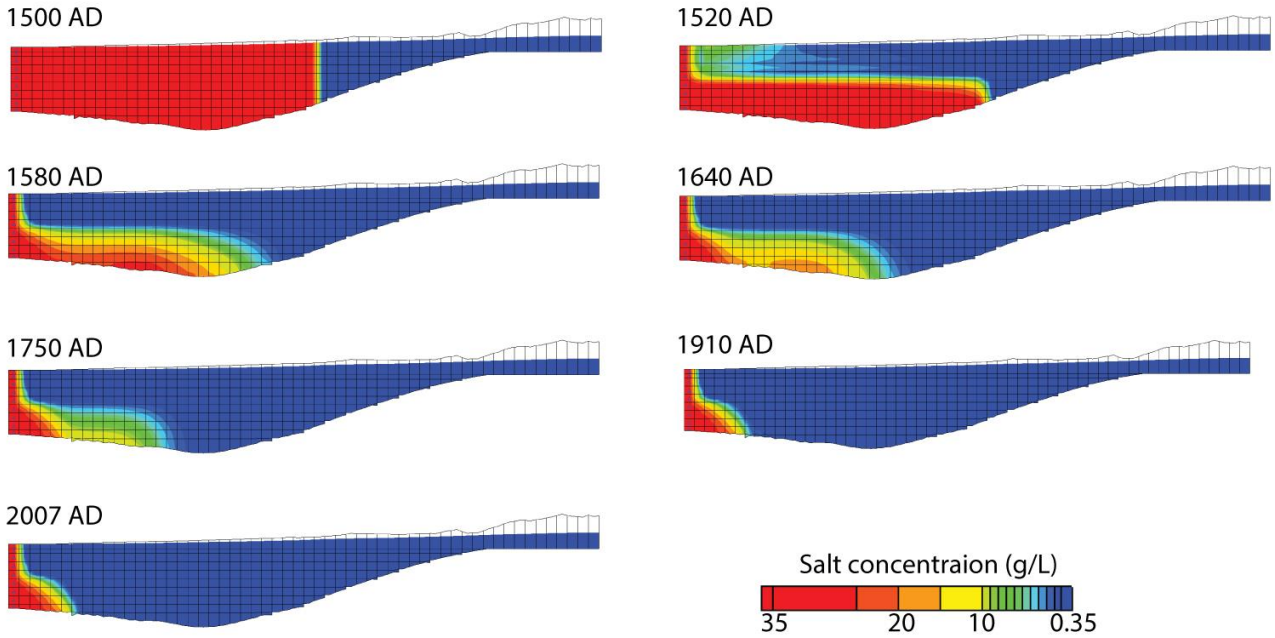

Figure 4.21: Cross sectional view of the evolution of the salinity distribution along the line C-C` (Figure 4.21). Vertical exaggeration 5:1.

Based on the evolution of the salinity distribution for the time period 1500 AD - 2007 AD it was made a map showing the relative flushing times for different parts of the aquifer (Figure 4.22). It is evident that the flushing times to a high degree follows the hydraulic conductivity distribution in the aquifer (Figure 4.18), with areas of high hydraulic conductivity having lower flushing time. It is however one distinct exception from this. In the west of the aquifer next to the sea, there is an area experiencing longer flushing time relative to its hydraulic conductivity value (27 m/d). This is due to the area being partially isolated and receiving little recharge, resulting in less flushing compared to the adjacent area with the same hydraulic conductivity (Figure 4.22).

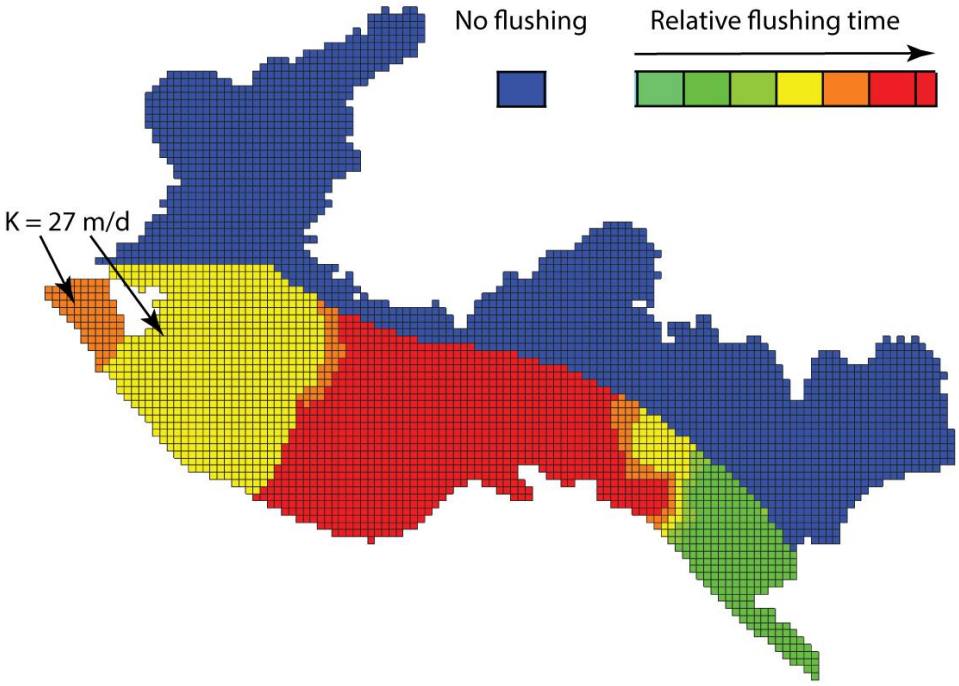

Figure 4.22: Relative flushing time of saline water in the Motril-Salobreña aquifer based on the paleo-hydrogeological simulation.

5 Discussion

5.1 Sedimentological model and hydrofacies

The construction of a sedimentological model allowed for a more detailed subdivision of hydrofacies. In previous studies on the Motril-Salobreña aquifer different hydrogeological units were differentiated based on direct interpolation between similar lithologies in adjacent boreholes, whereas in this study a more careful correlation was conducted by integrating information about depositional environments. Further, the natural intrinsic heterogeneity of each unit was considered by applying a range of possible values for hydraulic conductivity to each unit.

The study of the sedimentological environment made it possible to distinguish 7 major lithofacies from the lithological columns (Table 4.2), and based on this the aquifer was divided in 6 hydrofacies units (Figure 4.3). It was considered merging unit 5 and 6 as they show relatively similar values of hydraulic properties. However, the lithological columns showed that the amount of silts increased towards the sea compared to inland areas. Also, keeping them separated allows for more freedom in the calibration process as it is possible to give each unit a different limit, and consequently it was decided to keep them separated. Besides this, the remaining units exhibit distinct characterizations in sediment composition clearly indicating the influence of different depositional systems.

5.2 2D-model

5.2.1 Seawater intrusion

The results for hydraulic conductivity suggest that horizontal hydraulic conductivity greatly determines the extent of the seawater intrusion. For higher values of hydraulic conductivity the seawater intrusion penetrates further inland (Figure 4.4), due to the reduced head gradient in the groundwater system. In the presence of vertical heterogeneities the hydraulic conductivity at shallow parts influences the extent of the seawater intrusion the most (Figure 4.12), due to the high permeable formation in the top layer acting as a preferential flow path for the sea water. These results are in agreement with that found by others authors, who demonstrated the importance of preferential flow paths on seawater intrusions (Mulligan et al., 2007). The role of preferential flow paths has also been observed in karst coastal aquifers

where occurrence of conduits is one of the most important geological factors influencing the mixing between freshwater and seawater (e.g. Fleury et al., 2007).

Dispersion influences both the thickness of the mixing zone and the length the seawater intrusion would penetrate inland; with lower values increasing penetration distance and resulting in a sharper interface. The increased thickness observed is a result of the increased mixing between the two waters. Further, the increased mixing also leads to reduced penetration distance of the wedge toe due to the density reduction of the seawater, thus lowering the density gradient and the inflow of seawater into the aquifer. These results are in agreement with that found by Shoemaker (2004). Besides this, the nonlinear relationship observed shows that the penetration distance is more sensitive to changes in dispersivity when smaller values are applied (Figure 4.7, left). Connecting this to previous estimates of dispersivity in the Motril-Salobreña aquifer shows the dispersivity values of 30 and 65 applied in the aquifer (Calvache et al., 2009) would lead to a difference in penetration distance of 300 m (table 4.6).

The recharge to the aquifer influences the penetration distance of the seawater intrusion and the geometry of the mixing zone, with higher values of recharge significantly reducing the penetration distance and decreasing the thickness. When recharge is reduced more seawater penetrates inland due to the reduced head gradient in the aquifer. This again leads to more mixing between the waters, and thereby increases the thickness of the mixing zone. These results clearly shows the effect of the head gradient on seawater intrusions, with a difference of over 1000 meters observed between the highest and lowest values of recharge. The results are in agreement with observations made by previous authors (e.g. Li et al., 2015), who demonstrated the importance of recharge on seawater intrusions using a generic 2D numerical model.

5.2.2 Dynamic coastline

Since paleo-hydrogeological modeling is not a common objective in scientific literature, there were some methodological questions regarding how to establish the boundary conditions and how to implement it in the simulations that had to be addressed prior to constructing the paleo-model of the Motril-Salobreña aquifer.

One of the main questions when simulating the dynamic coastline was how to define the new cells added in each time slices. It was decided to add them as seawater after simulations showed no observable difference between the three options after 300 days; which compared to the time required for the groundwater system to reach equilibrium in the various cases was less than 1 %. However, if this percentage was considerable smaller which option is used would have to be reconsidered. When Delsman et al. (2014) applied paleo-hydrogeological modeling to study the historical evolution of the salinity distribution in the Netherlands, they initialized new cells with the same values as the surrounding cells, which in the case of a prograding coast used in this study would be similar to full saltwater.

The sensitivity analysis on hydraulic conductivity and recharge showed that both parameters influenced the time necessary for the aquifer to reach equilibrium with the new boundary conditions with respect to salinity distribution. The effect of recharge is clear; higher values decreases the time required to reach equilibrium due to the increased head gradient in the aquifer as more water enters. This enhances flushing of old marine water in the aquifer and thereby decreases the time required for the system to reach equilibrium.

Variations in hydraulic conductivity would both lead to increased and decreased time to reach equilibrium depending on the values that were applied (Figure 4.11). This happens because higher values of hydraulic conductivity increase the groundwater discharge through the aquifer. However, since the recharge is defined by field measurements, the hydraulic gradient in the aquifer will decrease, and thus reducing the groundwater discharge through the aquifer. Also, when hydraulic conductivity increases the penetration distance of the saltwater increases, leading to more saltwater needed to be flushed. This could possibly be the reason why the time increases for some values of hydraulic conductivity, and reduces for others.

The study of a low permeable formation within a high permeable formation showed that this sedimentological characteristic could lead to connate seawater. When the contrast in hydraulic conductivity between the two units is increased, the residual concentration will also increase. This is due to the low permeable formation becoming partially or fully isolated from surrounding cells. The isolation would further result in diffusion becoming the most important factor for flushing any saline water, as this is the only process that can reduce the concentration since no water can enter. Higher values of diffusion consequently leads to more solute transport between the cells, and thereby decreases the time needed to flush the cells.

The timeframe of the flushing process was consequently influenced by the contrast in hydraulic conductivity between the two formations as well as the diffusion coefficient. For hydraulic conductivity values similar to that observed in the Motril-Salobreña aquifer, flushing times could exceed 1200 years depending on the diffusion coefficient applied.

5.3 3D-numerical model of the Motril-Salobreña aquifer

A new numerical model of the Motril-Salobreña aquifer was constructed based on the defined set of hydrofacies. By integrating the hydrofacies in the model it was possible to better define the spatial distribution of hydrogeological properties in the aquifer, and obtain a more detailed map of the hydraulic properties in the aquifer.

The calibration of the model resulted in a RMSE of 0.77 m, which is quite low relative to the range in observed head (35.2 m). There are some uncertainty regarding the boundary conditions for the carbonate and the alluvial aquifer (Figure 3.13). These boundaries also had the most influence on the water table in unit 2, which the hydraulic properties in the unit were calibrated against. Consequently there are some uncertainties associated with the calibrated values of this unit. Hydraulic conductivity in this unit ranges from 45 – 150 m/d, corresponding to clean sand or gravel (Fetter, 2001), and specific yield corresponds to medium sand or medium gravel (Kresic, 2006). These values are in agreement with the lithology observed in the lithological columns and the estimates from grain size analysis, so the calibrated values are realistic and are assumed to be well calibrated, despite the uncertainty in the boundary conditions.

The variations in hydraulic conductivity within each unit were estimated using pilot points. In unit 2, 3, 5 and 6 estimated hydraulic conductivity takes the highest or lowest possible values within that unit (Table 4.14). The fact that hydraulic conductivity reaches the limits in 4 out of 6 units could indicate that the boundaries are defined too narrow. The limits were mainly based on the grain size analysis, which was conducted on 22 samples (Table 4.1). The uneven spatial distribution and limited amount of samples results in some uncertainty connected to the limits, especially regarding unit 5 and 6 which only contained one sample. However, according to the present knowledge about hydraulic conductivity in the aquifer the limits are appointed correctly, but future studies should address this by gaining more information about the hydraulic conductivities in the aquifer in an attempt to better delineate the limits.

5.4 Paleo-hydrogeological model and connate seawater

A paleo-hydrogeological model of the Motril-Salobreña aquifer including the progradation of the coastline during the period 4000 BC – 2007 AD has been constructed. By reconstructing the coastline movement of the aquifer it was possible to study the transient evolution of the salinity distribution in the aquifer and also the possibility of connate seawater. Paleo-hydrogeological modeling has also been proposed by previous authors (Delsman et al., 2014) as a way of better delineating the initial salinity conditions for variable density dependent models on seawater intrusions.

This is the first time a paleo-hydrogeological mode of the Motril-Salobreña has been constructed, and consequently there are some uncertainties connected to the methodology. When determining the recharge to the aquifer it was decided to use the average values of the time period 2001 – 2007 as a constant value for the period 4000 BC – 2001 AD, which is a simplification of the reality. The true values will be more dynamic, and climate variations can result in considerable different climatic conditions over the 6000 year long period. Moreover, the sensitivity analysis conducted on the 2D model showed the importance of recharge on flushing time, and consequently will the simplification on recharge result in some uncertainties regarding the estimated flushing times of the aquifer. Despite this, the model is assumed to capture the relative flushing times of the different areas in the aquifer, and the estimated values for flushing time gives a good indication on the timeframe needed to flush any saline water from the aquifer. For future paleo-hydrogeological studies in the Motril-Salobreña aquifer the main focus for improvement should be on better quantifying the historical recharge to the aquifer.

The salinity distribution obtained at the end of the period 1500 AD – 2007 AD in the paleo-hydrogeological model is identical to that obtained in the steady state simulation. This indicates that, in principle, the Motril-Salobreña aquifer can be considered to be in equilibrium with the current coastline position, despite the very rapid coastline progradation the aquifer has been subjected to over the last 500 years. The transient study of the salinity distribution in the aquifer showed a clear connection between flushing time and hydraulic conductivity (Figure 4.22). This resulted in different parts of the aquifer reaching equilibrium at different rates, with the deepest parts of the aquifer requiring over 400 years too flush all the saline water. The analysis of lateral changes in hydraulic conductivity (Figure 4.15)

demonstrated that heterogeneities can lead to preferential flow paths, and consequently that some areas of the aquifer can experience more flushing than others. The general idea of heterogeneities leading to preferential flow paths can be connected to the flushing of the Motril-Salobreña aquifer, and to the zonation of hydraulic conductivity observed in calibration process (Figure 4.18). Because of the lower hydraulic conductivity in zone B, water will not only move slower in this part of the aquifer, but there will also be less circulation of water as most of the water will favor the higher permeability found in zone A and C. This can also be connected to the long flushing time of layer 5-10 (Figure 4.21), as most of the freshwater will flow through the upper parts of the aquifer. Despite the paleo-hydrogeological model reaching equilibrium with the present day coastline, the uncertainty in the construction of the model indicate that some parts of the aquifer could still have connate water, despite the lack of any in the model.

Previous studies in the Motril-Salobreña aquifer has detected higher amounts of salt at a distances of 300 m and 1 km from the coast, and it has been speculated in that this could be connate seawater trapped within low permeable sediments (Crespo et al., 2012). The absence of connate seawater in the paleo-hydrogeological model can possibly be explained due to the use of pilot points in the calibration processes and the model discretization. The study of connate seawater using the 2D-model showed that one possible solution for connate water to occur is due to abrupt changes in hydraulic conductivity (Table 4.10). Pilot points do not include small scale heterogeneities and makes for a more gradual change, which could result in the model not capturing the abrupt contrast in hydraulic conductivity needed. Further, the grain size analysis estimated values below 0.001 m/d at 4 different depths in the aquifer (Table 4.1). This indicates that the variation in hydraulic conductivity is bigger in reality compared to that estimated by the model.

Despite the lack of connate water in the model, the results from the 2D-simulation indicate that the aquifer could contain connate water. The lowest values of hydraulic conductivity from the Motril-Salobreña aquifer estimated with the grain size distribution was 0.00036 m/d. Comparing this to similar values used in the generic 2D-model shows a flushing time between 600 - 1178 years depending on diffusion (table 4.10). From this it is possible to conclude that the variations in hydraulic conductivity observed in the Motril-Salobreña aquifer could lead to connate seawater, and thereby that some of the observed saline water in the Motril-Salobreña aquifer could be connate.

Based on the time estimates provided by the paleo-hydrogeological model it was constructed a map of the aquifer showing the flushing times in different parts (Figure 4.22). Due to the uncertainties in the estimates associated with the methodology, the map is best used a measure for flushing capacity of different areas of the aquifer relative to each other. Also, the map provides some insight in the recovery capacity of the aquifer in case of future seawater intrusions.

6 Conclusion

This thesis has applied the use of paleo-hydrogeological modeling to study the transient evolution of the salinity distribution in the Motril-Salobreña aquifer. In the process of constructing the model the following objectives were accomplished:

A sedimentological model of the aquifer was constructed by studying the lithological columns from the aquifer and combining this with the sedimentological history of the aquifer. This was used to map 7 major lithofacies in the aquifer, corresponding to different depositional systems. Based on the sedimentological model the aquifer was then divided in 6 hydrofacies units to be used in the construction of the numerical model. It was also considered the intrinsic heterogeneity of each unit resulting from natural depositional systems by defining a range of possible values for hydraulic conductivity within each unit.

A sensitivity analysis was conducted using a 2D synthetic model of a coastal aquifer on the most important parameters for seawater intrusions and their effect on the distance a seawater intrusion penetrates inland and the shape of its mixing zone. The parameters were: hydraulic conductivity, dispersion and recharge; and the following conclusions can be drawn on each parameter: (1) higher values of hydraulic conductivity increases the distance the seawater intrusion penetrates inland because of increased mixing between the two waters, and contrary lower values will reduce the distance; (2) higher values of dispersion increases mixing and thereby leading to a thicker mixing zone and reduces the distance the seawater intrusion penetrates inland; (3) higher recharge decreases the distance the seawater intrusion penetrates inland because of reduced head gradient in the aquifer.

Further, the 2D model was used to answer some practical question regarding paleo-hydrogeological modeling, and to study the influence of recharge and hydraulic conductivity on the evolution of the salinity distribution. Higher recharge was found decrease the time needed to reach equilibrium with the new boundary condition by increasing flushing of old seawater. Variations in hydraulic conductivity would result in both increased and decreased flushing time, depending on the value applied.

A 3D-numerical model of the Motril-Salobreña aquifer was constructed and calibrated for the period 2001 – 2004, and validated for the period 2004 – 2007, with a RMSE of 0.77 m and

0.83 m, respectively. The model successfully integrated the use of the defined hydrofacies in the calibration process to better describe the distribution of hydraulic conductivity in the aquifer. The variability in hydraulic conductivity within each hydrofacies unit was included in the model using 44 pilot points in the calibration process, with the final values for hydraulic conductivity estimated to range between 0.1 and 245 m/d.

The evolution of the salinity distribution in the Motril-Salobreña aquifer for the period 4000 BC – 2007 AD was studied using a paleo-hydrogeological model. The model simulated the evolution of the aquifer by changing the coastline position according to a historical reconstruction of the coastline (Jabaloy-Sánchez et al., 2014). Flushing of old saline water connected to earlier positions of the coastline was estimated to range between 20 and 400 years depending on the hydraulic conductivity and the recharge. Flushing times indicated that the Motril-Salobreña aquifer is in equilibrium with the current coastline position.

By studying the flushing time of saline water trapped within low permeable sediments (connate water) it was documented for conditions similar to that found in the Motril-Salobreña aquifer, flushing times could exceed 1100 years. This proves that some of the saline water found within the aquifer could be connected to earlier hydrogeological conditions.

References

ADEPELUMI, A. A., AKO, B., AJAYI, T., AFOLABI, O. & OMOTOSO, E. 2009. Delineation of saltwater intrusion into the freshwater aquifer of Lekki Peninsula, Lagos, Nigeria. *Environmental Geology,* 56**,** 927-933.

ALEXANDER, J. 1989. Delta or coastal plain? With an example of the controversy from the Middle Jurassic of Yorkshire. *Geological Society, London, Special Publications,* 41**,** 11-19.

ANDERSON, M. P. 1989. Hydrogeologic facies models to delineate large-scale spatial trends in glacial and glaciofluvial sediments. *Geological Society of America Bulletin,* 101**,** 501-511.

ANDERSON, M. P., WOESSNER, W. W. & HUNT, R. J. 2015. *Applied groundwater modeling: simulation of flow and advective transport*, Academic press.

APPELO, C. A. J. & POSTMA, D. 2005. *Geochemistry, groundwater and pollution*, CRC press.

ASPRION, U. & AIGNER, T. 1999. Towards realistic aquifer models: three-dimensional georadar surveys of Quaternary gravel deltas (Singen Basin, SW Germany). *Sedimentary Geology,* 129**,** 281-297.

AYRES, E. D. 2015. Modelling the impact of land-use change due to anthropogenic activity on hydrodynamics in an aquifer in Southern Spain.

BATH, A. H. & EDMUNDS, W. M. 1981. Identification of connate water in interstitial solution of chalk sediment. *Geochimica et Cosmochimica Acta,* 45**,** 1449-1461.

BEAR, J. & CHENG, A. H.-D. 2010. *Modeling groundwater flow and contaminant transport*, Springer Science & Business Media.

BEYER, W. 1964. Zur Bestimmung der Wasserdurchlässigkeit von Kiesen und Sanden aus der Kornverteilungskurve. *WWT,* 14**,** 165-168.

BISWAS, H. & MELESSE, A. M. 2016. Regional Scale Groundwater Flow Modeling for Wakel River Basin: A Case Study of Southern Rajasthan. *Landscape Dynamics, Soils and Hydrological Processes in Varied Climates.* Springer.

BOBBA, A. G. 2002. Numerical modelling of salt-water intrusion due to human activities and sea-level change in the Godavari Delta, India. *Hydrological Sciences Journal,* 47**,** S67-S80.

BOGGS, S. 1995. *Principles of sedimentology and stratigraphy*, Prentice Hall Upper Saddle River^ eNJ NJ.

BOGGS, S. 2006. *Principles of sedimentology and stratigraphy*, Pearson Prentice Hall.

BOUWER, H. 2002. Artificial recharge of groundwater: hydrogeology and engineering. *Hydrogeology Journal,* 10**,** 121-142.

BUTLER JR, J. J. 2005. Hydrogeological methods for estimation of spatial variations in hydraulic conductivity. *Hydrogeophysics.* Springer.

CALVACHE, M., IBÁÑEZ, S., DUQUE, C., MARTÍN‐ROSALES, W., LÓPEZ‐CHICANO, M., RUBIO, J., GONZÁLEZ, A. & VISERAS, C. 2009. Numerical modelling of the potential effects of a dam on a coastal aquifer in S. Spain. *Hydrological processes,* 23**,** 1268-1281.

CARLE, S. F., LABOLLE, E. M., WEISSMANN, G. S., VAN BROCKLIN, D. & FOGG, G. E. 1998. Conditional simulation of hydrofacies architecture: a transition probability/Markov approach. *Hydrogeologic models of sedimentary aquifers, concepts in hydrogeology and environmental geology,* 1**,** 147-170.

CARRERA, J., ALCOLEA, A., MEDINA, A., HIDALGO, J. & SLOOTEN, L. J. 2005. Inverse problem in hydrogeology. *Hydrogeology journal,* 13**,** 206-222.
CASTILLO, E. 1975. Hidrogeología de la Vega de Motril-Salobreña y sus bordes. *M. Thesis, Universidad de Granada, Granada,* 184.
COLEMAN, J. M. & WRIGHT, L. 1975. Modern river deltas: variability of processes and sand bodies.
CRESPO, F. J., LÓPEZ CHICANO, M., CALVACHE QUESADA, M. L., SÁNCHEZ ÚBEDA, J. P., DUQUE, C. & MARTÍN ROSALES, W. 2012. Estudio de las fuentes de salinización en el acuífero costero Motril-Salobreña (Granada).
CUSTODIO, E. 2005. Coastal aquifers as important natural hydrogeological structures. *Groundwater and Human Development. Selected Papers on Hydrogeology,* 6**,** 15-38.
CUSTODIO, E. 2010. Coastal aquifers of Europe: an overview. *Hydrogeology Journal,* 18**,** 269-280.
CUSTODIO, E. & BRUGGEMAN, G. 1987. *Groundwater problems in coastal areas*, Unesco.
DALRYMPLE, R. W. & JAMES, N. P. Facies Models 4. 2010. Geological Association of Canada.
DAVIS, J. C. & SAMPSON, R. J. 1986. *Statistics and data analysis in geology*, Wiley New York et al.
DELSMAN, J. R., HU-A-NG, K. R. M., VOS, P. C., DE LOUW, P. G. B., OUDE ESSINK, G. H. P., STUYFZAND, P. J. & BIERKENS, M. F. P. 2014. Paleo-modeling of coastal saltwater intrusion during the Holocene: an application to the Netherlands. *Hydrol. Earth Syst. Sci.,* 18**,** 3891-3905.
DEVLIN, J. F. 2015. HydrogeoSieveXL: an Excel-based tool to estimate hydraulic conductivity from grain-size analysis. *Hydrogeology Journal,* 23**,** 837-844.
DOHERTY, J. E. & HUNT, R. J. 2010. *Approaches to highly parameterized inversion: a guide to using PEST for groundwater-model calibration*, US Department of the Interior, US Geological Survey.
DUQUE, C. 2009. *Influencia antrópica sobre la hidrogeología del acuífero Motril-Salobreña [Anthropogenic influence on the hydrogeology of the Motril-Salobreña Aquifer].* Ph. D Thesis, University of Granada, Granada.
DUQUE, C., CALVACHE, M. L. & ENGESGAARD, P. 2010. Investigating river–aquifer relations using water temperature in an anthropized environment (Motril-Salobreña aquifer). *Journal of Hydrology,* 381**,** 121-133.
DUQUE, C., CALVACHE, M. L., PEDRERA, A., MARTÍN-ROSALES, W. & LÓPEZ-CHICANO, M. 2008. Combined time domain electromagnetic soundings and gravimetry to determine marine intrusion in a detrital coastal aquifer (Southern Spain). *Journal of Hydrology,* 349**,** 536-547.
DUQUE, C., LÓPEZ-CHICANO, M., CALVACHE, M. L., MARTÍN-ROSALES, W., GÓMEZ-FONTALVA, J. M. & CRESPO, F. 2011. Recharge sources and hydrogeological effects of irrigation and an influent river identified by stable isotopes in the Motril-Salobreña aquifer (Southern Spain). *Hydrological Processes,* 25**,** 2261-2274.
EATON, T. T. 2006. On the importance of geological heterogeneity for flow simulation. *Sedimentary Geology,* 184**,** 187-201.
EDMUNDS, W. M. & MILNE, C. Palaeowaters in coastal Europe: evolution of groundwater since the late Pleistocene. 2001. Geological Society of London.

EZZY, T., COX, M., O'ROURKE, A. & HUFTILE, G. 2006. Groundwater flow modelling within a coastal alluvial plain setting using a high-resolution hydrofacies approach; Bells Creek plain, Australia. *Hydrogeology Journal,* 14**,** 675-688.
FETTER, C. W. 2001. *Applied hydrogeology*, Prentice hall Upper Saddle River.
FLECKENSTEIN, J. H., NISWONGER, R. G. & FOGG, G. E. 2006. River‐aquifer interactions, geologic heterogeneity, and low‐flow management. *Groundwater,* 44**,** 837-852.
FLEURY, P., BAKALOWICZ, M. & DE MARSILY, G. 2007. Submarine springs and coastal karst aquifers: a review. *Journal of Hydrology,* 339**,** 79-92.
FREEZE, R. A. & CHERRY, J. A. 1979. *Groundwater*.
GALLOWAY, W. E. 1975. Process framework for describing the morphologic and stratigraphic evolution of deltaic depositional systems.
GALLOWAY, W. E. & HOBDAY, D. K. 2012. *Terrigenous clastic depositional systems: applications to fossil fuel and groundwater resources*, Springer Science & Business Media.
GALLOWAY, W. E. & SHARP JR, J. M. 1998a. Characterizing aquifer heterogeneity within terrigenous clastic depositional systems. *Hydrogeologic Models of Sedimentary Aquifers (Fraser, GS; Dowis, JM; editors). Society of Sedimentary Geologists***,** 85-90.
GALLOWAY, W. E. & SHARP JR, J. M. 1998b. Hydrogeology and characterization of fluvial aquifer systems. *Hydrogeologic Models of Sedimentary Aquifers (Fraser, GS; Dowis, JM; editors). Society of Sedimentary Geologists***,** 91-105.
GARCÍA-RUIZ, J. M. 2010. The effects of land uses on soil erosion in Spain: A review. *CATENA,* 81**,** 1-11.
GELHAR, L. W., WELTY, C. & REHFELDT, K. R. 1992. A critical review of data on field‐scale dispersion in aquifers. *Water resources research,* 28**,** 1955-1974.
GILBERT, G. K. 1885. *The topographic features of lake shores*, US Government Printing Office.
GUO, W. & LANGEVIN, C. D. 2002. User's guide to SEAWAT; a computer program for simulation of three-dimensional variable-density ground-water flow.
HAZEN, A. 1892. *Some physical properties of sands and gravels: with special reference to their use in filtration*, publisher not identified.
HEREDIA, J., MURILLO, J., GARCÍA-AROSTEGUI, J., RUBIO, J. Y. & LOPEZ-GETA, J. 2003. Influencia antrópica en un acuífero costero. *Consideraciones sobre la gestión hídrica del acuífero de Motril-Salobreña (España)[Anthropogenic influence on a coastal aquifer. Considerations on the hydraulic management of the Motril-Salobreña aquifer]., Rev. Latino-Amer. Hidrogeol,* 3**,** 73-83.
HILL, M. C. 1998. *Methods and guidelines for effective model calibration*, US Geological Survey Denver, CO, USA.
HOFFMANN, G. 1987. *Holozänstratigraphie und Küstenlinienverlagerung an der andalusischen Mittelmeerküste.* Doctoral thesis/PhD Doctoral thesis/PhD, Universität Bremen.
HUDON-GAGNON, E., CHESNAUX, R., COUSINEAU, P. & ROULEAU, A. 2015. A hydrostratigraphic simplification approach to build 3D groundwater flow numerical models: example of a Quaternary deltaic deposit aquifer. *Environmental Earth Sciences,* 74**,** 4671-4683.
JABALOY-SÁNCHEZ, A., LOBO, F. J., AZOR, A., MARTÍN-ROSALES, W., PÉREZ-PEÑA, J. V., BÁRCENAS, P., MACÍAS, J., FERNÁNDEZ-SALAS, L. M. & VÁZQUEZ-VÍLCHEZ, M. 2014. Six thousand years of coastline evolution in the Guadalfeo deltaic system (southern Iberian Peninsula). *Geomorphology,* 206**,** 374-391.

KHASKA, M., LA SALLE, C. L. G., LANCELOT, J., MOHAMAD, A., VERDOUX, P., NORET, A. & SIMLER, R. 2013. Origin of groundwater salinity (current seawater vs. saline deep water) in a coastal karst aquifer based on Sr and Cl isotopes. Case study of the La Clape massif (southern France). *Applied geochemistry,* 37**,** 212-227.

KLINGBEIL, R., KLEINEIDAM, S., ASPRION, U., AIGNER, T. & TEUTSCH, G. 1999. Relating lithofacies to hydrofacies: outcrop-based hydrogeological characterisation of Quaternary gravel deposits. *Sedimentary Geology,* 129**,** 299-310.

KOLBE, T., MARÇAIS, J., THOMAS, Z., ABBOTT, B. W., DE DREUZY, J.-R., ROUSSEAU-GUEUTIN, P., AQUILINA, L., LABASQUE, T. & PINAY, G. 2016. Coupling 3D groundwater modeling with CFC-based age dating to classify local groundwater circulation in an unconfined crystalline aquifer. *Journal of Hydrology*.

KOLTERMANN, C. E. & GORELICK, S. M. 1996. Heterogeneity in sedimentary deposits: A review of structure‐imitating, process‐imitating, and descriptive approaches. *Water Resources Research,* 32**,** 2617-2658.

KRESIC, N. 2006. *Hydrogeology and groundwater modeling*, CRC press.

LANGEVIN, C. D. 2003. Simulation of submarine ground water discharge to a marine estuary: Biscayne Bay, Florida. *Ground Water,* 41**,** 758-771.

LEBBE, L., JONCKHEERE, S. & VANDENBOHEDE, A. Modeling of historical evolution of salt water distribution in the phreatic aquifer in and around the silted up Zwin estuary mouth (Flanders, Belgium). Proceedings 20th Salt Water Intrusion Meeting, Naples, Florida, USA, 2008. 141-144.

LEMIEUX, J.-M. & SUDICKY, E. A. 2010. Simulation of groundwater age evolution during the Wisconsinian glaciation over the Canadian landscape. *Environmental fluid mechanics,* 10**,** 91-102.

LI, X., HU, B. X. & TONG, J. 2015. Numerical study on tide-driven submarine groundwater discharge and seawater recirculation in heterogeneous aquifers. *Stochastic Environmental Research and Risk Assessment***,** 1-15.

LIQUETE, C., ARNAU, P., CANALS, M. & COLAS, S. 2005. Mediterranean river systems of Andalusia, southern Spain, and associated deltas: A source to sink approach. *Marine Geology,* 222–223**,** 471-495.

LOBO, F. J., FERNANDEZ-SALAS, L. M., MORENO, I., SANZ, J. L. & MALDONADO, A. 2006. The sea-floor morphology of a Mediterranean shelf fed by small rivers, northern Alboran Sea margin. *Continental Shelf Research,* 26**,** 2607-2628.

MALDONADO, A. 2009. El Delta del Guadalfeo, XXVII Semana de Estudios del Mar. *Asociación de Estudios del Mar***,** 189–212.

MCDONALD, M. G. & HARBAUGH, A. W. 1988. A modular three-dimensional finite-difference ground-water flow model.

MULLIGAN, A. E., EVANS, R. L. & LIZARRALDE, D. 2007. The role of paleochannels in groundwater/seawater exchange. *Journal of Hydrology,* 335**,** 313-329.

NARAYAN, K., SCHLEEBERGER, C., CHARLESWORTH, P. & BISTROW, K. Effects of groundwater pumping on saltwater intrusion in the lower Burdekin Delta, North Queensland. MODSIM 2003 International Congress on modelling and simulation, 2003. 212-217.

NEMEC, W. 1990. Deltas== remarks on terminology and classification. *Coarse-Grained Deltas (Special Publication 10 of the IAS),* 27**,** 3.

NISWONGER, R. G. & PRUDIC, D. E. 2005. *Documentation of the streamflow-routing (SFR2) package to include unsaturated flow beneath streams--A modification to SFR1*, US Department of the Interior, US Geological Survey.

POESEN, J. & HOOKE, J. 1997. Erosion, flooding and channel management in Mediterranean environments of southern Europe. *Progress in Physical Geography,* 21**,** 157-199.
POETER, E. & GAYLORD, D. R. 1990. Influence of aquifer heterogeneity on contaminant transport at the Hanford Site. *Groundwater,* 28**,** 900-909.
POST, V. & ABARCA, E. 2010. Preface: saltwater and freshwater interactions in coastal aquifers. *Hydrogeology Journal,* 18**,** 1-4.
REHFELDT, K. R., BOGGS, J. M. & GELHAR, L. W. 1992. Field study of dispersion in a heterogeneous aquifer: 3. Geostatistical analysis of hydraulic conductivity. *Water Resources Research,* 28**,** 3309-3324.
REILLY, T. E. & HARBAUGH, A. W. 2004. *Guidelines for evaluating ground-water flow models*, US Department of the Interior, US Geological Survey Denver, CO, USA.
SCHEIBE, T. D. & MURRAY, C. J. 1998. Simulation of geologic patterns: A comparison of stochastic simulation techniques for groundwater transport modeling. *Hydrogeologic models of sedimentary aquifers: Concepts in Hydrogeology and Environmental Geology,* 1**,** 107-118.
SCHMIDT, K. D. & SHERMAN, I. 1987. Effect of irrigation on groundwater quality in California. *Journal of irrigation and drainage engineering,* 113**,** 16-29.
SHOEMAKER, W. B. 2004. Important observations and parameters for a salt water intrusion model. *Ground Water,* 42**,** 829-840.
SLICHTER, C. S. 1905. Field measurements of the rate of movement of underground waters. Govt. Print. Off.
SMALL, C. & NICHOLLS, R. J. 2003. A global analysis of human settlement in coastal zones. *Journal of Coastal Research***,** 584-599.
SMITH, A. J. 2004. Mixed convection and density‐dependent seawater circulation in coastal aquifers. *Water Resources Research,* 40.
STEYL, G. & DENNIS, I. 2010. Review of coastal-area aquifers in Africa. *Hydrogeology Journal,* 18**,** 217-225.
SUDICKY, E. A. 1986. A natural gradient experiment on solute transport in a sand aquifer: Spatial variability of hydraulic conductivity and its role in the dispersion process. *Water Resources Research,* 22**,** 2069-2082.
TELLAM, J. H. 1995. Hydrochemistry of the saline groundwaters of the lower Mersey Basin Permo-Triassic sandstone aquifer, UK. *Journal of Hydrology,* 165**,** 45-84.
VAN LOON, A. H., SCHOT, P. P., GRIFFIOEN, J., BIERKENS, M. F. P. & WASSEN, M. J. 2009. Palaeo-hydrological reconstruction of a managed fen area in The Netherlands. *Journal of Hydrology,* 378**,** 205-217.
WALTHER, M., DELFS, J.-O., GRUNDMANN, J., KOLDITZ, O. & LIEDL, R. 2012. Saltwater intrusion modeling: verification and application to an agricultural coastal arid region in Oman. *Journal of Computational and Applied Mathematics,* 236**,** 4798-4809.
WERNER, A. D., BAKKER, M., POST, V. E. A., VANDENBOHEDE, A., LU, C., ATAIE-ASHTIANI, B., SIMMONS, C. T. & BARRY, D. A. 2013. Seawater intrusion processes, investigation and management: Recent advances and future challenges. *Advances in Water Resources,* 51**,** 3-26.
WHO 2004. *Guidelines for drinking-water quality: recommendations*, World Health Organization.
ZAMARIN, J. 1928. Calculation of groundwater flow (in Russian). *Trudey I.V.H, Taskeni*.
ZHENG, C. & WANG, P. P. 1999. A modular three-dimensional multi-species transport model for simulation of advection, dispersion and chemical reactions of

contaminants in groundwater systems; documentation and user's guide. *US Army Engineer Research and Development Center Contract Report SERDP-99-1, Vicksburg, Mississippi, USA*.

ZWERTVAEGHER, A., FINKE, P., DE REU, J., VANDENBOHEDE, A., LEBBE, L., BATS, M., DE CLERCQ, W., DE SMEDT, P., GELORINI, V., SERGANT, J., ANTROP, M., BOURGEOIS, J., DE MAEYER, P., VAN MEIRVENNE, M., VERNIERS, J. & CROMBÉ, P. 2013. Reconstructing Phreatic Palaeogroundwater Levels in a Geoarchaeological Context: A Case Study in Flanders, Belgium. *Geoarchaeology,* 28**,** 170-189.